



SAPIENZA
UNIVERSITÀ DI ROMA

A systematic study of phenomenological implications of dim-6 operators

**Scuola di dottorato Vito Volterra
Dottorato di ricerca in Fisica – XXX Ciclo**

Candidate
Marco Fedele
ID number 1308444

Thesis Advisors
Prof. Giuseppe Degrassi
Dr. Luca Silvestrini

A thesis submitted as a partial fulfillment of the requirements
for the degree of Doctor of Philosophy in Physics
October 2017

Contents

Introduction and Motivations	3
I The Theoretical Framework	5
1 The Standard Model of Particle Physics	6
1.1 The Standard Model Lagrangian	6
1.1.1 Gauge Boson Masses	7
1.1.2 Neutral and Charged Currents	9
1.1.3 Fermion Masses	9
1.1.4 The Cabibbo-Kobayashi-Maskawa Matrix V_{CKM}	10
1.2 Equations of Motion	11
1.3 Renormalization Group Improved Perturbative Expansion	12
1.3.1 Renormalization	13
1.3.2 Renormalization Group	14
2 Effective Field Theories	16
2.1 Effective Lagrangians as a Tool to Search for New Physics Effects	16
2.2 Operator Product Expansion	17
2.3 Bottom-Up vs Top-Down	19
3 The Standard Model Effective Field Theory	21
3.1 dim-5 operators	22
3.2 dim-6 operators	22
3.2.1 The Warsaw basis	23
3.2.2 The Anomalous Dimension	30
3.3 Higher Dimension Operators	34

II	Anomalies in $b \rightarrow s$ transitions	35
4	The Theoretical Framework	37
4.1	Weak Hamiltonian and Amplitude	37
4.2	Helicity Amplitudes and Helicity Form Factors	39
4.3	Kinematic Distribution	42
4.4	Angular Observables	44
4.5	On (Non-)Factorizable Contributions to the Hadronic Hamiltonian .	47
4.6	Amplitudes for Other Decay Channels	48
5	Review of $b \rightarrow s$ Anomalies and Their Interpretations	50
5.1	Anomalies in $B \rightarrow K^* \mu^+ \mu^-$ Angular Analysis	51
5.2	Anomalies in Branching Fractions: the $B \rightarrow K \mu^+ \mu^-$ and the $B_s \rightarrow \phi \mu^+ \mu^-$ cases	53
5.3	Anomalies in Branching Fraction Ratios: the R_K and the R_{K^*} Observables	55
5.4	A Comprehensive Phenomenological Interpretation: the $C_{9\mu}^{\text{NP}} \simeq -1$ Case	57
5.5	An Alternative Interpretation: the Axial Solution	59
6	A Systematic Analysis of the $b \rightarrow s$ Anomalies Employing the SMEFT Framework	72
6.1	The Operators Involved	72
6.2	Previous Studies	75
6.3	Constraining the Couplings by Means of a Bayesian Analysis	77
6.4	Future Perspectives	83
III	Is the EFT Approach the Only Way?	85
7	Constraining the Trilinear Higgs Self-Coupling by Means of Precision Electroweak Measurements	88
7.1	λ_3 -dependent Contributions in m_W and $\sin^2 \theta_{\text{eff}}^{\text{lep}}$	90
7.2	Analytic Expressions	93
7.3	Resulting Bounds on the Trilinear Higgs Self-Coupling	98
7.4	On the Equivalence with a $(\Phi^\dagger \Phi)^n$ Theory	101
	Conclusions	105
	Bibliography	107

Introduction and Motivations

The Standard Model (SM) of particle physics has been producing reliable estimates to a high precision level in the last few decades. Moreover, the discovery of a scalar particle with properties consistent with the SM Higgs boson [1, 2], together with the fact that no Beyond Standard Model (BSM) particle has been detected so far, suggests that the New Physics (NP) scale Λ can be placed above the electro-weak symmetry breaking (EWSB) scale.

Therefore, an effective field theory built solely using the SM fields, called Standard Model Effective Field Theory (SMEFT), can be used to describe the low energy limit of BSM physics. This theory should be written adding to the renormalizable SM interactions further terms of higher dimensions, suppressed by suitable powers of the scale Λ and invariant under the SM gauge group. The schematic Lagrangian is

$$\mathcal{L}_{SMEFT} = \mathcal{L}_{SM} + \mathcal{L}_5 + \mathcal{L}_6 + \dots$$

\mathcal{L}_5 contains only the Weinberg operator, which can be used to provide masses to neutrinos. Assuming the conservation of baryon number, in \mathcal{L}_6 there are 59 operators, many of which have flavour indices (explicitly taking them into account, the number of operators grows up to 2499); a complete list can be found in [3]. The full one-loop anomalous dimension (AD) matrix needed for renormalization group evolution (RGE) of the dimension 6 operators has been recently computed [4–7]; several entries have been found to be of order 1, therefore suggesting a relevant mixing between some of these operators.

The SMEFT approach can be used to interpret several patterns of deviations in SM processes: it allows for model independent analysis, which is a particularly useful feature given our present lack of knowledge regarding the ultraviolet (UV) completion of the SM theory. The BSM fields can in fact be integrated out of the theory at the NP scale, in such a way that there is no evident sign of their presence at the EWSB scale, but their effects can be mimicked by means of the couplings of the higher dimension operators; it will therefore be possible to use experimental informations in order to constrain the bounds of the such couplings, which can be consequently reinterpreted as bounds on the NP scale once the SMEFT is mapped on the desired UV completion of the theory.

In my PhD project, I have focused my attention to phenomenological implications due to the effect of dimension 6 operators. As a first step of my project, I have partially recomputed the AD from Refs. [4–7], in order to check the correctness of their results. Subsequently, I have been involved in analyses concerning the status of the anomalies present in B physics, with a particular focus on $b \rightarrow s$ transitions. My work on the field, aiming at discerning the shape of the potential NP underlying such processes and potentially disentangling it from effects stemming from QCD effects, is reported in Refs. [8–11]. A systematic reinterpretation of such findings in the SMEFT framework is an original contribution to this PhD thesis, and is yet to be published. Moreover, I have spent some time working on the study of the trilinear Higgs self-coupling. Given the large room for NP effects to such coupling, induced by the present status of the experimental constraints, the (SM)EFT approach is not a phenomenologically-meaningful framework to employ in order to study potential BSM effects in this sector. Therefore, I have adopted an alternative method to approach the matter, exploiting the study of electroweak precision observables in order to further constrain the bound that can be put on the Higgs trilinear self-coupling [12].

The thesis is organized as follows. Part I is devoted to a review of the theoretical framework employed in my projects: Chapter 1 is focused on the SM theory, Chapter 2 briefly introduces the EFT approach and Chapter 3 describes the features of the SMEFT framework. The analyses of the anomalies in $b \rightarrow s$ transitions are reviewed in Part II: the effective Hamiltonian employed to build the observables of interest is described in Chapter 4; subsequently, a summary of the anomalies and their main interpretation is carried out in Chapter 5, while the results of the systematic SMEFT analysis is reported in Chapter 6. Finally, Part III is devoted to the study of the constraints that can be imposed on the Higgs trilinear self-coupling by means of precision electroweak measurements.

Part I

The Theoretical Framework

Chapter 1

The Standard Model of Particle Physics

1.1 The Standard Model Lagrangian

Our present knowledge of the strong and electroweak interactions is described by means of the Standard Model (SM) Lagrangian \mathcal{L}_{SM} . Its fundamental degrees of freedom are the spin one-half quarks and leptons, the spin one gauge bosons and the spin zero Higgs boson. It is invariant under $SU(3)$ gauge transformations for the strong interactions and under $SU(2) \times U(1)$ gauge transformations for the electroweak interactions; therefore, its gauge group structure is

$$SU(3)_c \times SU(2)_L \times U(1)_Y. \quad (1.1)$$

The Standard Model contains 3 kinds of quarks

$$Q_{L_i} = \begin{pmatrix} u_{L_i} \\ d_{L_i} \end{pmatrix} = (3, 2, 1/6), \quad u_{R_i} = (3, 1, 2/3), \quad d_{R_i} = (3, 1, -1/3), \quad (1.2)$$

and, if one considers the non-interacting ν_{R_i} , 3 kinds of leptons

$$L_{L_i} = \begin{pmatrix} \nu_{L_i} \\ l_{L_i} \end{pmatrix} = (1, 2, -1/2), \quad l_{R_i} = (1, 1, -1), \quad \nu_{R_i} = (1, 1, 0), \quad (1.3)$$

where i is the flavour index, that goes from 1 to 3 and implies the existence of a $SU(3)^5 \times U(1)^4$ flavour symmetry (note that there are only four $U(1)$ flavour symmetries because the fifth one is already present as the $U(1)_Y$ gauge symmetry). While the $SU(3)_c$ symmetry is unbroken, low energy phenomenology implies that $SU(2)_L \times U(1)_Y$ must be broken onto a $U(1)_{em}$ symmetry; besides, the different experimental values of quark and lepton masses imply that also the flavour symmetries need to be broken, in particular into a phenomenological $U(1)_B \times U(1)_L$

symmetry; moreover, the symmetry breaking must give mass to three out of the four gauge bosons (Z^0 , W^\pm), while the fourth one (the photon) remains massless. All this can be accomplished through the *Higgs mechanism* [13–15], which requires the introduction of a four-component scalar field that forms a complex doublet of $SU(2)_L$ with hypercharge $Y = 1/2$:

$$\varphi = \begin{pmatrix} \varphi^+ \\ \varphi^0 \end{pmatrix}. \quad (1.4)$$

This new field has the opposite quantum numbers of L_{Li} , and its Lagrangian can be written as

$$\mathcal{L}_H = D_\mu \varphi^\dagger D^\mu \varphi + \mu^2 \varphi^\dagger \varphi - \frac{\lambda}{4} (\varphi^\dagger \varphi)^2, \quad (1.5)$$

where D_μ is the covariant derivative

$$D_\mu = \partial_\mu - igW_\mu^i \frac{\sigma^i}{2} - i\frac{g'}{2}B_\mu, \quad (1.6)$$

W_μ^i and B_μ are respectively the gauge bosons of the $SU(2)_L$ and $U(1)_Y$ symmetries, and g and g' are the corresponding coupling constants. Note that both μ^2 and λ are positive constants so that the ground state breaks the symmetry, and performing a gauge transformation in a way such that $\langle \varphi^+ \rangle = 0$ and φ^0 becomes real, the Higgs doublet acquires the Vacuum Expectation Value (VEV)

$$\langle \varphi \rangle = \frac{1}{\sqrt{2}} \begin{pmatrix} 0 \\ v \end{pmatrix}, \quad \text{with} \quad v = \sqrt{\frac{\mu^2}{\lambda}}. \quad (1.7)$$

In the next sections we will see how the introduction of this new field affects the other SM fields.

1.1.1 Gauge Boson Masses

In order to compute the masses of the three massive gauge bosons, one has to analyze how the Lagrangian in Eq. (1.5) changes once the Higgs VEV is introduced; in particular, one has to study the term

$$\begin{aligned} \frac{1}{2} \begin{pmatrix} 0 & v \end{pmatrix} \left(gW_\mu^i \frac{\sigma^i}{2} + \frac{g'}{2} B_\mu \right) \left(gW_\mu^j \frac{\sigma^j}{2} + \frac{g'}{2} B_\mu \right) \begin{pmatrix} 0 \\ v \end{pmatrix} &= \frac{v^2}{8} \left(g^2 W_\mu^i W_\mu^i + g'^2 B_\mu B_\mu - 2gg' W_\mu^3 B_\mu \right) \\ &= \frac{v^2}{8} \left(g^2 (W_\mu^1)^2 + g^2 (W_\mu^2)^2 + (gW_\mu^3 - g'B_\mu)^2 \right). \end{aligned} \quad (1.8)$$

This term allow us to write the gauge boson mass eigenstates

$$W_\mu^\pm = \frac{1}{\sqrt{2}} (W_\mu^1 \mp W_\mu^2), \quad (1.9)$$

$$Z_\mu^0 = \frac{1}{\sqrt{g^2 + g'^2}}(gW_\mu^3 - g'B_\mu), \quad (1.10)$$

whose masses are

$$M_W = g \frac{v}{2}, \quad M_Z = \sqrt{g^2 + g'^2} \frac{v}{2}. \quad (1.11)$$

It is now possible to define the fourth mass eigenstate through the orthogonality with Z_μ^0 :

$$A_\mu^0 = \frac{1}{\sqrt{g^2 + g'^2}}(g'W_\mu^3 + gB_\mu), \quad M_A = 0. \quad (1.12)$$

Moreover, it is possible to express the covariant derivative

$$D_\mu = \partial_\mu - igW_\mu^i T^i - ig'Y B_\mu, \quad (1.13)$$

where $T^i = \frac{\sigma^i}{2}$ for SU(2) doublets and $T^i = 0$ for SU(2) singlets, in terms of the gauge boson mass eigenstates: inverting Eqs. (1.9), (1.10), (1.12) and defining

$$T^\pm = T^1 \pm T^2, \quad (1.14)$$

it is possible to write

$$D_\mu = \partial_\mu - \frac{ig}{\sqrt{2}}(W_\mu^+ T^+ + W_\mu^- T^-) - \frac{i}{\sqrt{g^2 + g'^2}} Z_\mu (g^2 T^3 - g'^2 Y) - \frac{igg'}{\sqrt{g^2 + g'^2}} A_\mu (T^3 + Y). \quad (1.15)$$

Observing now that the last term must be the one which describes the electromagnetic current, we obtain the relations

$$e = \frac{gg'}{\sqrt{g^2 + g'^2}}, \quad (1.16)$$

$$Q = T^3 + Y. \quad (1.17)$$

Furthermore, if one defines the weak mixing angle θ_W through the relation

$$\begin{pmatrix} Z_\mu^0 \\ A_\mu^0 \end{pmatrix} = \begin{pmatrix} \cos \theta_W & -\sin \theta_W \\ \sin \theta_W & \cos \theta_W \end{pmatrix} \begin{pmatrix} W_\mu^3 \\ B_\mu \end{pmatrix} \quad \Rightarrow \quad \sin \theta_W = \frac{g'}{\sqrt{g^2 + g'^2}}, \quad (1.18)$$

Eq. (1.15) may be written as

$$D_\mu = \partial_\mu - \frac{ig}{\sqrt{2}}(W_\mu^+ T^+ + W_\mu^- T^-) - \frac{ig}{\cos \theta_W} Z_\mu (T^3 - \sin^2 \theta_W Q) - ie A_\mu Q. \quad (1.19)$$

1.1.2 Neutral and Charged Currents

Once the covariant derivative is written in the form of Eq. (1.19), it is possible to obtain the fermions-bosons coupling terms and therefore the explicit form of the neutral and charged currents. In order to do so, one has to write the Lagrangian for chiral fermions:

$$\begin{aligned}\mathcal{L}_F &= \bar{L}_L^i i \not{D} L_L^i + \bar{l}_R^i i \not{D} l_R^i + \bar{Q}_L^i i \not{D} Q_L^i + \bar{u}_R^i i \not{D} u_R^i + \bar{d}_R^i i \not{D} d_R^i \\ &= g(W_\mu^+ J^+ + W_\mu^- J^-) + gZ_\mu^0 J_\mu^Z + eA_\mu J_\mu^{em} + K,\end{aligned}\quad (1.20)$$

where K is the kinetic terms

$$K = \bar{l}_L^i i \not{\partial} l_L^i + \bar{\nu}_L^i i \not{\partial} \nu_L^i + \bar{l}_R^i i \not{\partial} l_R^i + \bar{u}_L^i i \not{\partial} u_L^i + \bar{u}_R^i i \not{\partial} u_R^i + \bar{d}_L^i i \not{\partial} d_L^i + \bar{d}_R^i i \not{\partial} d_R^i, \quad (1.21)$$

and

$$J_\mu^+ = \frac{1}{\sqrt{2}}(\bar{\nu}_L^i \gamma^\mu l_L^i + \bar{u}_L^i \gamma^\mu d_L^i), \quad (1.22)$$

$$J_\mu^{em} = -\bar{l}_L^i \gamma^\mu l_L^i - \bar{l}_R^i \gamma^\mu l_R^i + \frac{2}{3}\bar{u}_L^i \gamma^\mu u_L^i + \frac{2}{3}\bar{u}_R^i \gamma^\mu u_R^i - \frac{1}{3}\bar{d}_L^i \gamma^\mu d_L^i - \frac{1}{3}\bar{d}_R^i \gamma^\mu d_R^i, \quad (1.23)$$

$$\begin{aligned}J_\mu^Z &= \frac{1}{\cos \theta_W} \left(\frac{1}{2} \bar{\nu}_L^i \gamma^\mu \nu_L^i + \left(-\frac{1}{2} + \sin^2 \theta_W \right) \bar{l}_L^i \gamma^\mu l_L^i + \sin^2 \theta_W \bar{l}_R^i \gamma^\mu l_R^i \right. \\ &\quad \left. + \left(\frac{1}{2} - \frac{2}{3} \sin^2 \theta_W \right) \bar{u}_L^i \gamma^\mu u_L^i + \left(-\frac{1}{2} + \frac{1}{3} \sin^2 \theta_W \right) \bar{d}_L^i \gamma^\mu d_L^i \right. \\ &\quad \left. - \frac{2}{3} \sin^2 \theta_W \bar{u}_R^i \gamma^\mu u_R^i + \frac{1}{3} \sin^2 \theta_W \bar{d}_R^i \gamma^\mu d_R^i \right).\end{aligned}\quad (1.24)$$

1.1.3 Fermion Masses

In order to let the fermions acquire masses, it is necessary to write a gauge invariant Yukawa Lagrangian which contains the interactions among fermions and the Higgs boson:

$$\mathcal{L}_Y = -(Y_d)_{ij} \bar{Q}_L^i \varphi d_R^j - (Y_u)_{ij} \bar{Q}_L^i \tilde{\varphi} u_R^j - (Y_l)_{ij} \bar{L}_L^i \varphi l_R^j + h.c. \quad (1.25)$$

where Y_i are the Yukawa couplings and $\tilde{\varphi}^\alpha = \epsilon^{\alpha\beta} \varphi_\beta^*$, with $\epsilon^{\alpha\beta}$ a totally antisymmetric matrix. Once the Higgs doublet acquires a VEV, the Lagrangian takes the form

$$\mathcal{L}_Y = -\frac{v}{\sqrt{2}}(Y_d)_{ij} \bar{d}_L^i d_R^j - \frac{v}{\sqrt{2}}(Y_u)_{ij} \bar{u}_L^i u_R^j - \frac{v}{\sqrt{2}}(Y_l)_{ij} \bar{l}_L^i l_R^j + h.c. \quad (1.26)$$

so that the fermions acquire the masses

$$(m_d)_{ij} = \frac{v}{\sqrt{2}}(Y_d)_{ij}, \quad (m_u)_{ij} = \frac{v}{\sqrt{2}}(Y_u)_{ij}, \quad (m_l)_{ij} = \frac{v}{\sqrt{2}}(Y_l)_{ij}. \quad (1.27)$$

It is now possible to write the Lagrangian in the mass eigenstate basis. In order to do so, it is first necessary to diagonalize the mass matrix m_ψ of fermion ψ through a bi-unitary transformation:

$$U_{\psi,L}^+ m_\psi U_{\psi,R} = m_\psi^D \equiv \text{diag}(m_1, m_2, m_3); \quad (1.28)$$

it is now possible to write the mass term in the form

$$\bar{\psi}_L m_\psi \psi_R = \bar{\psi}'_L m_\psi^D \psi'_R, \quad (1.29)$$

where we have defined the mass eigenstates

$$\psi'_L = U_{\psi,L}^+ \psi_L, \quad \psi'_R = U_{\psi,R}^+ \psi_R. \quad (1.30)$$

1.1.4 The Cabibbo-Kobayashi-Maskawa Matrix V_{CKM}

If one takes the currents from Eqs. (1.22)-(1.24) and expresses them in terms of the mass eigenstate basis defined by Eq. (1.30), it is straightforward to observe that the neutral currents remain unmodified: this implies that the Standard Model predicts the absence of tree-level *Flavour Changing Neutral Currents* (FCNC). Instead, the charged current J_μ^+ takes the form

$$J_\mu^+ = \frac{1}{\sqrt{2}} (\bar{\nu}_L^i \gamma^\mu U_L^l l_L^i + \bar{u}_L^i U_L^{u+} \gamma^\mu U_L^d d_L^i) \equiv \frac{1}{\sqrt{2}} (\bar{\tilde{\nu}}_L^i \gamma^\mu l_L^i + \bar{u}_L^i V_{CKM} \gamma^\mu d_L^i), \quad (1.31)$$

where we have redefined the mass-less neutrino field setting

$$\tilde{\nu}_L = U_L^{l+} \nu_L \quad (1.32)$$

and we have defined the Cabibbo-Kobayashi-Maskawa (CKM) matrix [16, 17]

$$V_{CKM} = U_L^{u+} U_L^d. \quad (1.33)$$

This matrix will not generally be diagonal, so that the Standard Model predicts the occurrence of *Flavour Changing Charged Currents* at tree-level.

We observe that CP violation in weak interactions requires the Yukawa matrices Y^d, Y^u to be complex. In the mass eigenstate basis they take the form

$$Y^d \rightarrow U_{Q_L}^+ Y^d U_{d_R}, \quad Y^u \rightarrow U_{Q_L}^+ Y^u U_{u_R}. \quad (1.34)$$

For 3 quark generations the Yukawa matrices contain 9 real parameters and 9 phases each; the three U matrices, which contain 9 angles and 17 phases (the 18th phase is related to the $U_B(1)$ symmetry), can be used to reduce the number of undetermined quantities so that there are only 9 physical real parameters and

1 physical phase: the 6 quarks masses, and 3 angles and 1 phase for the V_{CKM} matrix.

Following this observation, the standard way to parameterize the CKM matrix [18] is through the phase δ and the angles θ_{12}, θ_{13} and θ_{23} :

$$V_{CKM} = \begin{pmatrix} c_{12}c_{13} & s_{12}c_{13} & s_{13}e^{-i\delta} \\ -s_{12}c_{23} - c_{12}s_{23}s_{13}e^{i\delta} & c_{12}c_{23} - s_{12}s_{23}s_{13}e^{i\delta} & s_{23}c_{13} \\ s_{12}s_{23} - c_{12}c_{23}s_{13}e^{i\delta} & -c_{12}s_{23} - s_{12}c_{23}s_{13}e^{i\delta} & c_{23}c_{13} \end{pmatrix}, \quad (1.35)$$

where $c_{ij} = \cos \theta_{ij}$ and $s_{ij} = \sin \theta_{ij}$.

An approximation of the V_{CKM} matrix has been given by Wolfenstein [19], through a power series in the small parameter $\lambda = |V_{us}| \simeq 0.22$:

$$V_{CKM} = \begin{pmatrix} 1 - \frac{\lambda^2}{2} & \lambda & A\lambda^3(\rho - i\eta) \\ -\lambda & 1 - \frac{\lambda^2}{2} & A\lambda^2 \\ A\lambda^3(1 - \rho - i\eta) & -A\lambda^2 & 1 \end{pmatrix} + O(\lambda^4). \quad (1.36)$$

1.2 Equations of Motion

Putting together all the pieces from the previous section (and adding the kinetic terms for the gauge field strength tensors), it is possible to write down the SM Lagrangian:

$$\begin{aligned} \mathcal{L}_{\text{SM}} = & -\frac{1}{4}G_{\mu\nu}^A G^{A\mu\nu} - \frac{1}{4}W_{\mu\nu}^I W^{I\mu\nu} - \frac{1}{4}B_{\mu\nu} B^{\mu\nu} + (D_\mu \varphi^\dagger)(D^\mu \varphi) - \lambda \left(\varphi^\dagger \varphi - \frac{1}{2}v^2 \right)^2 \\ & + \bar{L}_L^i i \not{D} L_L^i + \bar{l}_R^i i \not{D} l_R^i + \bar{Q}_L^i i \not{D} Q_L^i + \bar{u}_R^i i \not{D} u_R^i + \bar{d}_R^i i \not{D} d_R^i \\ & - \left[(Y_d)_{ij} \bar{Q}_L^i \varphi d_R^j + (Y_u)_{ij} \bar{Q}_L^i \tilde{\varphi} u_R^j + (Y_l)_{ij} \bar{L}_L^i \varphi l_R^j + h.c. \right]. \end{aligned} \quad (1.37)$$

Starting from this Lagrangian, it is therefore possible to extract the Equation of Motion (EoM) for all the dynamical fields involved. In particular, for the Higgs field one obtains

$$D^2 \varphi_k - \lambda v^2 \varphi_k + 2\lambda(\varphi^\dagger \varphi)\varphi_k + \bar{Q}_L^j Y_u^\dagger u_R \epsilon_{jk} + \bar{d}_R Y_d Q_L^k + \bar{e}_R Y_e L_L^k = 0; \quad (1.38)$$

for the fermion fields, the EoM reads

$$\begin{aligned} i \not{D} Q_L^j &= Y_u^\dagger u_R \tilde{\varphi}_j + Y_d^\dagger d_R \varphi_j, & i \not{D} d_R &= Y_d Q_L^j \varphi^{\dagger j}, \\ i \not{D} u_R &= Y_u Q_L^j \tilde{\varphi}^{\dagger j}, & i \not{D} L_L^j &= Y_e^\dagger e_R \varphi_j, \\ i \not{D} e_R &= Y_e L_j \varphi^{\dagger j}; \end{aligned} \quad (1.39)$$

and for the gauge fields, one obtains

$$[D^\alpha, G_{\alpha\beta}]^A = g_3 j_\beta^A, \quad [D^\alpha, W_{\alpha\beta}]^I = g_2 j_\beta^I, \quad D^\alpha B_{\alpha\beta} = g_1 j_\beta, \quad (1.40)$$

where $[D^\alpha, F_{\alpha\beta}]$ is the covariant derivative in the adjoint representation. The gauge currents are

$$j_\beta^A = \sum_{\psi=u_R, d_R, Q_L} \bar{\psi} T^A \gamma_\beta \psi, \quad (1.41)$$

$$j_\beta^I = \frac{1}{2} \bar{Q}_L \tau^I \gamma_\beta Q_L + \frac{1}{2} \bar{L}_L \tau^I \gamma_\beta L_L + \frac{1}{2} \varphi^\dagger i \overleftrightarrow{D}_\beta^I \varphi, \quad (1.42)$$

$$j_\beta = \sum_{\psi=u_R, d_R, Q_L, e_R, L_L} \bar{\psi} y_i \gamma_\beta \psi + \frac{1}{2} \varphi^\dagger i \overleftrightarrow{D}_\beta \varphi, \quad (1.43)$$

where y_i are the fermions $U(1)$ hypercharges, and

$$\varphi^\dagger i \overleftrightarrow{D}_\beta \varphi = i\varphi^\dagger (D_\beta \varphi) - i(D_\beta \varphi^\dagger) \varphi, \quad (1.44)$$

$$\varphi^\dagger i \overleftrightarrow{D}_\beta^I \varphi = i\varphi^\dagger \tau^I (D_\beta \varphi) - i(D_\beta \varphi^\dagger) \tau^I \varphi. \quad (1.45)$$

1.3 Renormalization Group Improved Perturbative Expansion

Weak decays mediated by the exchange of the W boson may receive corrections by QCD loops, as the ones shown in Fig. 1.1. Those corrections may give rise to terms proportional to (denoting the external momenta by p , with $p^2 < 0$)

$$\alpha_S \ln \frac{M_W^2}{-p^2}, \quad (1.46)$$

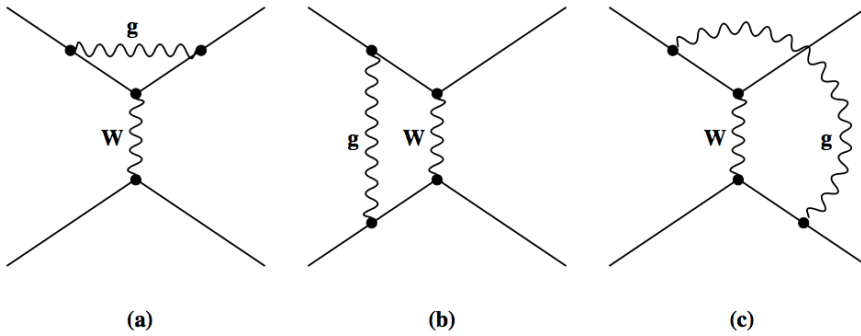


Figure 1.1: 1-loop QCD corrections to W mediated weak decays. Figure taken from Ref. [20].

where the logarithms, for $-p^2 \ll M_W^2$, may become large and eventually overcome the smallness of α_s , invalidating the perturbative expansion. This problem can be solved using a *Renormalization Group Improved Perturbative Expansion*; for a pedagogical introduction see [20]. Let us work out the steps necessary to obtain this feature.

1.3.1 Renormalization

In order to eliminate the divergences that may arise at loop level in Green Functions, calculated for example using *dimensional regularization* [21] in which one evaluates Feynman diagrams in $D = 4 - 2\epsilon$ space-time dimensions, the fields and the parameters present in the Lagrangian have to be renormalized through

$$A_{0\mu}^a = Z_3^{1/2} A_\mu^a, \quad q_0 = Z_q^{1/2} q, \quad g_{0,s} = Z_g g_s \mu^\epsilon, \quad m_0 = Z_m m, \quad (1.47)$$

where the “0” indicates bare quantities, A_μ^a is the renormalized gauge field, q is the renormalized quark field, g_s is the renormalized QCD coupling, μ is the renormalization scale and m is the renormalized quark mass; the Z_i factors are called renormalization constants, and are divergent quantities chosen in a way such that the divergences disappear in the observables written in terms of the renormalized quantities only. It should be stressed that since bare quantities are μ independent, g_s must be μ dependent and, since all Z_i have a perturbative expansion in g_s , they must all be μ dependent as well.

The value of the renormalization constants (scheme) is arbitrary, and the computationally simplest renormalization scheme is the *Minimal Subtraction* MS [22], in which the Z_i subtract only the divergences; in this scheme, the renormalization constants at Leading Order (LO) are

$$Z_q = 1 - \frac{\alpha_s}{4\pi} \frac{1}{\epsilon} C_F + O(\alpha_s^2), \quad (1.48)$$

$$Z_g = 1 - \frac{\alpha_s}{4\pi} \frac{1}{\epsilon} \left(\frac{11}{6} N_C - \frac{2}{6} n_f \right) + O(\alpha_s^2), \quad (1.49)$$

$$Z_3 = 1 - \frac{\alpha_s}{4\pi} \frac{1}{\epsilon} \left(\frac{2}{3} n_f - \frac{5}{3} N_C \right) + O(\alpha_s^2), \quad (1.50)$$

$$Z_m = 1 - \frac{\alpha_s}{4\pi} \frac{1}{\epsilon} 3C_F + O(\alpha_s^2), \quad (1.51)$$

where $C_F = 4/3$ is the relevant colour factor, N_C is the number of colours and n_f is the number of active quark flavours.

1.3.2 Renormalization Group

Given the independence of the bare quantities from μ , it is possible to write equations for the renormalized quantities which describe how they evolve as a function of μ .

Let us focus on the couplings, observing that it is possible to write

$$\mu \frac{d}{d\mu} g_0 = 0 = \mu \frac{d}{d\mu} (Z_g g \mu^\epsilon) = \left(\frac{1}{g} \mu \frac{\partial}{\partial \mu} g + \frac{1}{Z_g} \mu \frac{\partial}{\partial \mu} Z_g + \epsilon \right) Z_g g \mu^\epsilon, \quad (1.52)$$

so that

$$\mu \frac{\partial}{\partial \mu} g = -g\epsilon - \frac{g}{Z_g} \mu \frac{\partial}{\partial \mu} Z_g; \quad (1.53)$$

if now one defines the quantities

$$\beta(g(\mu), \epsilon) = \frac{\partial}{\partial \ln \mu} g, \quad \beta(g(\mu)) = -g \frac{d \ln Z_g}{d \ln \mu}, \quad (1.54)$$

Eq. (1.53) takes the form

$$\beta(g(\mu), \epsilon) = -g\epsilon - \beta(g(\mu)). \quad (1.55)$$

Defining now the quantity

$$\beta(g(\mu)) = g f(g), \quad \text{with} \quad f(g) = \frac{1}{Z_g} \frac{dZ_g}{d \ln \mu}, \quad Z_g = 1 + \sum_{k=1}^{\infty} \frac{1}{\epsilon^k} Z_{g,k}(g), \quad (1.56)$$

we can write

$$Z_g f(g) = \frac{dZ_g}{d \ln \mu} = \frac{dZ_g}{dg} \frac{dg}{d \ln \mu} = \beta(g(\mu), \epsilon) \frac{dZ_g}{dg}, \quad (1.57)$$

so that

$$f(g) \left(1 + \frac{1}{\epsilon} Z_{g,1} + \dots \right) = (-g f(g) - \epsilon g) \left(\frac{1}{\epsilon} \frac{d}{dg} Z_{g,1} + \dots \right). \quad (1.58)$$

Solving this equation order by order one obtains

$$f(g) = -g \frac{dZ_{g,1}}{dg}, \quad (1.59)$$

so that, taking the $\epsilon \rightarrow 0$ limit (or the $D \rightarrow 4$ limit) and using the definition in Eq. (1.49), one obtains the explicit form

$$\beta(g) = g^2 \frac{dZ_{g,1}}{dg} = -\frac{g^3}{16\pi^2} \left(\frac{11}{3} N_C - \frac{2}{3} N_F \right) \equiv -\frac{g^3}{16\pi^2} \beta_0. \quad (1.60)$$

Multiplying now both sides by $\frac{g}{4\pi}$ and remembering the definition in Eq. (1.54), one obtains

$$\frac{d\alpha_s}{d\ln\mu} = -2\beta_0 \frac{\alpha_s^2}{4\pi}, \quad (1.61)$$

whose solution, calculated using as upper bound M_W where $n_f = 5$, is

$$\alpha_s(\mu) = \frac{\alpha_s(M_W)}{1 - \frac{1}{2\pi}\beta_0\alpha_s(M_W)\ln\frac{M_W}{\mu}} = \alpha_s(M_W) \left[1 + \sum_n \left(\frac{1}{2\pi}\beta_0\alpha_s(M_W)\ln\frac{M_W}{\mu} \right)^n \right]. \quad (1.62)$$

Note that this procedure allows to resum all logarithms of the form

$$\left(\alpha_s(M_W)\ln\frac{M_W}{\mu} \right)^n, \quad (1.63)$$

therefore removing the large logarithms problem that may arise computing QCD corrections to weak decays (see below). Furthermore, the calculation of β at Next to Leading Order (NLO) would lead to a resummation of the logarithms

$$\alpha_s(M_W) \left(\alpha_s(M_W)\ln\frac{M_W}{\mu} \right)^n, \quad (1.64)$$

and so on.

Chapter 2

Effective Field Theories

2.1 Effective Lagrangians as a Tool to Search for New Physics Effects

The purpose of the effective Lagrangian method is to allow the study of a theory in the low energy limit, where the heavy particles can be removed from the Lagrangian keeping correctly into account their effects at low energies.

Those Lagrangians can be obtained by writing the most general terms which satisfy the symmetries of the theory at low energy; moreover, given the fact that at that particular energy scale the heavy particles cannot be produced, one has to explicitly take into account only terms containing the lightest ones. This process is called *integrating out* the heavy fields, and its consequences are described by the *decoupling theorem*: if the remaining low energy theory is renormalizable, then all effects of the heavy particles integrated out appear either as a renormalization of the coupling constants in the theory or else as terms with dimension $d > 4$ suppressed by appropriate powers of the heavy particles masses.

As an illustrative example, the basic effective Lagrangian for weak interactions is the *Fermi Lagrangian* [23]

$$\mathcal{L}_F \sim \frac{G_F}{\sqrt{2}} J_\mu^+ J^{+\mu}, \quad (2.1)$$

where the coefficient of the dimension 6 current-current operator is

$$\frac{G_F}{\sqrt{2}} = \frac{g^2}{8M_W^2} \propto \frac{1}{M_W^2}, \quad (2.2)$$

so that the Lagrangian has dimension 4. The W boson is integrated out in this theory, since it is produced at a scale much higher than the ones involved in such

processes. In turn, the theory develops a 4 fermion local interaction, responsible e.g. for the neutron decay. However, the effects of this particle are encoded in the effective coupling G_F , where the factor $1/M_W^2$ is produced when the W propagator is shrunk to a point, assuming $q^2 \ll M_W^2$.

Therefore, the Effective Field Theory (EFT) approach allows to build low-energy Lagrangians, where all the heavy degrees of freedom that can not be produced directly (but that can induce virtual effects) are removed from the theory, building in turn special local operators which include in their couplings the effects of such removed fields. This can be a really powerful tool, simplifying indeed several computations. Moreover, it can also be a useful way to probe NP: integrating away potentially-unknown BSM degrees of freedom, it is possible to use experimental information in order to constrain the bounds of the EFT couplings; subsequently, once the EFT theory will be matched to a UV completion of the theory, it will be possible to reinterpret such bounds as constraints on the parameter of the new theory. Hence, the EFT approach is one of the most employed tool when one wants to inspect the possible shape of NP.

2.2 Operator Product Expansion

Weak decays of hadrons are not easily described since they include both weak interactions, which mediate the decay, and strong interactions, which bind the quarks into hadrons, at different energy scales: the strong interactions are characterized by the typical hadronic energy scale of $O(1 \text{ GeV})$, much lower than the scale of weak interactions, of $O(M_{W,Z})$. Therefore, we need an effective theory for weak interactions capable of describing these decays, which can be obtained through the so-called *Operator Product Expansion* [20, 24, 25].

In order to obtain this effective theory, one has first to integrate out the W boson (as well as the t quark) and write the most general Hamiltonian, which is composed by all the possible local operators which can mediate the decay; this effective Hamiltonian will therefore take the form of a series of local operators $Q_i(\mu)$ whose contributions are weighted by the effective scale-dependent couplings $C_i(\mu)$, called *Wilson Coefficients*:

$$H_{eff} = \frac{4G_F}{\sqrt{2}} V_{q_1 q_2}^* V_{q_3 q_4} \sum_i C_i(\mu) Q_i(\mu); \quad (2.3)$$

the result of this procedure is illustrated in Fig. 2.1.

The next step is to consider the full theory H_{full} and calculate the amplitude at a given order; if now one calculates at the same order the matrix elements $\langle Q_i(\mu) \rangle$ of all the local operators included in H_{eff} , it is possible to perform the

matching

$$A_{full} = A_{eff}, \quad (2.4)$$

and to extract the values of the Wilson Coefficients $C_i(\mu)$. It is worth to note that, if a renormalization is applied to the effective Hamiltonian through the relation

$$\langle Q_i^{(0)} \rangle = Z_q^{-2} Z_{ij} \langle Q_j \rangle, \quad (2.5)$$

where Z_q is the quark field renormalization, the fields of the full Hamiltonian must be renormalized following the same scheme, in order to obtain a correct matching; furthermore, since in the matching infrared logarithms cancel out,

$$\alpha_S \ln \frac{M_W^2}{-p^2} \rightarrow \alpha_S \ln \frac{M_W^2}{-\mu^2}, \quad (2.6)$$

the matching has to be performed at a scale $\mu_W = O(M_W)$, in order to avoid the problem of large logarithms.

Now we can use the techniques of the Renormalization Group and evolve the Wilson Coefficients to the scale of the hadronic decay. In order to accomplish this process one has to note in the first place that the quantity $C_i(\mu)Q_i(\mu)$ is an observable: this means that it must be μ independent, so that

$$\mu \frac{dC_i}{d\mu} Q_i + \mu \frac{dQ_i}{d\mu} C_i = 0 \quad \Rightarrow \quad \mu \frac{dC_i}{d\mu} = -\frac{d \ln Q_i}{d \ln \mu} C_i; \quad (2.7)$$

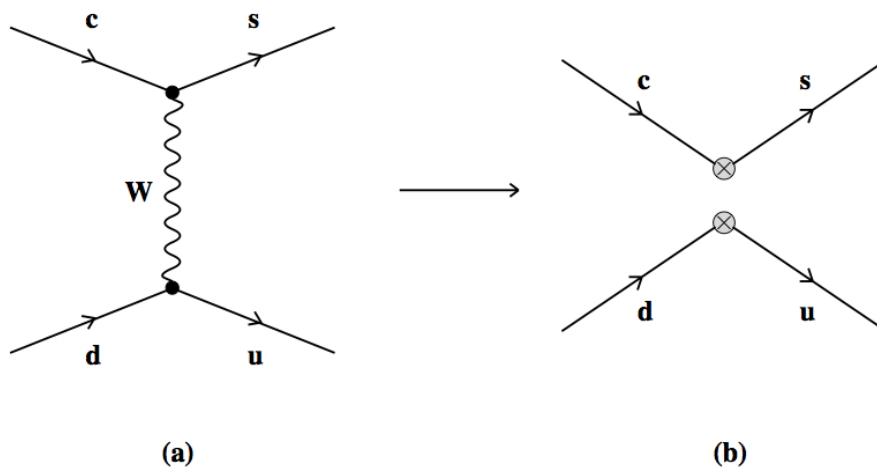


Figure 2.1: The W boson has been integrated out and its propagator has been contracted to a point. Figure taken from Ref. [20].

moreover, remembering that the bare quantity (2.5) has to be μ independent as well, one may diagonalize the matrix Z_{ij} and obtain the relation

$$\mu \frac{dZ_i}{d\mu} Q_i + \mu \frac{dQ_i}{d\mu} Z_i = 0 \quad \Rightarrow \quad \frac{d \ln Q_i}{d \ln \mu} = -\frac{d \ln Z_i}{d \ln \mu} \equiv -\gamma_i(g), \quad (2.8)$$

so that

$$\frac{dC_i(\mu)}{d \ln \mu} = \gamma_i(g) C_i(\mu) \quad \Rightarrow \quad C_i(\mu) = U_i(\mu, \mu_0) C_i(\mu_0), \quad (2.9)$$

where $U_i(\mu, \mu_0)$ is the function that governs the evolution of the quantity $C_i(\mu)$. Note that one has to pay attention to quark thresholds, given the change of the total flavour number at a scale $\mu_b = O(M_b)$.

Finally, one has to calculate the hadronic matrix elements $\langle Q_i(\mu) \rangle$ at the decay energy scale. This task, given the non-perturbative nature of the matrix elements, usually has to be performed on lattice QCD, which consists in discretizing the space-time, and therefore the fields, on a lattice. This introduces a momentum cut-off at the order $\frac{1}{a}$, where a is the lattice spacing, which regularizes QCD and allows numerical computation of non-perturbative objects. The continuum values can be obtained performing the $a \rightarrow 0$ extrapolation, which can be done once repeated calculations at different lattice spacings have been performed.

The main feature of the Operator Product Expansion is therefore to factorize the contributions to the amplitude into a short-distance, high energy term ($C_i(\mu)$) and a long-distance, low energy term ($\langle Q_i(\mu) \rangle$). Moreover, the product $C_i(\mu) \langle Q_i(\mu) \rangle$ is μ independent, and the large logarithms are automatically resummed through the implementation of the Renormalization Group method.

2.3 Bottom-Up vs Top-Down

As we have described at the beginning of this chapter, an EFT is built with the purpose to write down a low-energy Lagrangian, where the heavy degrees of freedom are removed and their effects are encoded in the couplings of local operators. This allows to build a theory where computations are simplified, or even feasible in the first place, and to study the indirect effects of some field at a scale way below the one where it can be produced.

These features make the EFT approach really appealing in present days: the LHC has yet to directly observe new particles, different from the SM ones. Moreover, it can also be possible that the NP scale is well above a few tens of TeV, hence beyond the grasp of a direct observation at the LHC. However, this does not mean that these new heavy degrees of freedom can not be produced at loop-level, hence contributing to SM-like processes in such a way that precise measurements

could detect their effects, effectively yielding an indirect NP observation. Therefore, following the EFT approach and studying the effects of such fields by means of effective couplings to local operators might be a useful probe on the hunt for NP.

With this situation in mind, it is interesting to conclude this chapter with a description of the two possible approaches one can make use of, when building an EFT. The first one is the Top-Down approach: in this first scheme, the underlying, high-energy theory is known. However, one might be interested in studying its effects at a low scale, lower than the production scale of one (or more) of the degrees of freedom present in the theory. Moreover, it is also possible that the underlying theory is cumbersome, and trying to directly apply it makes some computation heavily non-trivial. As we have already seen, this is the case of e.g. weak decays: the underlying theory - the SM - is well known, however directly applying it in order to compute hadron weak decays is utterly complicated. Therefore, it is convenient to integrate out the W boson and the top quark, and build an effective theory consisting of four-quark operators. Their effective couplings are functions of the W and top masses, which can be exactly computed performing the matching procedure described in Sec. 2.2. The Weak Effective Theory (WET) build in such a manner allows to perform computations in a feasible way, without losing any SM information but working in a viable environment which allows to resumming large logarithms.

A diametrically opposed approach is the Bottom-Up one: in this second scheme, one makes no assumptions on the underlying theory, and works in a model-independent framework. Once the field content of the low-energy theory is decided, along with its gauge symmetries, one simply has to build accordingly all the Lorentz invariant operators. The EFT couplings will be free parameters. Therefore, this approach could be really interesting for a generic NP search: given the present experimental status and the lack of informations regarding an UV completion of the SM, one can decide to make no assumptions at all on this completion. Therefore, it is possible to make predictions for a desired decay channel, compare them with experimental data and subsequently extract the values of the EFT couplings. If one (or more) of such couplings is to be found different from zero, this will be a signature of a NP effect: only then, it will be possible to look for those UV model capable of producing relevant operator, paying attention that such models do not produce also operators that would spoil other, “well-behaving” measurements.

Chapter 3

The Standard Model Effective Field Theory

As I have stated in the Introduction, the SM of particle physics has been extremely reliable in the last decades, producing an astonishing number of accurate estimates for a very large number of observables, confirmed by experimental data. However, several elements (e.g. Dark Matter, neutrino mass/oscillation, baryon asymmetry, gravity ...) point towards the fact that the SM is not the final theory of particle physics, but it has to be included in some more general framework.

Therefore, due to the lack of an UV completion of the SM, a useful way to study possible BSM effects consists of employing an EFT framework, following the Bottom-Up approach. In particular, given the lack of NP signals guiding us in the construction of such EFT, it is convenient to build this theory according to the following prescriptions:

- its gauge group should contain the SM one, $SU(3)_C \times SU(2)_L \times U(1)_Y$;
- it should be built using solely SM fields;
- it should contain all the possible Lorentz invariant terms.

The EFT built according to the above guidelines is called Standard Model Effective Field Theory (SMEFT), and can be a remarkably useful tool to describe the low energy limit of BSM physics. The schematic Lagrangian is

$$\mathcal{L}_{SMEFT} = \mathcal{L}_{SM}^{(d \leq 4)} + \sum_{d=5}^{\infty} \sum_i \left(\frac{1}{\Lambda} \right)^{(d-4)} c_i^{(d)} \mathcal{O}_i^{(d)}, \quad (3.1)$$

where d represent the operator dimension. For each dimension, following the aforementioned guidelines, it is possible to define a certain set of operators; however,

these sets might be redundant due to possible relations between different operators. Hence, by means of EoM, Fierz identities and integration by parts, it is possible to define a minimal basis for the operators for each dimension. The choice for the basis is of course irrelevant once physical observables are computed; however, given the process of interest, certain bases can be more suitable than others.

In the following sections we discuss the first terms appearing in Eq. (3.1), analyzing the number and the structure of such operators.

3.1 dim-5 operators

At dimension 5, only one operator structure survives, together with its hermitian conjugate [26]:

$$\mathcal{O}_{\nu\nu} = \epsilon_{jk}\epsilon_{mn}\varphi^j\varphi^m(l_p^k)^T C l_r^n + h.c. \equiv (\tilde{\varphi}^\dagger l_p)^T C (\tilde{\varphi}^\dagger l_r) + h.c. , \quad (3.2)$$

where C is the charge conjugation matrix, φ is the Higgs field, l is a left lepton field and p, r are flavour indices. Since both $\mathcal{O}_{\nu\nu}$ and its hermitian conjugate are symmetric in flavour indices, the total number of operators is equal to $2 \cdot \frac{n_f(n_f + 1)}{2}$, where n_f is the number of flavour present in the theory. Hence, in a single-flavour theory, only 2 independent dim-5 operators exist, while in a theory with $n_f = 3$ there are 12 independent operators.

The operator $\mathcal{O}_{\nu\nu}$, often referred to as “Weinberg operator”, violates the $B - L$ accidental symmetry (as all operators with an odd dimension [27, 28]), and is therefore expected to be heavily suppressed. It can be introduced in theories involving a right handed neutrino: if this new particle is heavy enough, it can be integrated out giving rise to the Weinberg operator at low energy. After EWSB, this operator generates a Majorana mass term for left-handed neutrinos, which is indirectly proportional to the NP scale Λ . This mechanism, where a very light left-handed neutrino is generated by means of a very heavy right-handed one, goes by the name of seesaw mechanism [29–32].

3.2 dim-6 operators

Dimension-6 operators are suppressed by two powers of the NP scale; however, most of the operators of this class do not violate any SM accidental symmetry (contrary to all dim-5 ones): hence, the overall suppression of such operators is expected to be lower. Moreover, there are plenty of NP models whose primary effects arise at the level of dim-6 operators, making this particular EFT a popular choice for BSM analysis at LHC [33].

The first dim-6 operators historically taken into account were four-fermion operators, and their study can go back to the pioneering work on weak interactions by Enrico Fermi [23]. The four-fermion operators sub-set was heavily used thereafter, but it was only in the Eighties that a first attempt to catalogue the full set of operators was carried over by Buchmuller and Wyler [34]. However this basis, consisting of 80 operators in a single-flavour theory, was missing one last operator and, more importantly, was redundant. Finally, in 2010, a first complete non-redundant basis was obtained by Grzadkowski, Iskrzynski, Misiak, and Rosiek [3]¹, obtained following the guidelines of reducing the number of derivatives as much as possible. As we stated above, this is just a possible choice for the basis: for instance, for the analysis of strongly-interacting light Higgs an ad hoc sub-basis (often referred to as the SILH basis) has been identified by Giudice, Grojean, Pomarol and Rattazzi [35], focusing on Higgs operators. Analogously, the HISZ sub-basis has been introduced by Hagiwara, Ishihara, Szalapski and Zeppenfeld [36] to study interactions between the Higgs and the vector bosons.

In the remainder of this thesis we will work with the Warsaw basis (and in general only with operators not violating the $B - L$ accidental symmetry), since it was the first complete dimension-6 basis to be computed, and moreover (as we will see) it is the only fully renormalized basis to date.

3.2.1 The Warsaw basis

The number of operators in this basis is quite big: in a single-flavour theory there are 59 independent operators², with this number growing up to 2499 in a theory with $n_f = 3$. This plethora of operators can be sub-divided in 8 classes, in terms of the field content and of the number of covariant derivatives contained in each of them. Hereafter, we will denote with φ a Higgs field, with D a covariant derivative, with X a gauge field strength tensor, with ψ a generic fermion field, with $l(e)$ a left (right) lepton field, with q a left quark field and with $u(d)$ an up-(down-)type right quark field. In the remainder of this section, we will briefly review the content of each class, showing why the basis is indeed non-redundant; in order to do so, we will extensively make use of the following tensor relations:

$$\tau_{jk}^I \tau_{mn}^I = 2\delta_{jn}\delta_{mk} - \delta_{jk}\delta_{mn}, \quad (3.3)$$

$$T_{\alpha\beta}^A T_{\kappa\lambda}^A = \frac{1}{2}\delta_{\alpha\lambda}\delta_{\kappa\beta} - \frac{1}{6}\delta_{\alpha\beta}\delta_{\kappa\lambda}, \quad (3.4)$$

¹Due to the difficulty in pronouncing the names of these authors, this basis is usually referred to as the “Warsaw basis”, in honor to the city where this work was carried out.

²The actual number of operators is 76, if one considers the Hermitian conjugate of non-Hermitian operators as a separate operator.

where τ^I is a rescaled Pauli matrix $\tau^I \equiv \sigma^I/2$ and T^A is a Gell-Mann matrix, and of Fierz identities, such as

$$(\bar{\psi}\gamma_\mu\psi)(\bar{\chi}\gamma_\mu\chi) = (\bar{\psi}\gamma_\mu\chi)(\bar{\chi}\gamma_\mu\psi). \quad (3.5)$$

- **1 : \mathbf{X}^3**

This first class contains all the operators involving 3 gauge field strength tensors (denoted by A, B and C in this section). The only non-vanishing independent Lorentz contraction reads $A_\mu{}^\nu B_\nu{}^\rho C_\rho{}^\mu$, and since each tensor is antisymmetric, the other two have from being different in order to prevent them to be symmetric resulting in a vanishing operator; moreover, this couple cannot be related by duality, feature that would make them symmetric and forbid the operator again. Hence, the only way to build a non-vanishing singlet is by means of the structure constants f^{ABC} or ϵ^{IJK} :

$$Q_G = f^{ABC} G_\mu^{A\nu} G_\nu^{B\rho} G_\rho^{C\mu}, \quad (3.6)$$

$$Q_{\tilde{G}} = f^{ABC} \tilde{G}_\mu^{A\nu} G_\nu^{B\rho} G_\rho^{C\mu}, \quad (3.7)$$

$$Q_W = \epsilon^{IJK} W_\mu^{I\nu} W_\nu^{J\rho} W_\rho^{K\mu}, \quad (3.8)$$

$$Q_{\tilde{W}} = \epsilon^{IJK} \tilde{W}_\mu^{I\nu} W_\nu^{J\rho} W_\rho^{K\mu}. \quad (3.9)$$

These operators have no flavour content, hence they are 4 independent of n_f , 2 CP -even and 2 CP -odd ones.

- **2 : φ^6**

Due to hypercharge, three of the Higgs fields of each operator of this class needs to be complex conjugated. We have then three $(\varphi^*\varphi)$ couples, each being either a singlet or a triplet. The three-triplet case vanishes since the three identical couples have to be saturated with an antisymmetric tensor, while the two-triplet one can be rewritten in terms of an overall singlet by means of Eq. (3.3); hence, the only surviving operator in this class is:

$$Q_H = (\varphi^\dagger\varphi)^3. \quad (3.10)$$

This operator has no flavour content, hence there is only 1 CP -even operator.

- **3 : $\varphi^4\mathbf{D}^2$**

Again, due to hypercharge, two of the Higgs fields of each operator of this class need to be complex conjugated. We can therefore build operators containing two singlets or two triplets; however, in the latter case, we can employ

Eq. (3.3) in order to rewrite these operators as products of singlets. After reducing the number of operators by means of EOM and integration by parts, we obtain the following final sub-set of independent operators:

$$Q_{H\Box} = (\varphi^\dagger\varphi)\Box(\varphi^\dagger\varphi), \quad (3.11)$$

$$Q_{HD} = (\varphi^\dagger D^\mu\varphi)^*(\varphi^\dagger D^\mu\varphi). \quad (3.12)$$

These operators have no flavour content, hence they are 2 CP -even operators.

- **4 : $\mathbf{X}^2\varphi^2$**

Once again, due to hypercharge, one of the Higgs fields of each operator of this class needs to be complex conjugated. We will therefore build all the possible operators containing either two singlets or two triplets, with an n -let containing Higgs fields and the other containing field strength tensors. Operators containing a single $W_{\mu\nu}^I$ tensor need to be contracted with a rescaled Pauli matrix τ^I , in order to obtain an operator which is an isospin singlet. The list of operators is the following:

$$Q_{HG} = (\varphi^\dagger\varphi)G_{\mu\nu}^A G^{A\mu\nu}, \quad (3.13)$$

$$Q_{H\tilde{G}} = (\varphi^\dagger\varphi)\tilde{G}_{\mu\nu}^A G^{A\mu\nu}, \quad (3.14)$$

$$Q_{HW} = (\varphi^\dagger\varphi)W_{\mu\nu}^I W^{I\mu\nu}, \quad (3.15)$$

$$Q_{H\tilde{W}} = (\varphi^\dagger\varphi)\tilde{W}_{\mu\nu}^I W^{I\mu\nu}, \quad (3.16)$$

$$Q_{HB} = (\varphi^\dagger\varphi)B_{\mu\nu} B^{\mu\nu}, \quad (3.17)$$

$$Q_{H\tilde{B}} = (\varphi^\dagger\varphi)\tilde{B}_{\mu\nu} B^{\mu\nu}, \quad (3.18)$$

$$Q_{HWB} = (\varphi^\dagger\tau^I\varphi)W_{\mu\nu}^I B^{\mu\nu}, \quad (3.19)$$

$$Q_{H\tilde{W}B} = (\varphi^\dagger\tau^I\varphi)\tilde{W}_{\mu\nu}^I B^{\mu\nu}. \quad (3.20)$$

These operators have no flavour content, hence they are 8, 4 CP -even and 4 CP -odd ones.

- **5 : $\psi^2\varphi^3$**

This class of operators contains two fermionic fields, forming a scalar current, coupled with a first Higgs field. Such currents, in order to combine with the two remaining Higgs fields, have to be isospin doublets and colour singlets: hence, the scalar current has the same shape of a Yukawa interaction, with the remaining Higgs forming the only non-vanishing isospin singlet available, $(\varphi^\dagger\varphi)$. Therefore we remain with 3 operators, each one along with its hermitian conjugate:

$$Q_{eH} = (\varphi^\dagger\varphi)(\bar{l}_p e_r\varphi), \quad (3.21)$$

$$Q_{uH} = (\varphi^\dagger \varphi)(\bar{q}_p u_r \tilde{\varphi}), \quad (3.22)$$

$$Q_{dH} = (\varphi^\dagger \varphi)(\bar{q}_p d_r \varphi). \quad (3.23)$$

Each family of operators, being non-Hermitian, is described by a $n_f \times n_f$ complex matrix, with n_f^2 CP-even operators coming from the real matrix elements, and n_f^2 CP-odd operators coming from the imaginary ones. Therefore, in a single-fermion theory we have 6 independent operators, 3 CP-even and 3 CP-odd, while in a theory with $n_f = 3$ there are 54 independent operators, 27 CP-even and 27 CP-odd ones.

- **6** : $\psi^2 \mathbf{X} \varphi$

This class of operators contains again two fermionic fields, combined this time in a tensorial antisymmetric form due to the presence of the field strength tensor. The Higgs field displays a Yukawa-like behavior due to hypercharge (i.e., contracted with a totally antisymmetric matrix when coupled to right-handed up-type quarks), while the $W_{\mu\nu}^I$ and $G_{\mu\nu}^A$ tensors need to be contracted either with a rescaled Pauli matrix τ^I or with a Gell-Mann matrix T^A , in order to obtain an operator which is an isospin and colour singlet, respectively. The final list contains 8 operators, each one along with its hermitian conjugate:

$$Q_{eW} = (\bar{l}_p \sigma^{\mu\nu} e_r) \tau^I \varphi W_{\mu\nu}^I, \quad (3.24)$$

$$Q_{eB} = (\bar{l}_p \sigma^{\mu\nu} e_r) \varphi B_{\mu\nu}, \quad (3.25)$$

$$Q_{uG} = (\bar{q}_p \sigma^{\mu\nu} T^A u_r) \tilde{\varphi} G_{\mu\nu}^A, \quad (3.26)$$

$$Q_{uW} = (\bar{q}_p \sigma^{\mu\nu} u_r) \tau^I \tilde{\varphi} W_{\mu\nu}^I, \quad (3.27)$$

$$Q_{uB} = (\bar{q}_p \sigma^{\mu\nu} u_r) \tilde{\varphi} B_{\mu\nu}, \quad (3.28)$$

$$Q_{dG} = (\bar{q}_p \sigma^{\mu\nu} T^A d_r) \varphi G_{\mu\nu}^A, \quad (3.29)$$

$$Q_{dW} = (\bar{q}_p \sigma^{\mu\nu} d_r) \tau^I \varphi W_{\mu\nu}^I, \quad (3.30)$$

$$Q_{dB} = (\bar{q}_p \sigma^{\mu\nu} d_r) \varphi B_{\mu\nu}. \quad (3.31)$$

Analogously to the previous class, each family of non-Hermitian operators is described by a $n_f \times n_f$ complex matrix, with n_f^2 CP-even operators coming from the real matrix elements, and n_f^2 CP-odd operators coming from the imaginary ones. Hence, in a single-fermion theory we have 16 independent operators, 8 CP-even and 8 CP-odd, while in a theory with $n_f = 3$ there are 144 independent operators, 72 CP-even and 72 CP-odd ones.

- **7** : $\psi^2 \varphi^2 \mathbf{D}$

This is the last class of operators containing two fermionic fields, contracted to form a vector current. The derivative will act on scalars only, since EOM

will reduce the operators with a derivative applied to a fermionic field to the ones of class 5. Therefore, the complete list of Hermitian operators is the following:

$$Q_{Hl}^{(1)} = (\varphi^\dagger i \overleftrightarrow{D}_\mu \varphi) (\bar{l}_p \gamma^\mu l_r), \quad (3.32)$$

$$Q_{Hl}^{(3)} = (\varphi^\dagger i \overleftrightarrow{D}_\mu^I \varphi) (\bar{l}_p \tau^I \gamma^\mu l_r), \quad (3.33)$$

$$Q_{He} = (\varphi^\dagger i \overleftrightarrow{D}_\mu \varphi) (\bar{e}_p \gamma^\mu e_r), \quad (3.34)$$

$$Q_{Hq}^{(1)} = (\varphi^\dagger i \overleftrightarrow{D}_\mu \varphi) (\bar{q}_p \gamma^\mu q_r), \quad (3.35)$$

$$Q_{Hq}^{(3)} = (\varphi^\dagger i \overleftrightarrow{D}_\mu^I \varphi) (\bar{q}_p \tau^I \gamma^\mu q_r), \quad (3.36)$$

$$Q_{Hu} = (\varphi^\dagger i \overleftrightarrow{D}_\mu \varphi) (\bar{u}_p \gamma^\mu u_r), \quad (3.37)$$

$$Q_{Hd} = (\varphi^\dagger i \overleftrightarrow{D}_\mu \varphi) (\bar{d}_p \gamma^\mu d_r). \quad (3.38)$$

Moreover, there also exists another non-Hermitian operator, together with its Hermitian conjugate:

$$Q_{Hud} = i(\tilde{\varphi}^\dagger D_\mu \varphi) (\bar{u}_p \gamma^\mu d_r). \quad (3.39)$$

The first seven families of operators, due to their Hermiticity, can be described each by means of a matrix of the form $H = S + iA$, where S is a real symmetric matrix, containing $n_e = n_f(n_f + 1)/2$ CP -even operators, while A is a real antisymmetric one, containing $n_o = n_f(n_f - 1)/2$ CP -odd operators. Considering also Q_{Hud} and its Hermitian conjugate, described by a $n_f \times n_f$ complex matrix, the total number of CP -even operators is $n_f(9n_f + 7)/2$ while the total number of CP -odd ones is $n_f(9n_f - 7)/2$. Therefore, in a single-fermion theory we have 9 independent operators, 8 CP -even and 1 CP -odd, while in a theory with $n_f = 3$ there are 81 independent operators, 51 CP -even and 30 CP -odd ones.

- **8** : ψ^4

The last class of dimension 6 operators is the most numerous: it contains four-fermion operators, each composed by two bilinears; to better describe them, it is useful to further group them, according to their chiral content.

- $(\bar{L}L)(\bar{R}R)$

The first sub-class is composed by the product of a left-handed with a right-handed current:

$$Q_{le} = (\bar{l}_p \gamma^\mu l_r) (\bar{e}_s \gamma^\mu e_t), \quad (3.40)$$

$$Q_{lu} = (\bar{l}_p \gamma^\mu l_r) (\bar{u}_s \gamma^\mu u_t), \quad (3.41)$$

$$Q_{ld} = (\bar{l}_p \gamma^\mu l_r)(\bar{d}_s \gamma^\mu d_t), \quad (3.42)$$

$$Q_{qe} = (\bar{q}_p \gamma^\mu q_r)(\bar{e}_s \gamma^\mu e_t), \quad (3.43)$$

$$Q_{qu}^{(1)} = (\bar{q}_p \gamma^\mu q_r)(\bar{u}_s \gamma^\mu u_t), \quad (3.44)$$

$$Q_{qu}^{(8)} = (\bar{q}_p \gamma^\mu T^A q_r)(\bar{u}_s \gamma^\mu T^A u_t), \quad (3.45)$$

$$Q_{qd}^{(1)} = (\bar{q}_p \gamma^\mu q_r)(\bar{d}_s \gamma^\mu d_t), \quad (3.46)$$

$$Q_{qd}^{(8)} = (\bar{q}_p \gamma^\mu T^A q_r)(\bar{d}_s \gamma^\mu T^A d_t). \quad (3.47)$$

All these operators are products of L and R Hermitian currents, each one containing n_e CP -even operators and n_o CP -odd operators, as explained below Eq. (3.39). Multiplying the two currents, there is a total of $8 \cdot (n_e^2 + n_o^2) = 4n_f^2(n_f^2 + 1)$ CP -even operators and of $8 \cdot 2n_e n_o = 4n_f^2(n_f^2 - 1)$ CP -odd operators. Hence, in a single-fermion theory we have 8 independent CP -even operators, while in a theory with $n_f = 3$ there are 648 independent operators, 360 CP -even and 288 CP -odd ones.

- $(\bar{L}L)(\bar{L}L)$

The second sub-class is composed by two vector currents containing only left-handed fermions:

$$Q_{ll} = (\bar{l}_p \gamma^\mu l_r)(\bar{l}_s \gamma^\mu l_t), \quad (3.48)$$

$$Q_{qq}^{(1)} = (\bar{q}_p \gamma^\mu q_r)(\bar{q}_s \gamma^\mu q_t), \quad (3.49)$$

$$Q_{qq}^{(3)} = (\bar{q}_p \gamma^\mu \tau^I q_r)(\bar{q}_s \gamma^\mu \tau^I q_t), \quad (3.50)$$

$$Q_{lq}^{(1)} = (\bar{l}_p \gamma^\mu l_r)(\bar{q}_s \gamma^\mu q_t), \quad (3.51)$$

$$Q_{lq}^{(3)} = (\bar{l}_p \gamma^\mu \tau^I l_r)(\bar{q}_s \gamma^\mu \tau^I q_t). \quad (3.52)$$

It is interesting to notice that the operator $Q_{ll}^{(3)}$ is redundant, since it can be written in terms of Q_{ll} by applying Eq. (3.3) and then Eq. (3.5)³. Analogously, a $Q_{qq}^{(8)}$ operator composed by two colour octets is redundant due to Eqs. (3.3)-(3.5).

The $Q_{lq}^{(1,3)}$ operators are products of two different Hermitian currents so, analogously to the $(\bar{L}L)(\bar{R}R)$ family, there is a total of $2 \cdot (n_e^2 + n_o^2) = n_f^2(n_f^2 + 1)$ CP -even operators and of $2 \cdot 2n_e n_o = n_f^2(n_f^2 - 1)$ CP -odd operators. However, one can not apply the same procedure to the remaining operators, where the two currents are equal and we

³It is worth to mention that the same procedure does not work for $Q_{qq}^{(3)}$ as well, since Eq. (3.5) Fierzes also the colour indices, in such a way that it is not possible to rewrite this operator in terms of $Q_{ll}^{(1)}$ only.

therefore have four fields whose flavour indices transform under the same $SU(n_F)$ flavour group. These 3 operators, following group theory prescriptions that can be found e.g. in Refs. [37, 38], transform each as a $\mathbf{1} + adj + adj + \bar{a}a + \bar{s}s$, where $\mathbf{1}$ is a singlet containing 1 CP -even operator, adj is an adjoint representation containing $(n_f - 1)(n_f + 2)/2$ CP -even operators and $n_f(n_f - 1)/2$ CP -odd operators, $\bar{a}a$ is the $T_{[k,l]}^{[i,j]}$ representation, antisymmetric in both higher and lower indices and containing $n_f(n_f - 3)(n_f^2 + n_f + 2)/8$ CP -even operators and $n_f(n_f - 3)(n_f - 1)(n_f + 2)/8$ CP -odd operators, and $\bar{s}s$ is the $T_{\{k,l\}}^{\{i,j\}}$ representation, symmetric in both higher and lower indices and containing $n_f(n_f - 1)(n_f + 1)(n_f + 2)/8$ CP -even operators and $n_f(n_f - 1)(n_f^2 + 3n_f - 2)/8$ CP -odd operators. Hence, in a single-fermion theory we have 5 independent CP -even operators, while in a theory with $n_f = 3$ there are 297 independent operators, 171 CP -even and 126 CP -odd ones.

- $(\bar{R}R)(\bar{R}R)$

The following sub-class is composed by two currents containing only right-handed fermions:

$$Q_{ee} = (\bar{e}_p \gamma^\mu e_r)(\bar{e}_s \gamma^\mu e_t), \quad (3.53)$$

$$Q_{uu} = (\bar{u}_p \gamma^\mu u_r)(\bar{u}_s \gamma^\mu u_t), \quad (3.54)$$

$$Q_{dd} = (\bar{d}_p \gamma^\mu d_r)(\bar{d}_s \gamma^\mu d_t), \quad (3.55)$$

$$Q_{eu} = (\bar{e}_p \gamma^\mu e_r)(\bar{u}_s \gamma^\mu u_t), \quad (3.56)$$

$$Q_{ed} = (\bar{e}_p \gamma^\mu e_r)(\bar{d}_s \gamma^\mu d_t), \quad (3.57)$$

$$Q_{ud}^{(1)} = (\bar{u}_p \gamma^\mu u_r)(\bar{d}_s \gamma^\mu d_t), \quad (3.58)$$

$$Q_{ud}^{(8)} = (\bar{u}_p \gamma^\mu T^A u_r)(\bar{d}_s \gamma^\mu T^A d_t). \quad (3.59)$$

For this sub-class as well, due to eqs. (3.3)-(3.5), $Q_{ud}^{(8)}$ is the only non-redundant operator containing colour octets, due to the different field content of the two currents.

Analogously to the previous class, the Q_{eu} , Q_{ed} and $Q_{ud}^{(1,8)}$ operators each contain a total of $(n_e^2 + n_o^2)$ CP -even operators and of $2n_e n_o$ CP -odd operators, while the Q_{uu} and Q_{dd} operators both transform as a $\mathbf{1} + adj + adj + \bar{a}a + \bar{s}s$. The operator Q_{ee} is a special case: the Fierz identity of Eq. (3.5) transform the operator into itself, implying that it is symmetric in both e and \bar{e} indices, and therefore that it transforms as a $\mathbf{1} + adj + \bar{s}s$. Therefore, in a single-fermion theory we have 7 independent CP -even operators, while in a theory with $n_f = 3$ there are 450 independent operators, 255 CP -even and 195 CP -odd.

- $(\bar{L}R)(\bar{L}R)$

This sub-class is composed by either two scalar currents or two tensor ones, with the barred fermions always being the left ones. The operator list is the following, each one along with its hermitian conjugate:

$$Q_{quqd}^{(1)} = (\bar{q}_p^j u_r) \epsilon_{jk} (\bar{q}_s^k d_t), \quad (3.60)$$

$$Q_{quqd}^{(8)} = (\bar{q}_p^j T^A u_r) \epsilon_{jk} (\bar{q}_s^k T^A d_t), \quad (3.61)$$

$$Q_{lequ}^{(1)} = (\bar{l}_p^j e_r) \epsilon_{jk} (\bar{q}_s^k u_t), \quad (3.62)$$

$$Q_{lequ}^{(3)} = (\bar{l}_p^j \sigma_{\mu\nu} e_r) \epsilon_{jk} (\bar{q}_s^k \sigma^{\mu\nu} u_t). \quad (3.63)$$

Due to non-Hermiticity, each family of operators is described by two $n_f \times n_f$ complex matrices, with a total of n_f^4 CP-even operators and n_f^4 CP-odd ones. Hence, in a single-fermion theory we have 8 independent operators, 4 CP-even and 4 CP-odd, while in a theory with $n_f = 3$ there are 648 independent operators, 324 CP-even and 324 CP-odd ones.

- $(\bar{L}R)(\bar{R}L)$

The final sub-class is composed by just one scalar operator, along with its hermitian conjugate:

$$Q_{ledq} = (\bar{l}_p e_r) (\bar{d}_s q_t). \quad (3.64)$$

This last operator is again non-Hermitian, hence described by two $n_f \times n_f$ complex matrices, with a total of n_f^4 CP-even operators and n_f^4 CP-odd ones. Therefore, in a single-fermion theory we have 2 independent operators, 1 CP-even and 1 CP-odd, while in a theory with $n_f = 3$ there are 162 independent operators, 81 CP-even and 81 CP-odd ones.

3.2.2 The Anomalous Dimension

The computation of the AD for dimension 6 operators, needed to perform the RGE of the respective Wilson coefficients, has been slowly performed for several decades [36, 39–52]. However, most of the early studies were focused only on small sub-sets of the operators, often without even taking into account the mixing between the different classes of operators described in the previous section.

Presently, the Warsaw basis is the only basis for which a complete computation of the one-loop AD has been fully performed [4–7]⁴. These results agreed

⁴The computation was performed in a rescaled basis for convenience, but it is straightforward to obtain the results for the original basis by scaling back the rescaled operators.

		$g^3 X^3$	H^6	$H^4 D^2$	$g^2 X^2 H^2$	$y\psi^2 H^3$	$gy\psi^2 XH$	$\psi^2 H^2 D$	ψ^4
		1	2	3	4	5	6	7	8
$g^3 X^3$	1	g^2	0	0	1	0	0	0	0
H^6	2	0	λ, g^2	$g^4, g^2\lambda, \lambda^2$	$g^6, g^4\lambda$	y^4	0	y^4	0
$H^4 D^2$	3	0	0	g^2, λ	g^4	y^2	0	y^2	0
$g^2 X^2 H^2$	4	g^4	0	1	g^2, λ	0	y^2	1	0
$y\psi^2 H^3$	5	0	0	g^2, y^2	g^4	g^2, λ, y^2	$g^2\lambda, g^4, g^2y^2$	g^2, λ, y^2	y^2
$gy\psi^2 XH$	6	g^4	0	0	g^2	1	g^2, y^2	1	1
$\psi^2 H^2 D$	7	0	0	y^2	g^4	y^2	g^2y^2	g^2, λ, y^2	y^2
ψ^4	8	0	0	0	0	0	g^2y^2	y^2	g^2, y^2

		$g^3 X^3$	H^6	$H^4 D^2$	$g^2 X^2 H^2$	$y\psi^2 H^3$	$gy\psi^2 XH$	$\psi^2 H^2 D$	ψ^4
		1	2	3	4	5	6	7	8
$g^3 X^3$	1	0	0	0	1	0	0	0	0
H^6	2	$g^6\lambda$	0	$g^2\lambda, \lambda^2$	λg^4	λy^2	0	$\lambda g^2, \lambda y^2$	0
$H^4 D^2$	3	g^6	0	g^2	g^4	0	g^2y^2	g^2	0
$g^2 X^2 H^2$	4	g^4	0	0	0	0	0	0	0
$y\psi^2 H^3$	5	g^6	0	g^2, λ, y^2	g^4	y^2	$g^2\lambda, g^2y^2$	g^2, λ, y^2	λ, y^2
$gy\psi^2 XH$	6	g^4	0	0	0	0	g^2, y^2	1	1
$\psi^2 H^2 D$	7	g^6	0	g^2	g^4	0	g^2y^2	g^2, y^2	g^2, y^2
ψ^4	8	g^6	0	0	0	0	g^2y^2	g^2, y^2	g^2, y^2

Table 3.1: The form of the one-loop AD matrix for the coefficients of the rescaled dimension six operators [5–7]. The scaling factors are shown next to each operator class. The upper table gives entries generated by direct contribution from a 1PI one-loop diagram. The lower table gives entries which are generated after EOM are employed to remove redundant operators, hence not directly generated by means of 1PI diagrams. There are also y^2 contributions to be added to all diagonal entries except the first one, stemming from Higgs wave-function renormalization.

with the small subsets computed before, supplementing such results with several new elements. A scheme of the non-null entries of the AD matrix is shown in Tab. 3.1, where the contributions are divided in two classes: the first one comes from the direct mixing between dim-6 operators, with AD entries stemming from the computation of 1 particle-irreducible (1PI) diagrams; however, a second set of contributions has to be taken in consideration when redundant operators are removed from the basis by means of the EOM: even though these operators are not present in the final basis, one must keep track of their effects in order to fully compute the one-loop AD. The effect of this kind of contribution is often recovered by taking a look at 1 particle-reducible (1PR) diagrams, in a similar fashion as one must do when adding penguin operators to the four-quark operators of the Lagrangian needed to study weak decays [53, 54]: penguin operators do need to be taken into account to properly renormalize the theory, but using the EOM is possible to re-write them in terms of four-quark operators.

As a first step in my PhD program, I recomputed several of the entries of the AD, namely all those stemming from 1PI diagrams. This computation was performed since a systematic cross-check of the computation from Refs. [4–7] was lacking in the literature. All the results obtained were found in perfect agreement with their results. In the rest of this section, I will illustrate the procedure I followed to perform this cross-check.

The computation of the AD of a set of operators is closely connected to the ultraviolet (UV) divergences renormalization of such operators, due to the following relation between the AD matrix $\hat{\gamma}$ and the renormalization matrix \hat{Z} :

$$\hat{\gamma} = \hat{Z}^{-1} \frac{d\hat{Z}}{d \ln \mu}. \quad (3.65)$$

Bearing this in mind, the calculation of the AD is carried out after performing the following preliminary operations:

- the Feynman rules for the dimension 6 Lagrangian \mathcal{L}_6 are obtained using the FeynRules package [55], after creating a suitable model file;
- all relevant one-loop diagrams are written employing the FeynArts package [56].

Once these operations are carried out, the actual computation can be performed. The employed algorithm is the Passarino-Veltman reduction [57]: this algorithm allows to rewrite all tensor integrals in terms of well-known scalar ones. A recent review can be found in Appendix A of Ref. [58], while here I will cover only the main features of the method.

The computation of a generic one loop diagram requires calculating integrals of the following form:

$$I_N \sim \int \frac{d^4 l}{(2\pi)^4} \frac{\mathcal{N}(l)}{(l^2 - m_1^2)((l + q_1)^2 - m_2^2) \dots ((l + q_{N-1})^2 - m_N^2)}, \quad (3.66)$$

where N is the number of external particles (with momentum p_i) and $q_i = \sum_{j=1}^i p_j$. The numerator $\mathcal{N}(l)$ is a polynomial function of the loop momentum l , and a scalar integral is the special case where $\mathcal{N}(l) = 1$. It is important to stress the fact that power counting implies that a UV divergence appears in I_N only if $\mathcal{N}(l)$ contains a tensor of rank $r \geq 2N - 4$; hence, only one-point and two-point scalar integrals are UV divergent. In the presence of UV divergences, the integrals require regularization; a conventional scheme is dimensional regularization [21], where the number of dimensions of the space-time is set to $D = 4 - 2\epsilon$, and the limit $\epsilon \rightarrow 0$ is performed at the end of the computation. As a result, the integration measure in Eq. (3.66) is changed to

$$\frac{d^4 l}{(2\pi)^4} \rightarrow \frac{d^D l}{(2\pi)^D}. \quad (3.67)$$

The Passarino-Veltman reduction scheme makes use of Lorentz invariance in order to reduce the tensor integrals to scalar ones. Focusing for example on $N = 1, 2$, the one-point and two-point integrals can be written as

$$A_0(m) = \frac{1}{i\pi^{D/2}} \int d^D l \frac{1}{(l^2 - m^2)}, \quad (3.68)$$

$$B_0, B^\mu, B^{\mu\nu}(p_1, m_1, m_2) = \frac{1}{i\pi^{D/2}} \int d^D l \frac{1, l^\mu, l^{\mu\nu}}{(l^2 - m_1^2)((l + p_1)^2 - m_2^2)}; \quad (3.69)$$

hence, it is possible to expand in terms of so-called form factors the two-point tensor integrals:

$$B^\mu = p_1^\mu B_1, \quad (3.70)$$

$$B^{\mu\nu} = g^{\mu\nu} B_{00} + p_1^\mu p_1^\nu B_{11}. \quad (3.71)$$

By contracting these equations with p_1 and $g^{\mu\nu}$, all form factors can be expressed in terms of the well-known scalar integrals A_0 and B_0 .

The renormalization matrix (and hence the AD matrix) can be finally obtained by taking in consideration the coefficients of the divergent parts of the diagrams (i.e. the coefficients of the ϵ^{-1} terms of the scalar integrals); these coefficients can be extracted employing the following relations:

$$\text{Div}[A_0(m)] = m^2, \quad \text{Div}[B_0(p_1, m_1, m_2)] = 1, \quad (3.72)$$

and remembering that the one-point and two-point scalar integrals are the only scalar integrals to develop a UV divergence.

3.3 Higher Dimension Operators

A systematic study of operators with dimension higher than 6 has been started only recently [59, 60]. Such study is limited by the rapidly increasing growing number of such operators [61]: for instance, there are 30 (1542) dimension 7 operators and 993 (44807) dimension 8 operators in a theory with one (three) flavours. Moreover, given such an enormous number of operators involved, it was necessary to develop new techniques based on Hilbert Series in order to catalogue them in a systematic and “usable” way [62].

However, operators with higher dimension are usually considered as sub-leading with respect to the widely employed and studied dimension six ones, given the higher suppression induced by the NP scale. Therefore, it is common to neglect operators with dimension higher than six in phenomenological analyses, unless there are particular reasons to include them, usually dictated by a specific choice of symmetries [63]. Nevertheless, one has to keep in mind that observables are built from squared amplitudes: this means that the effects of squared dimension six operators are of the same order of the ones stemming from the interference between SM operators and dimension eight ones. Hence, once the future experiments will become sensitive to quadratic dimension six operators effects, dimension eight operators will have to be taken into account as well.

Part II

Anomalies in $b \rightarrow s$ transitions

In the decades that have followed the original formulation of flavour mixing [16], the flavour structure of the SM has been experimentally tested and well established. On the one side, the tremendous progress on the experimental facilities has probed the flavour structure of the SM to a high level of precision [64]; on the other side, a substantial effort has been carried on by the theoretical community to go well beyond leading order computations [65]. In this flavour “precision tests” context, radiative and (semi)leptonic $\Delta B = 1$ processes, related at the quark level to $b \rightarrow s\gamma, s\ell\ell$ transitions, occupy a special place in probing the SM and its possible extensions in terms of NP models [66, 67].

Firstly, this is due to the fact that these rare B meson decays belong to the class of FCNC processes. These processes are among the most sensitive probes of BSM Physics, thanks to the GIM mechanism [68]: the flavour structure of the SM allows for FCNC starting only at the loop level. Hence, there is significant room for heavy new degrees of freedom to sizably contribute to these rare processes.

Secondly, from the experimental side, the study of rare B meson decays offers us some of the most precise measurements amongst the $|\Delta F| = 1$ processes. For instance, the inclusive Branching Fraction of $B \rightarrow X_s\gamma$ has been measured with a relative uncertainty of a few percent [69–71], while the study of an exclusive mode such as $B \rightarrow K^*\ell\ell$ allows for a detailed analysis of the angular distribution of the four final state particles, yielding rich experimental information in terms of angular functions of the dilepton invariant mass, with full kinematic coverage of the latter [72] and – starting from Ref. [73] – also with available experimental correlations among the angular observables.

Finally, the occurrence of several so-called anomalies has been arising in the last few years within the family of $\Delta B = 1$ processes. These anomalies, if confirmed, would point to the presence of NP underling the $b \rightarrow s\gamma, s\ell\ell$ transitions [74–83]. Therefore, a coherent study of this pattern of anomalies performed by means of the SMEFT, trying to find a systematic explanation of the experimental data, could provide an interesting insight of the shape of NP (if these anomalies would be indeed confirmed by future experiments).

Chapter 4

The Theoretical Framework

In this chapter we review out all the equations needed to define the observables displaying the recent anomalies in $b \rightarrow s\gamma, sl\ell$ transitions, further analyzed in the following chapter. We will first study the $B \rightarrow V\ell^+\ell^-$ decays, with V being a vector meson (e.g., a K^* or a ϕ), and then we will easily obtain formulae for the $B \rightarrow V\gamma$ and $B \rightarrow P\ell^+\ell^-$ decays, with P being a pseudoscalar meson (e.g., a K).

4.1 Weak Hamiltonian and Amplitude

The $b \rightarrow s\gamma, sl\ell$ transitions can be described by means of the $\Delta B = 1$ WET Hamiltonian [84–86] which can be split in two parts, a hadronic one and a semileptonic one:

$$H_{eff}^{\Delta B=1} = H_{eff}^{had} + H_{eff}^{sl+\gamma}, \quad (4.1)$$

where

$$H_{eff}^{had} = \frac{4G_F}{\sqrt{2}} \sum_{p=u,c} \lambda_p \left[C_1 P_1^p + C_2 P_2^p + \sum_{i=3,\dots,6} C_i P_i + C_{8g} Q_{8g} \right], \quad (4.2)$$

$$H_{eff}^{sl+\gamma} = \frac{4G_F}{\sqrt{2}} \lambda_t \left[C_7 Q_{7\gamma} + C_7' Q_{7\gamma}' + C_9 Q_{9V} + C_9' Q_{9V}' + C_{10} Q_{10A} + C_{10}' Q_{10A}' \right. \\ \left. + C_S Q_S + C_S' Q_S' + C_P Q_P + C_P' Q_P' \right]. \quad (4.3)$$

The operators P_i are defined as

$$P_1 = (\bar{s}_L \gamma_\mu T^a p_L) (\bar{p}_L \gamma^\mu T^a b_L), \quad (4.4)$$

$$P_2 = (\bar{s}_L \gamma_\mu p_L) (\bar{p}_L \gamma^\mu b_L), \quad (4.5)$$

$$P_3 = (\bar{s}_L \gamma_\mu b_L) \sum_q (\bar{q} \gamma^\mu q), \quad (4.6)$$

$$P_4 = (\bar{s}_L \gamma_\mu T^a b_L) \sum_q (\bar{q} \gamma^\mu T^a q), \quad (4.7)$$

$$P_5 = (\bar{s}_L \gamma_{\mu_1} \gamma_{\mu_2} \gamma_{\mu_3} b_L) \sum_q (\bar{q} \gamma^{\mu_1} \gamma^{\mu_2} \gamma^{\mu_3} q), \quad (4.8)$$

$$P_6 = (\bar{s}_L \gamma_{\mu_1} \gamma_{\mu_2} \gamma_{\mu_3} T^a b_L) \sum_q (\bar{q} \gamma^{\mu_1} \gamma^{\mu_2} \gamma^{\mu_3} T^a q), \quad (4.9)$$

and the operators Q_i are defined as

$$Q_{7\gamma} = \frac{e}{16\pi^2} \hat{m}_b \bar{s} \sigma_{\mu\nu} P_R F^{\mu\nu} b, \quad (4.10)$$

$$Q_{8g} = \frac{g_s}{16\pi^2} \hat{m}_b \bar{s} \sigma_{\mu\nu} P_R G^{\mu\nu} b, \quad (4.11)$$

$$Q_{9V} = \frac{\alpha_{em}}{4\pi} (\bar{s} \gamma_\mu P_L b) (\bar{\ell} \gamma^\mu \ell), \quad (4.12)$$

$$Q_{10A} = \frac{\alpha_{em}}{4\pi} (\bar{s} \gamma_\mu P_L b) (\bar{\ell} \gamma^\mu \gamma^5 \ell), \quad (4.13)$$

$$Q_S = \frac{\alpha_{em}}{4\pi} \frac{\hat{m}_b}{m_W} (\bar{s} P_R b) (\bar{\ell} \ell), \quad (4.14)$$

$$Q_P = \frac{\alpha_{em}}{4\pi} \frac{\hat{m}_b}{m_W} (\bar{s} P_R b) (\bar{\ell} \gamma^5 \ell). \quad (4.15)$$

The primed operators Q'_i are obtained from the operators Q_i by substituting $P_R \rightarrow P_L$, $P_L \rightarrow P_R$ in the quark bilinears. T^a are the $SU(3)_c$ generators, g_s denotes the strong coupling constant, e denotes the electromagnetic coupling constant, $\alpha_{em} = e^2/(4\pi)$ and \hat{m}_b is the b -quark mass in the \overline{MS} scheme at the scale m_b . In principle, $H_{eff}^{sl+\gamma}$ could also contain the tensor operators

$$Q_T = \frac{e^2}{(4\pi)^2} (\bar{s} \sigma_{\mu\nu} b) (\bar{\ell} \sigma^{\mu\nu} \ell), \quad Q_{T5} = \frac{e^2}{(4\pi)^2} (\bar{s} \sigma_{\mu\nu} b) (\bar{\ell} \sigma^{\mu\nu} \gamma_5 \ell); \quad (4.16)$$

however, these operators can not be generated in the SM, so they are usually neglected.

We can now compute the decay amplitude A of a B meson decaying into a vector meson V (e.g. a K^* or a ϕ) and a lepton pair. The contribution of the semileptonic Hamiltonian can be factorized in a sum of products of hadronic and leptonic currents:

$$A^{sl} = \langle V \ell^+ \ell^- | H_{eff}^{sl+\gamma} | \bar{B} \rangle = L_V^\mu a_{V\mu} + L_A^\mu a_{A\mu} + L_S a_S + L_P a_P + L_{TL}^\mu a_{TL\mu} + L_{TR}^\mu a_{TR\mu}, \quad (4.17)$$

where, using the relation

$$(\bar{s} \sigma_{\mu\nu} P_{R(L)} b) (\bar{\mu} \sigma^{\mu\nu} P_{R(L)} \mu) = \frac{4}{q^2} (\bar{s} q_\nu \sigma^{\mu\nu} P_{R(L)} b) (\bar{\mu} q_\rho \sigma^{\mu\rho} P_{R(L)} \mu), \quad (4.18)$$

we have defined

$$L_V^\mu = \langle \ell^+ \ell^- | \bar{\ell} \gamma^\mu \ell | 0 \rangle, \quad (4.19)$$

$$L_A^\mu = \langle \ell^+ \ell^- | \bar{\ell} \gamma^\mu \gamma^5 \ell | 0 \rangle, \quad (4.20)$$

$$L_S = \langle \ell^+ \ell^- | \bar{\ell} \ell | 0 \rangle, \quad (4.21)$$

$$L_P = \langle \ell^+ \ell^- | \bar{\ell} \gamma^5 \ell | 0 \rangle, \quad (4.22)$$

and

$$a_{V\mu} = \frac{4G_F}{\sqrt{2}} \frac{e^2}{16\pi^2} \lambda_t \left[C_9 \langle V | \bar{s} \gamma_\mu P_L b | \bar{B} \rangle + C'_9 \langle V | \bar{s} \gamma_\mu P_R b | \bar{B} \rangle \right. \\ \left. + 2 \frac{\hat{m}_b}{q^2} \left(C_7 q^\nu \langle V | \bar{s} \sigma_{\mu\nu} P_R b | \bar{B} \rangle + C'_7 q^\nu \langle V | \bar{s} \sigma_{\mu\nu} P_L b | \bar{B} \rangle \right) \right], \quad (4.23)$$

$$a_{A\mu} = \frac{4G_F}{\sqrt{2}} \frac{e^2}{16\pi^2} \lambda_t \left[C_{10} \langle V | \bar{s} \gamma_\mu P_L b | \bar{B} \rangle + C'_{10} \langle V | \bar{s} \gamma_\mu P_R b | \bar{B} \rangle \right], \quad (4.24)$$

$$a_S = \frac{4G_F}{\sqrt{2}} \frac{e^2}{16\pi^2} \lambda_t \frac{\hat{m}_b}{m_W} \left[C_S \langle V | \bar{s} P_R b | \bar{B} \rangle + C'_S \langle V | \bar{s} P_L b | \bar{B} \rangle \right], \quad (4.25)$$

$$a_P = \frac{4G_F}{\sqrt{2}} \frac{e^2}{16\pi^2} \lambda_t \frac{\hat{m}_b}{m_W} \left[C_P \langle V | \bar{s} P_R b | \bar{B} \rangle + C'_P \langle V | \bar{s} P_L b | \bar{B} \rangle \right]. \quad (4.26)$$

The contribution of the hadronic Hamiltonian does not naively factorize, but with the insertion of two electromagnetic currents to mediate the semileptonic decay the amplitude takes the form

$$A^{had} = -i \frac{e^2}{q^2} \int dx^4 e^{-iq \cdot x} \langle \ell^+ \ell^- | j_\mu^{em, lept}(x) | 0 \rangle \int dy^4 e^{iq \cdot y} \langle V | T \{ j^{\mu, had}(y) H_{eff}^{had}(0) \} | \bar{B} \rangle \\ \equiv \frac{e^2}{q^2} L_V^\mu a_\mu^{had}, \quad (4.27)$$

in such a manner that its contribution can be absorbed in (4.23):

$$a_{V\mu} = \frac{4G_F}{\sqrt{2}} \frac{e^2}{16\pi^2} \lambda_t \left[C_9 \langle V | \bar{s} \gamma_\mu P_L b | \bar{B} \rangle + C'_9 \langle V | \bar{s} \gamma_\mu P_R b | \bar{B} \rangle \right. \\ \left. + 2 \frac{\hat{m}_b}{q^2} \left(C_7 q^\nu \langle V | \bar{s} \sigma_{\mu\nu} P_R b | \bar{B} \rangle + C'_7 q^\nu \langle V | \bar{s} \sigma_{\mu\nu} P_L b | \bar{B} \rangle \right) + \frac{16\pi^2}{q^2} a_\mu^{had} \right]. \quad (4.28)$$

4.2 Helicity Amplitudes and Helicity Form Factors

In this section we carry out the decomposition of the leptonic currents in spins and helicities, using the completeness relation

$$\eta_{\mu\nu} = \epsilon_{t,\mu} \epsilon_{t,\nu}^* - \sum_{\lambda=\pm 1,0} \epsilon_\mu(1,\lambda) \epsilon_\nu^*(1,\lambda), \quad (4.29)$$

where $\epsilon_\mu(1, \lambda)$ denotes a spin-1 helicity triplet of polarisation 4-vectors for a vector particle of four-momentum q^μ and mass $\sqrt{q^2}$, and $\epsilon_t^\mu = q^\mu / \sqrt{q^2}$.

Using the fact that all leptonic currents are conserved, except for L_A^μ , we get that all their contractions with $\epsilon_{t,\mu}$ are equal to zero; observing now that

$$q_\mu L_A^\mu = 2m_l L_P, \quad (4.30)$$

we can write the amplitude in the following form:

$$A = - \sum_{\lambda=\pm 1,0} \mathcal{L}_V(\lambda) H_V(\lambda) - \sum_{\lambda=\pm 1,0} \mathcal{L}_A(\lambda) H_A(\lambda) + \mathcal{L}_S H_S + \mathcal{L}_P H_P, \quad (4.31)$$

where

$$\mathcal{L}_V(\lambda) = \epsilon_\mu(\lambda) L_V^\mu, \quad H_V(\lambda) = \epsilon_\mu^*(\lambda) a_V^\mu, \quad (4.32)$$

$$\mathcal{L}_A(\lambda) = \epsilon_\mu(\lambda) L_A^\mu, \quad H_A(\lambda) = \epsilon_\mu^*(\lambda) a_A^\mu, \quad (4.33)$$

$$\mathcal{L}_S(\lambda) = L_S, \quad H_S(\lambda) = a_S, \quad (4.34)$$

$$\mathcal{L}_P(\lambda) = L_P, \quad H_P(\lambda) = a_P + \frac{2m_l}{q^2} q_\mu a_A^\mu. \quad (4.35)$$

The quantities H_V , H_A , H_P and H_S are called *helicity amplitudes*. Working with these amplitudes is particularly useful, since they allow us to study directly how the non-factorizable effects coming from the hadronic Hamiltonian contribute to the observables, as we will discuss in the following sections.

In order to define explicitly those amplitudes we first need to define the following helicity form factors:

$$-im_B \tilde{V}_{L(R)\lambda}(q^2) = \langle V(\lambda) | \bar{s} \not{\epsilon}^*(\lambda) P_{L(R)} b | \bar{B} \rangle, \quad (4.36)$$

$$m_B^2 \tilde{T}_{L(R)\lambda}(q^2) = \epsilon^{*\mu}(\lambda) q^\nu \langle V | \bar{s} \sigma_{\mu\nu} P_{L(R)} b | \bar{B} \rangle, \quad (4.37)$$

$$im_B \tilde{S}_{L(R)}(q^2) = \langle V(\lambda=0) | \bar{s} P_{L(R)} b | \bar{B} \rangle. \quad (4.38)$$

We can now write the explicit form of the helicity amplitudes:

$$H_V(\lambda) = -iN \left\{ C_9 \tilde{V}_{L\lambda} + C'_9 \tilde{V}_{R\lambda} + \frac{m_B^2}{q^2} \left[\frac{2\hat{m}_b}{m_B} (C_7 \tilde{T}_{L\lambda} + C'_7 \tilde{T}_{R\lambda}) - 16\pi^2 h_\lambda \right] \right\}, \quad (4.39)$$

$$H_A(\lambda) = -iN (C_{10} \tilde{V}_{L\lambda} + C'_{10} \tilde{V}_{R\lambda}), \quad (4.40)$$

$$H_S = iN \frac{\hat{m}_b}{m_W} (C_S \tilde{S}_L + C'_S \tilde{S}_R), \quad (4.41)$$

$$H_P = iN \left\{ \frac{\hat{m}_b}{m_W} (C_P \tilde{S}_L + C'_P \tilde{S}_R) + \frac{2m_\mu m_B}{q^2} \left[C_{10} \left(\tilde{S}_L - \frac{m_s}{m_b} \tilde{S}_R \right) + C'_{10} \left(\tilde{S}_R - \frac{m_s}{m_b} \tilde{S}_L \right) \right] \right\}, \quad (4.42)$$

where

$$N = -\frac{4G_F m_B}{\sqrt{2}} \frac{e^2}{16\pi^2} \lambda_t \quad (4.43)$$

is a normalization factor, and

$$h_\lambda = \frac{i}{m_B^2} \epsilon^{\mu*}(\lambda) a_\mu^{had} \quad (4.44)$$

contains all the non-factorizable effects coming from the hadronic Hamiltonian.

Note that parity invariance of strong interactions allow us to write down the following relations:

$$\tilde{V}_{L\lambda} = -\eta(-1)^L \tilde{V}_{R,-\lambda} \equiv \tilde{V}_\lambda, \quad (4.45)$$

$$\tilde{T}_{L\lambda} = -\eta(-1)^L \tilde{T}_{R,-\lambda} \equiv \tilde{T}_\lambda, \quad (4.46)$$

$$\tilde{S}_L = -\eta(-1)^L \tilde{S}_R \equiv \tilde{S}, \quad (4.47)$$

where L is the angular momentum and η is the intrinsic parity of the vector meson V ; this means that there are seven independent helicity form factors for spin ≥ 1 and three for spin 0. It is now possible to rescale the helicity-0 form factors as

$$V_0(q^2) = \frac{2m_B \sqrt{q^2}}{\rho^{1/2}} \tilde{V}_0(q^2), \quad (4.48)$$

$$T_0(q^2) = \frac{2m_B^3}{\sqrt{q^2} \rho^{1/2}} \tilde{T}_0(q^2), \quad (4.49)$$

$$S(q^2) = -\frac{2m_B(m_b + m_s)}{\rho^{1/2}} \tilde{S}(q^2), \quad (4.50)$$

where

$$\rho = 4m_B^2 |\vec{k}|^2, \quad (4.51)$$

and \vec{k} is 3-momentum of the recoiling \bar{K}^* in the \bar{B} rest frame,

$$\vec{k}^2 = \frac{m_B^4 + (m_{K^*}^2 - q^2)^2 - 2m_B^2(m_{K^*}^2 + q^2)}{4m_B^2}. \quad (4.52)$$

Defining for the remaining helicities

$$V_\pm(q^2) \equiv \tilde{V}_\pm(q^2), \quad T_\pm(q^2) \equiv \tilde{T}_\pm(q^2), \quad (4.53)$$

it is possible to express these form factors in terms of the traditional transverse form factors [87, 88]:

$$V_\pm(q^2) = \frac{1}{2} \left[\left(1 + \frac{m_V}{m_B}\right) A_1(q^2) \mp \frac{\rho^{1/2}}{m_B(m_B + m_V)} V(q^2) \right], \quad (4.54)$$

$$V_0(q^2) = \frac{1}{2m_V\rho^{1/2}(m_B + m_V)} \left[(m_B + m_V)^2(m_B^2 - q^2 - m_V^2)A_1(q^2) - \rho A_2(q^2) \right], \quad (4.55)$$

$$T_{\pm}(q^2) = \frac{m_B^2 - m_V^2}{2m_B^2} T_2(q^2) \mp \frac{\rho^{1/2}}{2m_B^2} T_1(q^2), \quad (4.56)$$

$$T_0(q^2) = \frac{m_B}{2m_V\rho^{1/2}} \left[(m_B^2 + 3m_V^2 - q^2)T_2(q^2) - \frac{\rho}{(m_B^2 - m_V^2)} T_3(q^2) \right], \quad (4.57)$$

$$S(q^2) = A_0(q^2). \quad (4.58)$$

4.3 Kinematic Distribution

Let us now take a further step, and consider the final state particles of the decay (produced when the vector meson V decays into a pair of long-lived particles). In this section we will consider, without any loss of generality, the case where the vector meson is a K^* : the full decay channel is therefore

$$\bar{B}(p) \rightarrow \bar{K}^*(k) [\rightarrow \bar{K}(k_1)\pi(k_2)] \ell^+(q_1)\ell^-(q_2), \quad (4.59)$$

where $\bar{K} = \bar{K}^0$ or K^- and $\pi = \pi^+$ or π^0 (when ϕ is the vector meson, the final state mesons are a K^+ and a K^-). Let us define the angles θ_K , θ_l and ϕ as illustrated in Fig. 4.1. We first define, in the \bar{B} rest frame,

$$\mathbf{e}_l = \frac{\mathbf{p}_{l^-} \times \mathbf{p}_{l^+}}{|\mathbf{p}_{l^-} \times \mathbf{p}_{l^+}|}, \quad \mathbf{e}_k = \frac{\mathbf{p}_{\bar{K}} \times \mathbf{p}_{\pi}}{|\mathbf{p}_{\bar{K}} \times \mathbf{p}_{\pi}|}, \quad \hat{z} = \frac{\mathbf{p}_{\bar{K}} + \mathbf{p}_{\pi}}{|\mathbf{p}_{\bar{K}} + \mathbf{p}_{\pi}|}. \quad (4.60)$$

We can now define ϕ in the interval $[0, 2\pi)$ through the relations

$$\sin \phi = (\mathbf{e}_l \times \mathbf{e}_k) \cdot \hat{z}, \quad \cos \phi = \mathbf{e}_l \cdot \mathbf{e}_k. \quad (4.61)$$

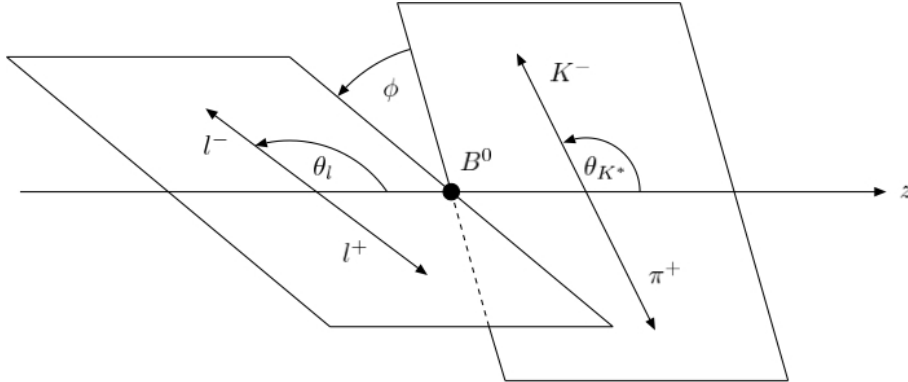


Figure 4.1: Definition of kinematic variables in the decay $B^0 \rightarrow K^{*0}(\rightarrow K^- \pi^+) \ell^+ \ell^-$. Figure taken from Ref. [89].

Hence, ϕ is the angle between the normals to the planes defined by $K^-\pi^+$ and $\ell^+\ell^-$ in the rest frame of the B meson, θ_l is defined as the angle between the direction of flight of the \bar{B} and the ℓ^- in the dilepton rest frame, and θ_K is defined as the angle between the direction of motion of the \bar{B} and the \bar{K} in the di-meson rest frame; both angles are defined in the interval $[0, \pi)$.

Making the assumption that the \bar{K}^* is a narrow resonance which decays, we should make the replacement

$$|\bar{K}^*; \lambda\rangle \rightarrow \sqrt{b} \int d\Omega_K Y_1^\lambda(\theta, \phi_K) |\theta_K; \phi_K\rangle, \quad (4.62)$$

where θ_K is previously defined, ϕ_K is the angle between the x axis and the projection of the former onto the xy plane and $b \equiv BF(K^* \rightarrow K\pi) \approx 1$.

Squaring the amplitude and summing over lepton spins allow us to write the fully differential decay rate as

$$\begin{aligned} \frac{d^{(4)}\Gamma}{dq^2 d(\cos\theta_\ell) d(\cos\theta_K) d\phi} &= \frac{9}{32\pi} \left(I_1^s \sin^2\theta_K + I_1^c \cos^2\theta_K + (I_2^s \sin^2\theta_K + I_2^c \cos^2\theta_K) \cos 2\theta_\ell \right. \\ &\quad + I_3 \sin^2\theta_K \sin^2\theta_\ell \cos 2\phi + I_4 \sin 2\theta_K \sin 2\theta_\ell \cos \phi \\ &\quad + I_5 \sin 2\theta_K \sin \theta_\ell \cos \phi + (I_6^s \sin^2\theta_K + I_6^c \cos^2\theta_K) \cos \theta_\ell \\ &\quad + I_7 \sin 2\theta_K \sin \theta_\ell \sin \phi + I_8 \sin 2\theta_K \sin 2\theta_\ell \sin \phi \\ &\quad \left. + I_9 \sin^2\theta_K \sin^2\theta_\ell \sin 2\phi \right). \end{aligned} \quad (4.63)$$

The angular coefficients I_i are functions of q^2 , and can be expressed in terms of the helicity amplitudes defined in Eqs. (4.39)-(4.42) as

$$I_1^c = F \left\{ \frac{1}{2} (|H_V^0|^2 + |H_A^0|^2) + |H_P^0|^2 + \frac{2m_l^2}{q^2} (|H_V^0|^2 - |H_A^0|^2) + \beta^2 |H_S^0|^2 \right\}, \quad (4.64)$$

$$I_1^s = F \left\{ \frac{\beta^2 + 2}{8} (|H_V^+|^2 + |H_V^-|^2 + (V \rightarrow A)) + \frac{m_l^2}{q^2} (|H_V^+|^2 - |H_V^-|^2) - (V \rightarrow A) \right\}, \quad (4.65)$$

$$I_2^c = -F \frac{\beta^2}{2} (|H_V^0|^2 + |H_A^0|^2), \quad (4.66)$$

$$I_2^s = F \frac{\beta^2}{2} (|H_V^+|^2 + |H_V^-|^2) + (V \rightarrow A), \quad (4.67)$$

$$I_3 = -F \frac{\beta^2}{2} \text{Re} [H_V^+ (H_V^-)^*] + (V \rightarrow A), \quad (4.68)$$

$$I_4 = F \frac{\beta^2}{4} \text{Re} [(H_V^+ + H_V^-) (H_V^0)^*] + (V \rightarrow A), \quad (4.69)$$

$$I_5 = F \left\{ \frac{\beta}{4} \text{Re} [(H_V^- - H_V^+) (H_A^0)^*] + (V \leftrightarrow A) - \frac{\beta m_l}{\sqrt{q^2}} \text{Re} [H_S^* (H_V^+ + H_V^-)] \right\}, \quad (4.70)$$

$$I_6^s = F\beta \operatorname{Re} [H_V^-(H_A^-)^* - H_V^+(H_A^+)^*], \quad (4.71)$$

$$I_6^c = 4F \frac{\beta m_l}{\sqrt{q^2}} \operatorname{Re} [H_S^* H_V^0], \quad (4.72)$$

$$I_7 = F \left\{ \frac{\beta}{2} \operatorname{Im} [(H_A^+ + H_A^-)(H_V^0)^*] + (V \leftrightarrow A) - \frac{\beta m_l}{\sqrt{q^2}} \operatorname{Im} [H_S^*(H_V^- + -H_V^+)] \right\}, \quad (4.73)$$

$$I_8 = F \frac{\beta^2}{4} \operatorname{Im} [(H_V^- - H_V^+)(H_V^0)^*] + (V \rightarrow A), \quad (4.74)$$

$$I_9 = F \frac{\beta^2}{4} \operatorname{Im} [H_V^+(H_V^-)^*] + (V \rightarrow A), \quad (4.75)$$

where

$$F = \frac{\rho^{1/2} \beta q^2}{3 \times 2^5 \pi^3 m_B^3} BF(K^* \rightarrow K\pi), \quad \beta = \sqrt{1 - \frac{4m_l^2}{q^2}}, \quad (4.76)$$

and ρ is defined in Eq. (4.51).

It is worth to notice that it is possible to study the CP-conjugate decay $B \rightarrow K^* \ell^+ \ell^-$ in an analogous way, obtaining a decay rate with the same form of Eq. (4.63) with the following substitutions:

$$I_{1s(c),2s(c),3,4,7} \rightarrow \bar{I}_{1s(c),2s(c),3,4,7}, \quad I_{5,6s(c),8,9} \rightarrow -\bar{I}_{5,6s(c),8,9}, \quad (4.77)$$

where the angles are defined as in the \bar{B} decays, with $K^- \rightarrow K^+$. All the \bar{I}_i 's are equal to the I_i 's, but with all the weak phases conjugated.

4.4 Angular Observables

We have now all the ingredients needed in order to define all the relevant observables. Taking into account both the I_i angular coefficients and their CP-conjugate counterparts, it is possible to define the following quantities:

$$\Sigma_i = \frac{I_i + \bar{I}_i}{2}, \quad \Delta_i = \frac{I_i - \bar{I}_i}{2}. \quad (4.78)$$

As a first step, we can now define the “usual” observables: the branching ratio, its longitudinal component and the forward-backward asymmetry, which can be defined in terms of the averaged angular coefficients as:

$$\Gamma' = \frac{1}{2} \frac{d\Gamma + d\bar{\Gamma}}{dq^2} = \frac{1}{4} [(3\Sigma_{1c} - \Sigma_{2c}) + 2(3\Sigma_{1s} - \Sigma_{2s})],$$

$$F_L = \frac{3\Sigma_{1c} - \Sigma_{2c}}{4\Gamma'}, \quad A_{FB} = -\frac{3\Sigma_{6s}}{4\Gamma'}. \quad (4.79)$$

In the limit $q^2 \gg m_\ell^2$ the terms proportional to m_ℓ^2/q^2 can be dropped from the angular coefficients in Eqs. (4.64)-(4.75), and moreover the helicity amplitude $H_P \rightarrow 0$ (since it is proportional to m_i/q^2 in the SM). In this limit, one therefore obtains further relations connecting the angular coefficients, which can be exploited in order to reduce the number of independent observables. These relations can be written as:

$$\Sigma_{1c} = -\Sigma_{2c}, \quad \Sigma_{1s} = 3\Sigma_{2s}, \quad (4.80)$$

and they simplify the expressions for F_L and Γ' to

$$F_L = \frac{\Sigma_{1c}}{\Gamma'} \quad \text{and} \quad \Gamma' = \Sigma_{1c} + 4\Sigma_{2s}. \quad (4.81)$$

Focusing now on angular observables, two different prescriptions have been advocated in the past [90, 91] in order to define these observables, and both have been used for experimental analyses [72–74, 77, 78, 92, 93]. These two definitions can be easily related to each other, since they are (obviously) equal from the physical point of view.

As a first possibility, following [90] one can define

$$S_i = \frac{I_i + \bar{I}_i}{2\Gamma'}, \quad A_i = \frac{I_i - \bar{I}_i}{2\Gamma'}. \quad (4.82)$$

On the other hand, in an attempt to reduce the uncertainties coming from form factors and hadronic contributions one can define a new set with suitable ratios of angular coefficients [91, 94–96]:

$$P_1 = \frac{\Sigma_3}{2\Sigma_{2s}}, \quad P_2 = \frac{\Sigma_{6s}}{8\Sigma_{2s}}, \quad P_3 = -\frac{\Sigma_9}{4\Sigma_{2s}}, \quad (4.83)$$

$$P'_4 = \frac{\Sigma_4}{\sqrt{-\Sigma_{2s}\Sigma_{2c}}}, \quad P'_5 = \frac{\Sigma_5}{2\sqrt{-\Sigma_{2s}\Sigma_{2c}}}, \quad P'_6 = -\frac{\Sigma_7}{2\sqrt{-\Sigma_{2s}\Sigma_{2c}}}, \quad P'_8 = -\frac{\Sigma_8}{\sqrt{-\Sigma_{2s}\Sigma_{2c}}}.$$

Experimentally, these observables are measured in binned data cut in regions of q^2 , the dilepton invariant mass. Hence, working without any loss of generality in the basis of Refs. [91, 94–96], the following convention has to be applied in order to define the experimentally binned observables starting from the analytic expressions:

$$\langle P_1 \rangle = \frac{\langle \Sigma_3 \rangle}{2 \langle \Sigma_{2s} \rangle}, \quad \langle P_2 \rangle = \frac{\langle \Sigma_{6s} \rangle}{8 \langle \Sigma_{2s} \rangle}, \quad \langle P_3 \rangle = -\frac{\langle \Sigma_9 \rangle}{4 \langle \Sigma_{2s} \rangle},$$

$$\begin{aligned}
\langle P'_4 \rangle &= \frac{\langle \Sigma_4 \rangle}{\sqrt{-\langle \Sigma_{2s} \Sigma_{2c} \rangle}}, & \langle P'_5 \rangle &= \frac{\langle \Sigma_5 \rangle}{2\sqrt{-\langle \Sigma_{2s} \Sigma_{2c} \rangle}}, \\
\langle P'_6 \rangle &= -\frac{\langle \Sigma_7 \rangle}{2\sqrt{-\langle \Sigma_{2s} \Sigma_{2c} \rangle}}, & \langle P'_8 \rangle &= -\frac{\langle \Sigma_8 \rangle}{2\sqrt{-\langle \Sigma_{2s} \Sigma_{2c} \rangle}},
\end{aligned} \tag{4.84}$$

where it should be noted that the relevant quantity is the ratio of binned angular coefficients rather than the binned ratios, since:

$$\langle \Sigma_i \rangle = \int_{q_{min}^2}^{q_{max}^2} \Sigma(q^2) dq^2. \tag{4.85}$$

Furthermore, the binned Branching Fraction, F_L and A_{FB} are defined as:

$$\langle \Gamma' \rangle = \langle \Sigma_{1c} + 4\Sigma_{2s} \rangle, \quad \langle F_L \rangle = \frac{\langle 3\Sigma_{1c} - \Sigma_{2c} \rangle}{4\langle \Gamma' \rangle}, \quad \langle A_{FB} \rangle = -\frac{3\langle \Sigma_{6s} \rangle}{4\langle \Gamma' \rangle}. \tag{4.86}$$

It is now important to stress that the theory definitions of these observables are not the same as the ones used for the experimental measurements, due to the difference in the definitions of the kinematic variable between the two cases; the numerical results between the two definitions are connected by [97, 98]:

$$P_2^{\text{Exp}} = -P_2^{\text{T}}, \quad P_3^{\text{Exp}} = -P_3^{\text{T}}, \quad P_4^{\text{Exp}} = -\frac{1}{2}P_4^{\text{T}} \quad \text{and} \quad P_8^{\text{Exp}} = -\frac{1}{2}P_8^{\text{T}}, \tag{4.87}$$

where the superscript Exp implies experimental definitions, while the subscript T implies theory ones. While the sign difference is due to the change in the definition of the kinematic variables, the factors of two come from the difference in the definitions of the variables themselves.

Finally, it is possible to define the connection between the two different sets of observables.

$$\begin{aligned}
P_1 &= A_T^{(2)} = \frac{2S_3}{1 - F_L}, & P_2 &= -\frac{2}{3} \frac{A_{FB}}{1 - F_L}, & P_3 &= -\frac{S_9}{1 - F_L} \\
P'_4 &= \frac{2S_4}{\sqrt{F_L(1 - F_L)}}, & P'_5 &= \frac{S_5}{\sqrt{F_L(1 - F_L)}}, & P'_6 &= -\frac{S_7}{\sqrt{F_L(1 - F_L)}}, \\
P'_8 &= -\frac{2S_8}{\sqrt{F_L(1 - F_L)}}.
\end{aligned} \tag{4.88}$$

In the above relations, both the left and the right hand sides refer to the definitions of the kinematic variables used in theory computations.

4.5 On (Non-)Factorizable Contributions to the Hadronic Hamiltonian

Before concluding the theoretical study of the $B \rightarrow V\ell^+\ell^-$ decays, it is mandatory to further analyze the factorizable and non-factorizable corrections to the $\Delta B = 1$ Hamiltonian $\mathcal{H}_{\text{eff}}^{\Delta B=1}$ in Eq. (4.1).

Concerning the semi-leptonic part of the Hamiltonian, $\mathcal{H}_{\text{eff}}^{\text{sl}+\gamma}$ in Eq. (4.3), such contribution clearly factorizes into the product of hadronic form factors and leptonic tensors to all orders in strong interactions. However, the hadronic part described by the matrix elements of $\mathcal{H}_{\text{eff}}^{\text{had}}$ in Eq. (4.2) factorize only in the infinite m_b limit below the charm threshold [100–102]. Moreover, working in the infinite mass limit one can exploit the heavy quark symmetry in order to reduce the number of independent form factors from seven to two soft form factors [103–105]. Therefore, in this limit, the amplitudes have simpler expressions that guided the community towards the definition of the aforementioned optimized observables, dominated by short distance physics [89, 95, 106]. However, it is mandatory to try to understand how important are the departures from the infinite mass limit, with particular care to the $q^2 \simeq 4m_c^2$ region (which is where, as we will see in the next chapter, most of the anomalies have been found).

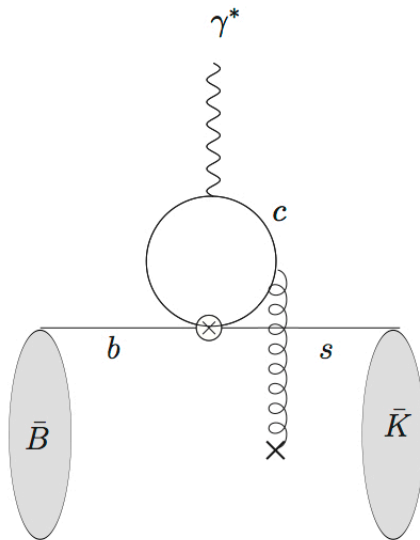


Figure 4.2: Non-factorizable contribution due to a soft gluon exchange in the $B^0 \rightarrow K^*\gamma^*$ matrix element. The circled cross represents the insertion of the four quark local operator $Q_{1,2}^c$. Figure taken from Ref. [99].

Concerning factorized amplitudes, these can be described using the full set of form factors, which have been estimated using QCD sum rules at low q^2 [87, 88, 107–109]. Such computations, and in particular the latest results from Ref. [88] providing the full correlation matrix, show a reasonably accurate estimate of low q^2 values, with a high compatibility with the lattice estimate at high q^2 [110]. It is interesting to note that using full QCD form factors reintroduces some hadronic uncertainties into optimized observables; however, such uncertainties have been estimated in refs. [91, 94, 96, 111–117].

On the other hand, particular care has to be taken when considering the non-factorizable contribution present in the matrix element of the Hamiltonian in Eq. (4.2) involving a $c\bar{c}$ loop, as shown in Fig. 4.2. Working in the infinite mass limit, the QCD factorization approach can be exploited in order to compute such term, up to $\mathcal{O}(\alpha_s)$ corrections [101, 118]. However, if one is interested in corrections beyond the leading power, the contribution of $Q_{1,2}^c$ to the $\bar{B} \rightarrow \bar{K}^*\gamma^*$ amplitude has been estimated using light-cone sum rules only at $q^2 \sim 1 \text{ GeV}^2$, in the single soft-gluon approximation [99]. While this is a seminal contribution, it is important to stress the fact that additional soft-gluon exchanges are suppressed by a factor $1/(q^2 - 4m_c^2)$, hence worsening the approximation as q^2 increases and eventually breaking it down at $q^2 \sim 4m_c^2$. In Ref. [99] the authors proposed also a model to extend their results in the whole low- q^2 phenomenological region, based on an extrapolation of their result at $q^2 \sim 1 \text{ GeV}^2$ with a description of the resonant region based on dispersion relations. While this model is reasonable, it is nevertheless spoiled by the large uncertainties present in the transition region from $q^2 \sim 4 \text{ GeV}^2$ to $m_{J/\psi}^2$.

It is interesting to notice that the community is well aware of this issue, which might reduce the reliability of the theoretical computation carried out for these decay channel and put at stake the claim of NP [8–11, 97, 114, 117, 119–122]. However, new efforts have been lately carried out in order to fully grasp the effects lying beyond such non-factorizable contributions, even though a conclusive computation is still lacking [123, 124].

4.6 Amplitudes for Other Decay Channels

Starting from the computations of previous sections, it is now straightforward to obtain analogous results for the $B \rightarrow V\gamma$ and $B \rightarrow P\ell^+\ell^-$ decays, with P being a pseudoscalar meson (e.g., a K).

Regarding the radiative decay, it's easy to observe that it is described by a simple subset of the amplitudes of the semileptonic one. The exact relation is the

following:

$$\begin{aligned}
\mathcal{A}(\bar{B} \rightarrow V(\lambda)\gamma(\lambda)) &= \lim_{q^2 \rightarrow 0} \frac{q^2}{e} H_V(q^2 = 0; \lambda) \\
&= \frac{iNm_B^2}{e} \left[\frac{2\hat{m}_b}{m_B} (C_7 \tilde{T}_\lambda(0) - C'_7 \tilde{T}_{-\lambda}(0)) - 16\pi^2 h_\lambda(q^2 = 0) \right],
\end{aligned} \tag{4.89}$$

where the helicity can be only ± 1 .

In a similar fashion, the amplitude for the $B \rightarrow P\ell^+\ell^-$ decay can be obtained considering only the subset of helicity-0 amplitudes. It is worth to mention that, for a pseudoscalar, we have the following relations between the helicity and the transverse form factors [108]:

$$V_0(q^2) = if_+(q^2), \tag{4.90}$$

$$T_0(q^2) = i \frac{2m_B}{(m_B + m_P)} f_T(q^2), \tag{4.91}$$

$$S(q^2) = \frac{1 + \frac{m_s}{m_b}}{1 - \frac{m_s}{m_b}} \frac{m_B^2 - m_M^2}{\rho^{1/2}} f_0(q^2). \tag{4.92}$$

Chapter 5

Review of $b \rightarrow s$ Anomalies and Their Interpretations

The recent years of experimental results in B physics have been characterized by the emergence of a striking pattern of anomalies, observed in multiple independent studies of some rare $b \rightarrow s$ transitions [125].

The first part of this chapter will be devoted to reviewing the present status of the anomalies: I will first discuss the measurements of the angular analysis of the $B \rightarrow K^* \mu^+ \mu^-$ decay [74, 78, 80, 82, 126], followed by an analysis of the measurements of the $B \rightarrow \phi \mu^+ \mu^-$ [77] and $B \rightarrow K \mu^+ \mu^-$ [75, 81] Branching Fractions. Subsequently, I will describe the measurement of R_K [76] and R_{K^*} [83], the ratios between the muonic Branching Fraction and the electronic one in the $B \rightarrow K \ell^+ \ell^-$ and the $B \rightarrow K^* \ell^+ \ell^-$ channels, respectively.

After this review, I will focus on the possible comprehensive interpretations of such a striking pattern of anomalies. Many early studies showed how a rather simple and fascinating explanation could be achieved advocating NP effects in the muonic vectorial operator Q_{9V}^μ [66, 98, 117, 127, 128]: the results of the fits showed that the introduction of a BSM correction $\Delta C_9^\mu \simeq -1$ is enough to account for all the anomalies, offering an appealing systematic explanation of the $\Delta B = 1$ anomalies.

However, the global picture might not be as simple as that. In the final part of this chapter I will describe the work that we have done on the subject, trying to cast some light on what might be the real origin of these anomalies. Indeed, we first focused on the angular analysis of the $B \rightarrow K^* \mu^+ \mu^-$ decay alone, showing how the size of the anomaly is directly connected with the treatment of the non-factorizable hadronic contribution: the widely used estimate of such term is based on a LCSR computation [99], which however lacks of some potentially-non-negligible contributions, as explained in Sec. 4.5; therefore, we allowed for larger (but in the same ballpark) effects, obtaining that this SM effect could indeed be the

reason behind the experimental discrepancies, without however being able to rule out the NP explanation [8–10]. On the other hand, once the R_K and R_{K^*} ratios are taken into account, a SM-only explanation is no longer viable; nevertheless, allowing once again for larger hadronic effects in the $B \rightarrow K^* \mu^+ \mu^-$ decay unveils the possibility of a new BSM explanation, requiring NP effects in the electronic axial operator Q_{10A}^e [11].

5.1 Anomalies in $B \rightarrow K^* \mu^+ \mu^-$ Angular Analysis

The first element in this pattern of anomalies occurred with the measurement of the angular analysis of the $B \rightarrow K^* \mu^+ \mu^-$ decay. The first partial angular measurement was carried out in 2013 by LHCb, with an analysis based on a data sample corresponding to an integrated luminosity of 1.0fb^{-1} [74]¹. The data was divided in 6 q^2 bins, where q^2 is the invariant lepton mass, with a total of 24 independent measurements. Agreement with the SM was observed for 23 of the 24 measure-

¹Due to the limited number of signal candidates, i.e. 883, it was not possible to fit the data to the full differential distribution: consequently, the data was “folded” in order to reduce the number of parameters in the fit, resulting with a measurement of only 4 of the 8 independent angular observables.

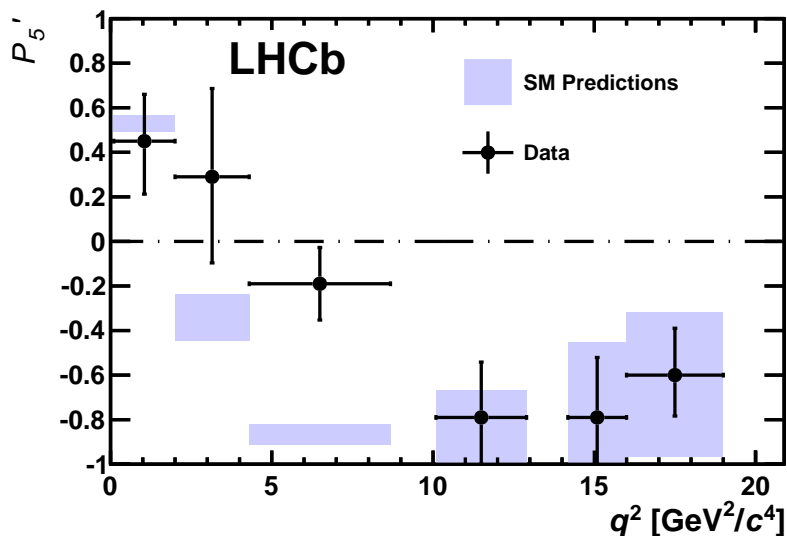


Figure 5.1: Measured values for the P'_5 observable (black points) performed by LHCb, based on a data sample corresponding to an integrated luminosity of 1.0fb^{-1} [74], to be compared with SM predictions from Ref. [95] (blue bands).

ments, with a 3.7σ local discrepancy observed in the $4.30 < q^2 < 8.68 \text{ GeV}^2/c^4$ bin of the P'_5 observable compared with the SM prediction in Ref. [95], as shown in Fig. 5.1.

The anomaly was subsequently confirmed by the 2015 analysis of the full Run 1 LHCb dataset, corresponding to an integrated luminosity of 3.0fb^{-1} [78]. The larger amount of signal candidates (equal to 2398 ± 57 events) allowed for the first time for a full angular analysis, with each angular observable subdivided in 7 q^2 bins. Once again, a local discrepancy was found in the “central” bins of the P'_5 observable, namely $4.0 < q^2 < 6.0 \text{ GeV}^2/c^4$ and $6.0 < q^2 < 8.0 \text{ GeV}^2/c^4$, with a global discrepancy showing a 3.4σ significance compared to the SM predictions of Ref. [116].

The following year, also the Belle collaboration performed a measurement of the P'_5 observable, for the first time both for the muonic and the electronic channel [79, 80]. Due to the very limited number for signal candidates (127 ± 15 for the electron channel and 185 ± 17 for the muonic one), only two bins per observable were measured, with a bigger relative uncertainty compared to LHCb ones. Nevertheless, while the electron channel was found in agreement with the SM predictions in Ref. [129], the muonic one displayed a 2.6σ discrepancy in the highest bin, namely $4.0 < q^2 < 8.0 \text{ GeV}^2/c^4$, in the same direction of the one found by LHCb.

To corroborate even more the picture of the “ P'_5 anomaly”, two new independent measurements of this angular observable have been released at the beginning of 2017 by ATLAS [82] and CMS [126] collaborations, showing in the former a 2.7σ tension in the $4.0 < q^2 < 6.0 \text{ GeV}^2/c^4$ bin between data and the SM prediction in Ref. [116], while a perfect agreement was found in the latter.

A summary of all the latest experimental measurements, compared to SM predictions from Refs. [116, 128], can be found in Fig. 5.2.² It is worth to stress again that these SM predictions, however, suffer from a possible under-estimation of the hadronic contribution: in fact, their treatment of such contribution is based on the LCSR computation of Ref. [99], which lacks some potentially non-negligible contributions, namely the consideration of multiple soft-gluon emissions. Hence, this observable cannot be viewed as a theoretically “clean” one. Therefore, due to lack of a firm control of QCD power corrections in this channel, the discrepancies obtained comparing experimental results to SM predictions on this decay channel should be taken *cum grano salis*.

²https://twiki.cern.ch/twiki/pub/LHCbPhysics/RareDecayConferenceMaterial/P5p_Including_ATLAS_CMS_Belle.pdf

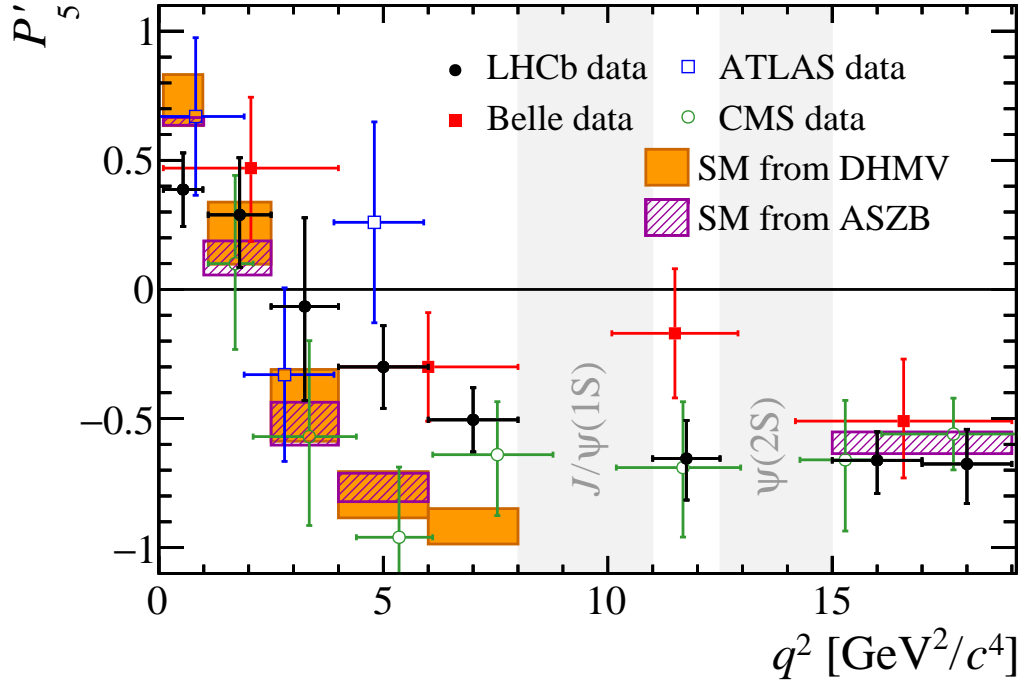


Figure 5.2: Latest measured values for the P'_5 observable performed by LHCb [78] (black points), Belle [79, 80] (red points), ATLAS [82] (blue points) and CMS [126] (green points), to be compared with SM predictions from Ref. [116] (orange bands) and Ref. [128] (purple bands).

5.2 Anomalies in Branching Fractions: the $B \rightarrow K\mu^+\mu^-$ and the $B_s \rightarrow \phi\mu^+\mu^-$ cases

The second anomaly in the context of $b \rightarrow s$ transitions is dated 2014, when the Branching Fraction of the $B \rightarrow K\mu^+\mu^-$ decay was first measured [75]. The analysis was carried out on the complete LHCb Run 1 dataset, with the observable being subdivided in 17 q^2 bins. While each measurement is in agreement with its SM prediction from Ref. [130], in the low- q^2 region they consistently show lower values compared to the theory computation, as shown in Fig. 5.3. Although this measurement would not be particularly appealing to NP hunters by itself, the fact that the (small) discrepancy between theory and data was found in the same q^2 region as the P'_5 one induced some authors to also take this measurement into account, as an hint of an underlying NP picture affecting the $b \rightarrow s$ transitions scenario.

This possibility was further corroborated in 2015, when the LHCb collaboration

made available the measurements of the Branching Fraction for the $B_s \rightarrow \phi \mu^+ \mu^-$ decay, making use of the complete Run 1 dataset [77]. The observable was measured in 6 q^2 bins, and compared with the SM predictions from Ref. [130]. Once again, data showed lower values relatively to the theory computation in the low- q^2 region, with a local discrepancy of about 3σ in the $2.0 < q^2 < 5.0 \text{ GeV}^2/c^4$ bin, as can be seen looking at Fig. 5.4.

It is worth noting that the latter mode suffers from the same “pollution” coming from hadronic physics as the one affecting the angular analysis of the $B \rightarrow K^* \mu^+ \mu^-$ decay, and hence this observable might not be viewed as a totally “clean” one; on the other hand, the theoretical computation of the hadronic part for the former channel seems to be under control [131], hence pointing to NP as the only possible explanation of such an experimental behavior, in the case that future experiments will further confirm the present trend.

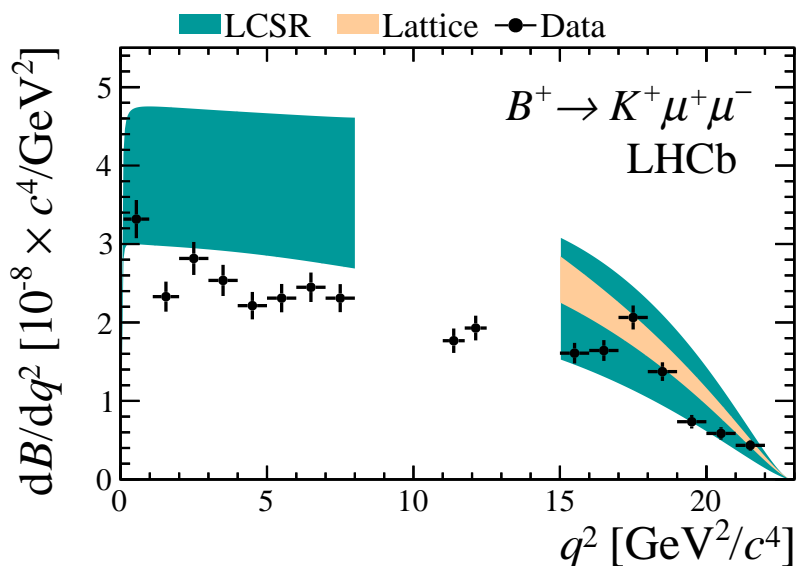


Figure 5.3: Measured values of the differential Branching Fraction of the $B^+ \rightarrow K^+ \mu^+ \mu^-$ decay (black points) performed by LHCb, based on a data sample corresponding to an integrated luminosity of 3.0fb^{-1} [75], to be compared with the SM predictions from Ref. [130] (green/orange bands).

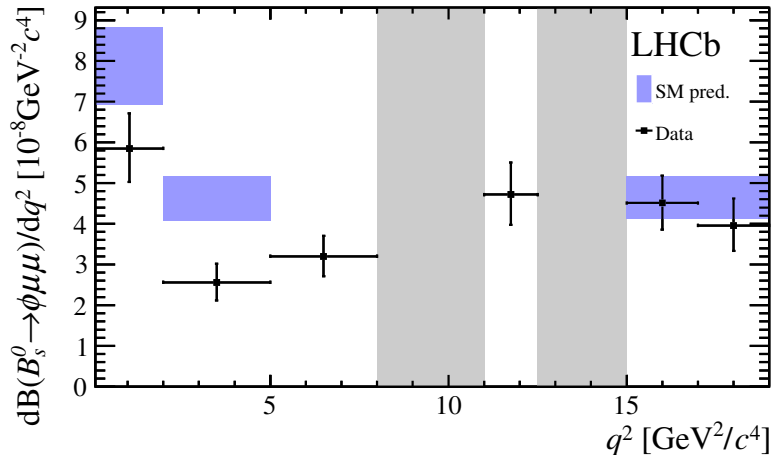


Figure 5.4: Measured values of the differential Branching Fraction of the $B_s^0 \rightarrow \phi\mu^+\mu^-$ decay (black points) performed by LHCb, based on a data sample corresponding to an integrated luminosity of 3.0fb^{-1} [77], to be compared with the SM predictions from Refs. [88, 128] (blue bands).

5.3 Anomalies in Branching Fraction Ratios: the R_K and the R_{K^*} Observables

One of the most intriguing measurements came out in 2014, when the LHCb collaboration presented for the first time the measurement of the ratio between the muonic Branching Fraction and the electronic one in the $B^+ \rightarrow K^+\ell^+\ell^-$ channel [76]:

$$\begin{aligned}
 R_{K_{[1,6]}} &\equiv \frac{Br(B^+ \rightarrow K^+\mu^+\mu^-)}{Br(B^+ \rightarrow K^+e^+e^-)} \\
 &= 0.745^{+0.090}_{-0.074} \pm 0.036,
 \end{aligned}
 \tag{5.1}$$

where the subscript refers to the q^2 bin of the measurement, i.e. $1.0 < q^2 < 6.0 \text{ GeV}^2/c^4$. This experimental value shows a deviation of about 2.6σ with respect to the standard theoretical prediction: indeed, the SM value of R_K in the bin provided by the LHCb collaboration is expected to be equal to unity beyond the percent level of accuracy [132, 133]. Moreover, contrary to most of the observables analyzed so far, R_K is the first one to be regarded as insensitive to QCD effects [132]: hence, it can be really viewed as a “clean” observable, and used as a genuine probe for NP effects in $b \rightarrow s$ transitions. It was the first real smoking gun for NP, and further confirmation of its deviation compared to the SM value

by future experiments would definitely point towards the presence of BSM physics in rare B decays.

The most fascinating measurement, however, came out only in 2017, when the measurement of the ratio between the muonic Branching Fraction and the electronic one in the $B \rightarrow K^* \mu^+ \mu^-$ channel was first announced by the LHCb collaboration [83]:

$$R_{K^*_{[0.045,1.1]}} \equiv \frac{Br(B \rightarrow K^* \mu^+ \mu^-)}{Br(B \rightarrow K^* e^+ e^-)} \quad (5.2)$$

$$= 0.660^{+0.110}_{-0.070} \pm 0.024 ,$$

$$R_{K^*_{[1.1,6]}} = 0.685^{+0.113}_{-0.069} \pm 0.047 . \quad (5.3)$$

These measurements have been performed in two separate bins, namely $0.045 < q^2 < 1.1 \text{ GeV}^2/c^4$ and $1.1 < q^2 < 6.0 \text{ GeV}^2/c^4$, in order to isolate in the first

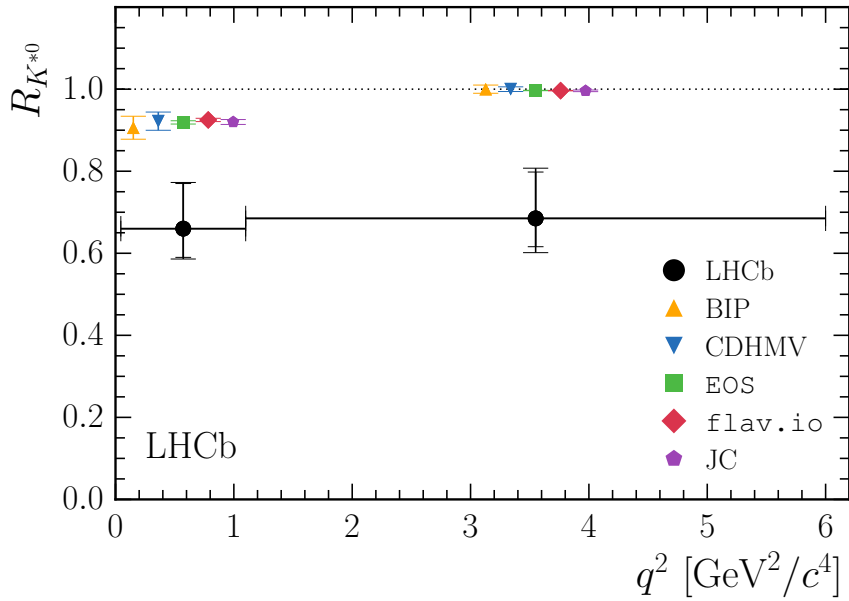


Figure 5.5: Measured values of the $R_{K^{*0}}$ ratio between the differential branching fractions of the $B \rightarrow K^* \mu^+ \mu^-$ and the $B \rightarrow K^* e^+ e^-$ decays (black points) performed by LHCb, based on a data sample corresponding to an integrated luminosity of 3.0 fb^{-1} [83], to be compared with SM predictions from Refs. [133] (orange points), [121] (blue points), [134] (green points), [135] (red points) and [117] (purple points).

bin the effects coming from the proximity to the di-muon threshold. The results confirmed the R_K pattern, showing again a discrepancy of about 2σ with respect to the expected SM predictions from Refs. [117, 121, 133–135], which are in turn all agreeing between each other and predicting a value close to unity to a very good accuracy for the central- q^2 bin and close to 0.9 for the low- q^2 one (due to the aforementioned threshold effects). Once again, this measurement can be viewed as “clean” relatively to hadronic effects, and an explanation in terms of NP effects is the only viable one in case of a further confirmation by future experiments.

5.4 A Comprehensive Phenomenological Interpretation: the $C_{9\mu}^{\text{NP}} \simeq -1$ Case

After the first few anomalies started to arise, the desire to find a comprehensive interpretation of such a pattern drove several phenomenological and theoretical studies towards this common goal.

From the model building point of view, the measurements of R_K and R_{K^*} were definitely the most informative ones: they indeed hint at UV completion of the SM displaying a very characterizing Lepton Flavour Universality violation (LFUV). The most promising of such models capable of accounting for the experimental deviations involve the presence of either leptoquarks and/or Z' gauge bosons, through diagrams such as the ones depicted in Fig. 5.6. Such models were already analyzed after the first few anomalies came out, as can be easily observed looking at the literature [136–166]. However, once the R_{K^*} measurement was announced, this field attracted many researchers with a flourishing production of papers within just a few months [167–213].

On the phenomenological point of view, a first viable scenario was already pointed out when the first NP fits were performed after the measurements of the first anomalies [66, 98, 117, 127, 128]: remarkably simple and straightforward,

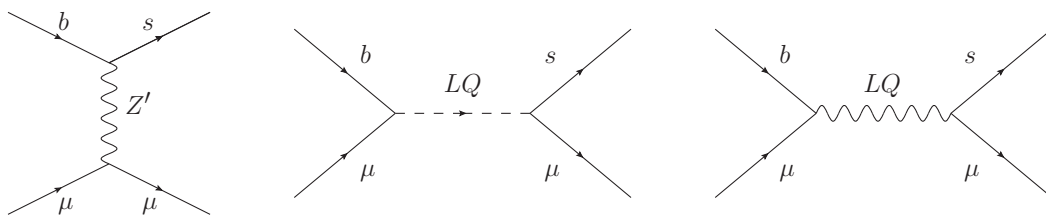


Figure 5.6: Examples of possible NP mediators responsible for the $b \rightarrow s$ anomalies: a Z' gauge boson (left), a scalar leptoquark (center) and a vector leptoquark (right).

it requires just the introduction of NP effects in the vector semi-muonic current Q_{9V}^μ . Indeed, the results of all these studies evidenced how the introduction of a $C_{9\mu}^{\text{NP}} \simeq -1$ was enough to account for all the anomalies, and as new measurements came out this scenario kept being reinforced: this can be easily seen looking at Fig. 5.7, summarizing the results of most of the latest global fits performed after the

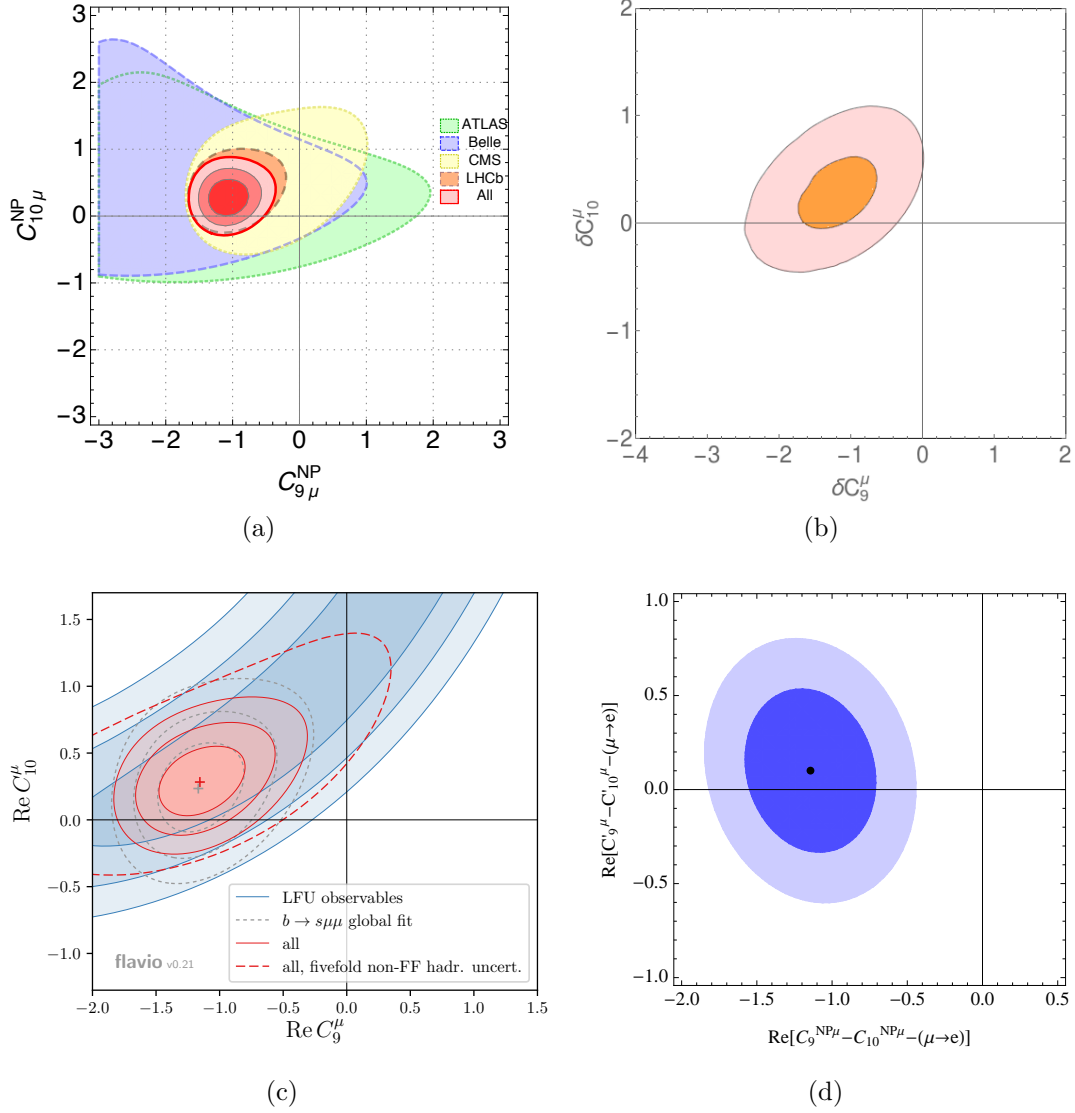


Figure 5.7: Some results for $C_{9\mu}^{\text{NP}}$ and $C_{10\mu}^{\text{NP}}$ obtained from the global fit of all present $b \rightarrow s$ anomalies. In panel (a) are shown the results from Ref. [214]; panel (b) reports the results from Ref. [215]; in panel (c) are displayed the results from Ref. [216] and in panel (d) are reported the results from Ref. [217].

announcement of the R_{K^*} measurements, involving all the present experimental data [214–217]. It is worth to mention that this NP solution has been found out also by the two remaining global fits performed on that very same day: apart from the one I carried out with my collaborators [11] and that I am going to thoroughly describe in the following section, it was pointed out also by the authors of Ref. [218], who however carried out most of their analysis in a $SU(2) \times U(1)$ basis. I will review their work in the following chapter, devoted to SMEFT interpretation of the anomalies.

All the aforementioned global fits investigated also less simple scenarios, where pairs of NP WC were taken in consideration with specific connection between the BSM couplings, guided by specific UV completions. The most promising results (i.e. the best fitting ones) were obtained on two scenarios: the first one involves both vectorial and axial semi-muonic currents, related according to the prescription $C_{9\mu}^{\text{NP}} = -C_{10\mu}^{\text{NP}}$, while the second one relies on both left-handed and right-handed vectorial semi-muonic currents, following the requirement that $C_{9\mu}^{\text{NP}} = -C'_{9,\mu}{}^{\text{NP}}$. Both scenarios fit well the experimental data, even though goodness-of-fit tests pointed towards the $C_{9\mu}^{\text{NP}}$ -only scenario as the best fitting one. It is interesting to notice that all these global fits allowed for several viable NP scenarios, induced by different UV models; however, all of the scenarios definitely agree on the requirement of a $C_{9\mu}^{\text{NP}} \neq 0$ in order to explain the anomalies.

5.5 An Alternative Interpretation: the Axial Solution

After the P_5' anomaly was first measured and the first NP fits started to appear, my collaborators and I decided to start investigating this matter. In particular, we noticed that regarding the treatment of non-perturbative hadronic power corrections, all the community relied on the phenomenological model of Ref. [99]. However, as already stressed in Sec. 4.5, this model misses potentially relevant contributions stemming from the inclusion of multiple soft gluons emissions. Therefore, we decided to perform the analysis reported in Ref. [8] and subsequently updated in Refs. [9, 10]: the goal was to extract the size of such contributions directly from experimental information, employing the LCSR results from Ref. [99] only in the reliable q^2 region, i.e. $q^2 \leq 1 \text{ GeV}^2$, while allowing this contribution to grow approaching the $c\bar{c}$ threshold.

In order to do so, we performed a Bayesian analysis where the main focus was put on the hadronic parameters h_λ appearing in Eq. (4.39), describing the non-factorizable power corrections. Following the definition introduced in Refs. [114], we generalized such corrections parametrizing them by means of the following

Taylor expansion:

$$\begin{aligned}
h_\lambda(q^2) &= \frac{\epsilon_\mu^*(\lambda)}{m_B^2} \int d^4x e^{iqx} \langle \bar{K}^* | T \{ j_{\text{em}}^\mu(x) \mathcal{H}_{\text{eff}}^{\text{had}}(0) \} | \bar{B} \rangle \\
&= h_\lambda^{(0)} + \frac{q^2}{1 \text{ GeV}^2} h_\lambda^{(1)} + \frac{q^4}{1 \text{ GeV}^4} h_\lambda^{(2)}.
\end{aligned} \tag{5.4}$$

The choice of such an expansion, where we decided to keep terms up to the quartic order, was motivated by looking at the shape of Eq. (4.39): indeed, the first two terms of this expansion can be reinterpreted as a (NP) modification of C_7 and C_9 respectively³, while the term $h_\lambda^{(2)}$, introduced in order to allow for a growth of non-perturbative power corrections approaching the $c\bar{c}$ threshold, cannot be reinterpreted as a BSM effect.

It is now mandatory to stress the following point regarding NP searches in this kind of processes: until a more accurate theoretical estimate of $h_\lambda(q^2)$ over the full kinematic range is known, it is not possible to disentangle long-distance, SM contributions such as $h_\lambda^{(0,1)}$ from possible NP ones affecting the size of $C_{7,9}$. This means that, if the result of a SM fit points to a solution with $h_\lambda^{(0,1)}$ producing a non-factorizable contribution compatible in size with the one extracted in Ref. [99] by means of dispersion relations, it is not possible to determine whether the effect is indeed a SM one, or a NP-induced one.

With this caveat in mind, we first performed a SM fit letting the complex parameters $h_\lambda^{(0,1,2)}$ vary in the range $|h_\lambda^{(0,1,2)}| < 2 \times 10^{-3}$, with no constrain on the phase and using flat priors. We imposed for $q^2 \leq 1 \text{ GeV}^2$ the results from Ref. [99], given in terms of the quantities $\tilde{g}^{\mathcal{M}_i}$ which are related to the h_λ as follows:

$$\tilde{g}^{\mathcal{M}_1} = -\frac{1}{2C_1} \frac{16m_B^3(m_B + m_{K^*})\pi^2}{\sqrt{\lambda(q^2)}V(q^2)q^2} (h_-(q^2) - h_+(q^2)), \tag{5.5}$$

$$\tilde{g}^{\mathcal{M}_2} = -\frac{1}{2C_1} \frac{16m_B^3\pi^2}{(m_B + m_{K^*})A_1(q^2)q^2} (h_-(q^2) + h_+(q^2)), \tag{5.6}$$

$$\begin{aligned}
\tilde{g}^{\mathcal{M}_3} &= \frac{1}{2C_1} \left[\frac{64\pi^2 m_B^3 m_{K^*} \sqrt{q^2} (m_B + m_{K^*})}{\lambda(q^2) A_2(q^2) q^2} h_0(q^2) \right. \\
&\quad \left. - \frac{16m_B^3\pi^2(m_B + m_{K^*})(m_B^2 - q^2 - m_{K^*}^2)}{\lambda(q^2) A_2(q^2) q^2} (h_-(q^2) + h_+(q^2)) \right].
\end{aligned} \tag{5.7}$$

The results for the parameters defining the non-factorizable power corrections h_λ are reported in Fig. 5.8: it is interesting to notice that $|h_-^{(2)}|$ is different from

³Rigorously speaking, $h_\lambda^{(0,1)}$ should be first multiplied by q^2 -dependent form factors, if one want to exactly perform such reinterpretation; however, as can be easily checked looking at Ref. [88], the q^2 dependance of such form factors is so mild that they won't spoil the identification with the current level of precision.

zero at more than 95.45% probability, thus disfavouring the interpretation of the hadronic correction as NP effects to the operators $Q_{7,9}$. In order to compare such results for h_λ with the results for $\tilde{g}^{\mathcal{M}_i}$ from Ref. [99], the reader may look at Fig. 5.9. It is easy to check that the contribution increases while approaching the $c\bar{c}$ threshold, as it should given the growing effect of multiple soft-gluon emissions, displaying an appreciable q^2 dependence induced by $|h_-^{(2)}|$. However, the results are still in the same ballpark as the ones from Ref. [99], hence potentially not beyond the expected size within the SM.

It is now interesting to take a look at the observables obtained including such hadronic contributions. In Fig. 5.10 we show the results for the angular observables in the S basis of the full fit to the LHCb measurements from Refs. [72, 78] reported in Tab. 5.1. The corresponding numerical results are reported in the “full fit” column of Tab. 5.1. It’s easy to check that, with the hadronic contributions obtained by our fit, it is possible to generate an S_5 (and hence a P'_5) compatible with experimental data.

Aside from the full fit, we also produced predictions for each observable on each bin, and the relative p -value. For uncorrelated observables, such as the BR’s, this was done simply removing the experimental information on the respective observable. On the other hand, this procedure had to be generalized for correlated observables in order to take both theoretical and experimental correlations into account; since the angular observables are correlated in each bin, we proceeded removing all the experimental information in on bin at a time from the fit in order to obtain the predictions; the fit produced a correlation matrix for such predicted observables, which was added to the experimental one and used to compute the corresponding log likelihood and, consequently, the p -value.

For completeness and easy comparison, in Tab. 5.1 we report also the results and predictions for the optimized observable P'_5 , which is however not independent from the other observables in Tab. 5.1 and hence not directly used in the fit.

The bottom line of our first work in this field was therefore that, given both the present hadronic uncertainties and the present experimental data, looking at the $B \rightarrow K^* \mu^+ \mu^-$ decay alone is not enough to determine whether NP is present in $b \rightarrow s$ transitions. Indeed, we showed that an underestimation of hadronic effects due to non-factorizable power corrections, which are still not under total control in the SM, could very well be the reason behind the discrepancies between the SM predictions of Refs. [116, 128] and the experimental measurements from LHCb [78], Belle [79, 80] and ATLAS [82].

Par.	Abs. value	Phase (rad)
$h_0^{(0)}$	$(5.7 \pm 2.0) \cdot 10^{-4}$	3.57 ± 0.55
$h_0^{(1)}$	$(2.3 \pm 1.6) \cdot 10^{-4}$	0.1 ± 1.1
$h_0^{(2)}$	$(2.8 \pm 2.1) \cdot 10^{-5}$	-0.2 ± 1.7
$h_+^{(0)}$	$(7.9 \pm 6.9) \cdot 10^{-6}$	0.1 ± 1.7
$h_+^{(1)}$	$(3.8 \pm 2.8) \cdot 10^{-5}$	-0.7 ± 1.9
$h_+^{(2)}$	$(1.4 \pm 1.0) \cdot 10^{-5}$	3.5 ± 1.6
$h_-^{(0)}$	$(5.4 \pm 2.2) \cdot 10^{-5}$	3.2 ± 1.4
$h_-^{(1)}$	$(5.2 \pm 3.8) \cdot 10^{-5}$	0.0 ± 1.7
$h_-^{(2)}$	$(2.5 \pm 1.0) \cdot 10^{-5}$	0.09 ± 0.77

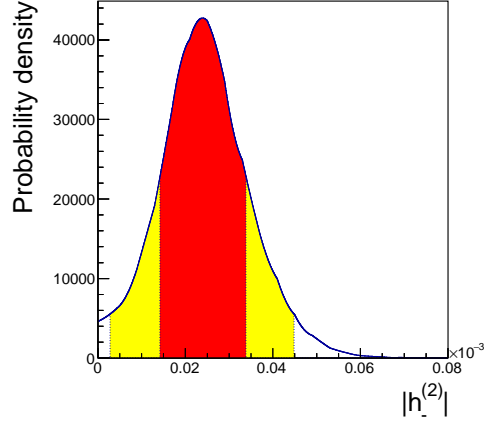


Figure 5.8: Left: results of the full fit for the h_λ parameters, obtained employing the results from Ref. [99] only for $q^2 \simeq 1 \text{ GeV}^2$. Right: p.d.f. for the absolute value of $h_-^{(2)}$; the red (yellow) colours identify the 68% (95%) probability region.

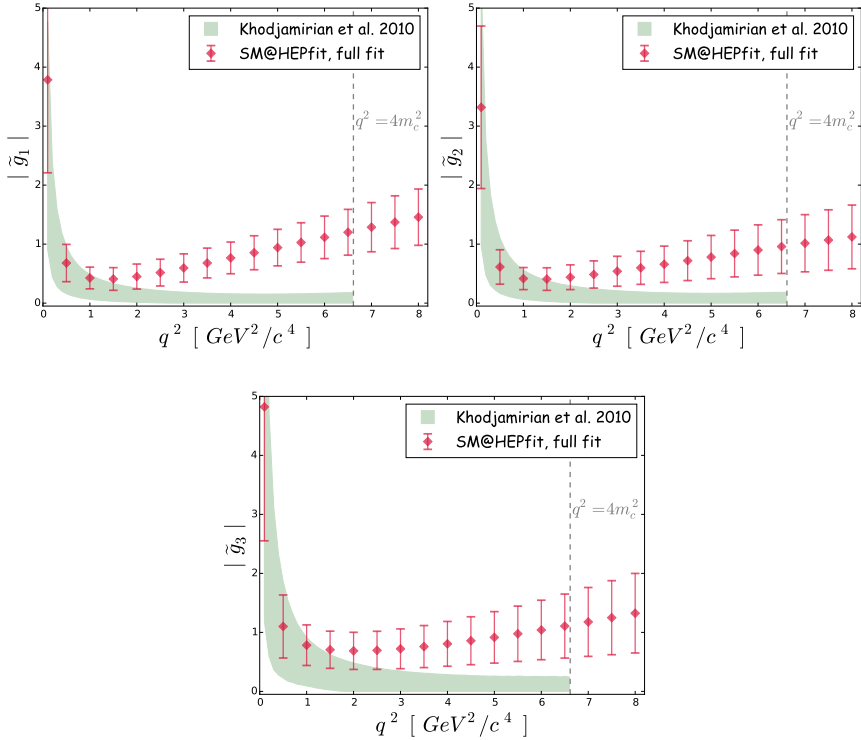


Figure 5.9: Results of the fit for $|\tilde{g}_{1,2,3}|$ defined in ref. [99] as a function of q^2 together with the phenomenological parametrization suggested in the same paper.

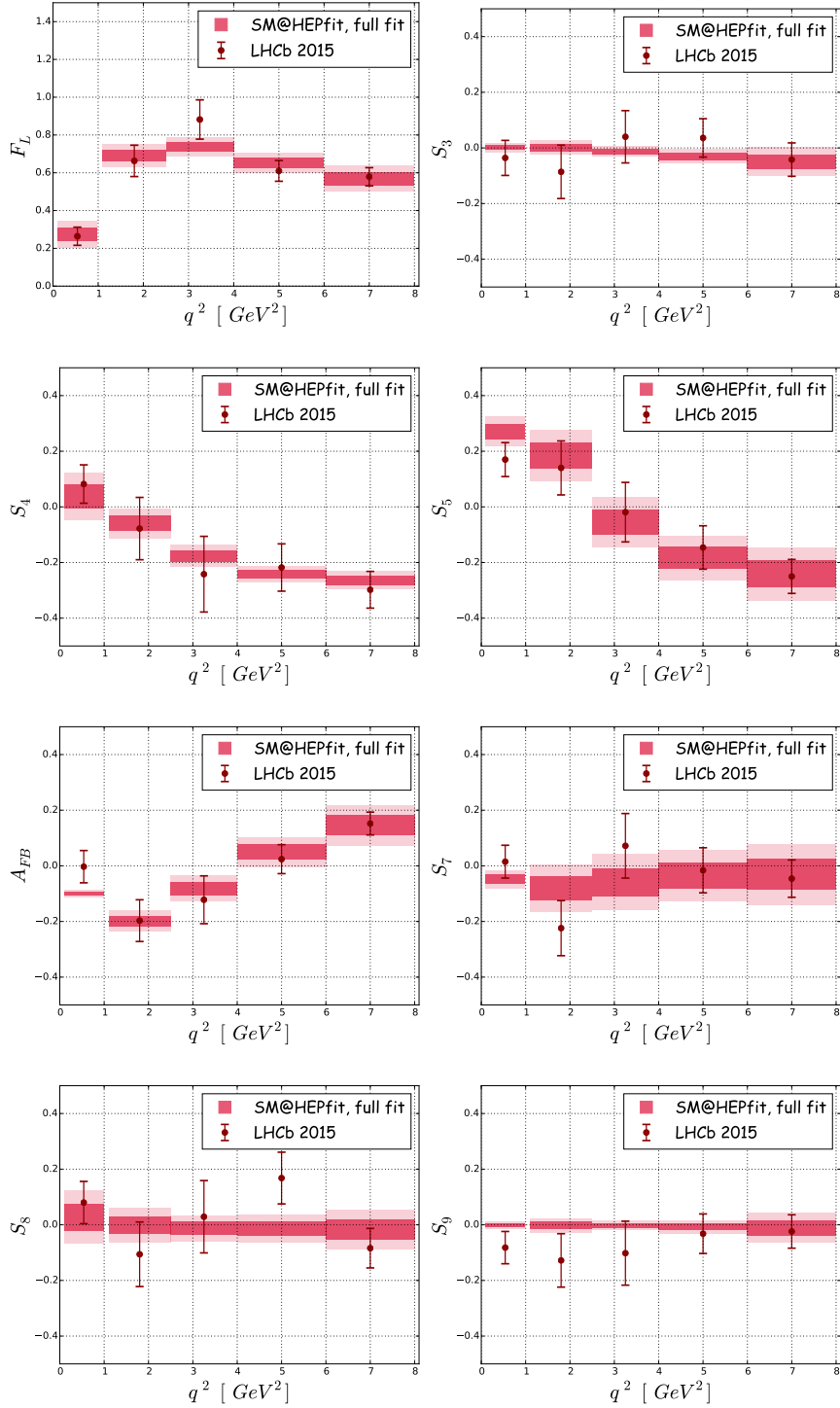


Figure 5.10: Results of the full fit and experimental results for the $B \rightarrow K^* \mu^+ \mu^-$ angular observables, obtained employing the results from Ref. [99] only for $q^2 \simeq 1 \text{ GeV}^2$. The darker (lighter) colours identify the 68% (95%) probability regions.

q^2 bin [GeV ²]	Observable	measurement	full fit	prediction	p – value
[0.1, 0.98]	F_L	0.264 ± 0.048	0.275 ± 0.035	0.257 ± 0.035	0.13
	S_3	-0.036 ± 0.063	0.002 ± 0.008	0.002 ± 0.008	
	S_4	0.082 ± 0.069	0.037 ± 0.042	-0.025 ± 0.047	
	S_5	0.170 ± 0.061	0.271 ± 0.027	0.301 ± 0.024	
	A_{FB}	-0.003 ± 0.058	-0.102 ± 0.006	-0.104 ± 0.006	
	S_7	0.015 ± 0.059	-0.049 ± 0.016	-0.043 ± 0.017	
	S_8	0.080 ± 0.076	0.027 ± 0.048	-0.004 ± 0.046	
	S_9	-0.082 ± 0.058	-0.002 ± 0.007	-0.002 ± 0.007	
	P'_5	0.387 ± 0.142	0.774 ± 0.094	0.881 ± 0.082	
	[1.1, 2.5]	F_L	0.663 ± 0.083	0.691 ± 0.030	0.688 ± 0.034
S_3		-0.086 ± 0.096	0.000 ± 0.013	0.001 ± 0.013	
S_4		-0.078 ± 0.112	-0.059 ± 0.027	-0.070 ± 0.032	
S_5		0.140 ± 0.097	0.183 ± 0.046	0.208 ± 0.057	
A_{FB}		-0.197 ± 0.075	-0.198 ± 0.019	-0.200 ± 0.022	
S_7		-0.224 ± 0.099	-0.081 ± 0.042	-0.056 ± 0.049	
S_8		-0.106 ± 0.116	-0.003 ± 0.031	-0.004 ± 0.033	
S_9		-0.128 ± 0.096	-0.002 ± 0.013	0.002 ± 0.013	
P'_5		0.298 ± 0.212	0.410 ± 0.099	0.460 ± 0.120	0.51
[2.5, 4]		F_L	0.882 ± 0.104	0.739 ± 0.025	0.729 ± 0.028
	S_3	0.040 ± 0.094	-0.012 ± 0.009	-0.014 ± 0.010	
	S_4	-0.242 ± 0.136	-0.176 ± 0.020	-0.179 ± 0.021	
	S_5	-0.019 ± 0.107	-0.055 ± 0.045	-0.055 ± 0.052	
	A_{FB}	-0.122 ± 0.086	-0.082 ± 0.023	-0.082 ± 0.025	
	S_7	0.072 ± 0.116	-0.059 ± 0.050	-0.080 ± 0.055	
	S_8	0.029 ± 0.130	-0.012 ± 0.023	-0.012 ± 0.023	
	S_9	-0.102 ± 0.115	-0.003 ± 0.009	-0.003 ± 0.009	
	P'_5	-0.077 ± 0.354	-0.130 ± 0.100	-0.130 ± 0.120	0.89
	[4, 6]	F_L	0.610 ± 0.055	0.653 ± 0.026	0.661 ± 0.030
S_3		0.036 ± 0.069	-0.030 ± 0.013	-0.030 ± 0.015	
S_4		-0.218 ± 0.085	-0.241 ± 0.014	-0.239 ± 0.016	
S_5		-0.146 ± 0.078	-0.183 ± 0.040	-0.205 ± 0.046	
A_{FB}		0.024 ± 0.052	0.050 ± 0.027	0.067 ± 0.032	
S_7		-0.016 ± 0.081	-0.034 ± 0.046	-0.037 ± 0.055	
S_8		0.168 ± 0.093	-0.015 ± 0.025	-0.026 ± 0.026	
S_9		-0.032 ± 0.071	-0.007 ± 0.012	-0.012 ± 0.014	
P'_5		-0.301 ± 0.160	-0.388 ± 0.087	-0.440 ± 0.100	0.46
[6, 8]		F_L	0.579 ± 0.048	0.569 ± 0.034	0.517 ± 0.070
	S_3	-0.042 ± 0.060	-0.050 ± 0.026	-0.006 ± 0.054	
	S_4	-0.298 ± 0.066	-0.264 ± 0.016	-0.224 ± 0.037	
	S_5	-0.250 ± 0.061	-0.241 ± 0.048	-0.164 ± 0.100	
	A_{FB}	0.152 ± 0.041	0.146 ± 0.036	0.099 ± 0.077	
	S_7	-0.046 ± 0.067	-0.031 ± 0.055	0.010 ± 0.110	
	S_8	-0.084 ± 0.071	-0.017 ± 0.035	0.039 ± 0.055	
	S_9	-0.024 ± 0.060	-0.011 ± 0.027	0.018 ± 0.047	
	P'_5	-0.505 ± 0.124	-0.491 ± 0.098	-0.330 ± 0.200	0.46
	[0.1, 2] [2, 4.3] [4.3, 8.68]	BR $\cdot 10^7$	0.58 ± 0.09	0.65 ± 0.04	0.67 ± 0.04
0.29 ± 0.05			0.33 ± 0.03	0.35 ± 0.04	0.35
0.47 ± 0.07			0.45 ± 0.05	0.47 ± 0.11	1.0
	BR $_{B \rightarrow K^* \gamma} \cdot 10^5$	4.33 ± 0.15	4.35 ± 0.14	4.61 ± 0.56	0.63

Table 5.1: Experimental results (with symmetrized errors) from Refs. [72, 78], results from the full fit, predictions and p -values for $B \rightarrow K^* \mu^+ \mu^-$ BR's and angular observables, obtained employing the results from Ref. [99] only for $q^2 \simeq 1 \text{ GeV}^2$. The predictions are obtained removing the corresponding observable from the fit. For the angular observables, experimentally correlated in each bin, the predictions are obtained removing from the fit all angular observables in one bin at a time. See the text for details. The results for BR($B \rightarrow K^* \gamma$) (including the experimental value from refs. [219–222]) and for the optimized observable P'_5 are also reported. The latter is however not explicitly used in the fit as a constraint, since it is not independent of F_L and S_5 .

However, once the experimental results for the Branching Fractions ratios are taken into account, the situation changes: non-factorizable correction, independent from their size, cannot be responsible of LFUV since they are completely washed out in ratios; moreover, as already pointed out in Sec. 5.2, the hadronic contribution in $B \rightarrow K\mu^+\mu^-$ is under control according to Ref. [131], making R_K more clean and reliable from the theoretical point of view. Therefore, barring experimental flukes in both LHCb measurements of R_K [76] and R_{K^*} [83], NP has to be the lone physical explanation underling such experimental deviations.

Nevertheless, in our following work [11] we inspected whether a more conservative approach on the size of non-factorizable power corrections could have effects on the sensitivity to NP and, more importantly, whether it could also unveil different NP scenarios not viable when a more “dogmatic” approach is used. In order to do so, we tested several NP scenarios in both approaches: a Phenomenological Model Driven (PMD) one, which relies on the phenomenological model from Ref. [99], and a Phenomenological and Data Driven (PDD) approach, which makes use of the results of Ref. [99] only for $q^2 \leq 1 \text{ GeV}^2$ and allows for larger values as q^2 grows.

To address the necessity to compare different scenarios and discriminate their validity, we used the Information Criterion [223, 224], defined as

$$IC = -2\overline{\log L} + 4\sigma_{\log L}^2, \quad (5.8)$$

where $\overline{\log L}$ is the log-likelihood average and $\sigma_{\log L}^2$ is its variance. The introduction of the second term in Eq. (5.8) is really important, since it takes into account the effective number of parameters in the model, hence allowing for a meaningful comparison of models with different number of parameters. This quantity is built in such a way that smaller IC values point towards preferred models.

As a first step in our analysis, we started analyzing the most widely studied NP scenario in both our approaches: the $C_{9\mu}^{\text{NP}} \neq 0$ scenario, where we also allowed for a non-null $C_{10\mu}^{\text{NP}}$ (indicated as the scenario **(II)** in Ref. [11]). The NP results for such analyses are shown in Fig. 5.11, with the left green panel displaying the PMD approach results while the right red panel displays the PDD ones. It is easy to observe that the PMD results are compatible with the ones obtained by the remaining global fits from Refs. [214–217], shown in Fig. 5.7, with an evidence for NP at more than 5σ . On the other hand, the PDD result shows a significantly reduced NP evidence, roughly between 3σ and 4σ , with a slightly improved IC value due to the effect of hadronic corrections in accommodating data.

The second scenario object of our interest already drew attention in the past: the one involving both C_9^{NP} and C_{10}^{NP} , with $C_{10,\mu,e}^{\text{NP}} = -C_{9,\mu,e}^{\text{NP}}$ (indicated as the scenario **(V)** in Ref. [11]); for completeness, we also allowed for a $C_7^{\text{NP}} \neq 0$. The results are shown in Fig. 5.12, for both the PMD and the PDD approach. In both

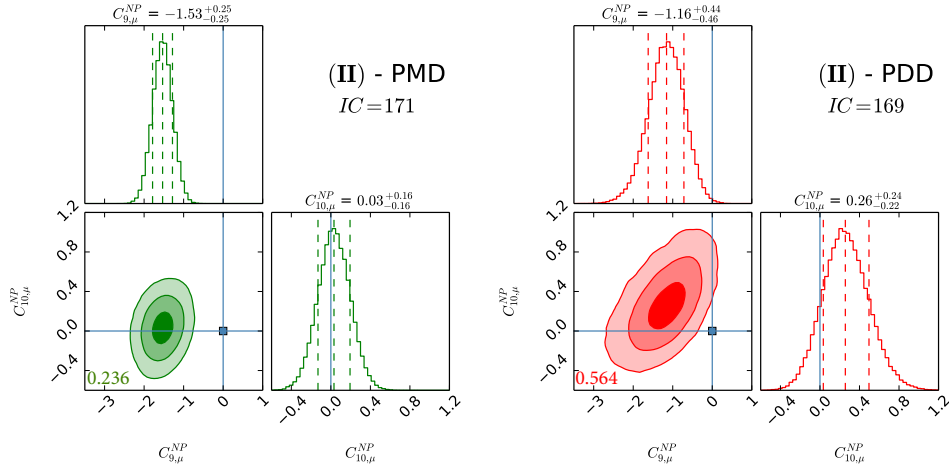


Figure 5.11: The fit result for the scenario involving $C_{9,\mu}^{NP}$ and $C_{10,\mu}^{NP}$. Here and in the following, PMD approach results are shown in the left green panel, while PDD ones are in the right red panel. In the 1D distributions we show the 16th, 50th and 84th percentile, marked with the dashed lines, while in the correlation plots (where the correlation is also reported) we show the 1, 2 and 3 σ contours, in decreasing degrees of transparency. The blue square and lines identify the SM limit. We also report IC values for the two approaches (see Eq. (5.8)).

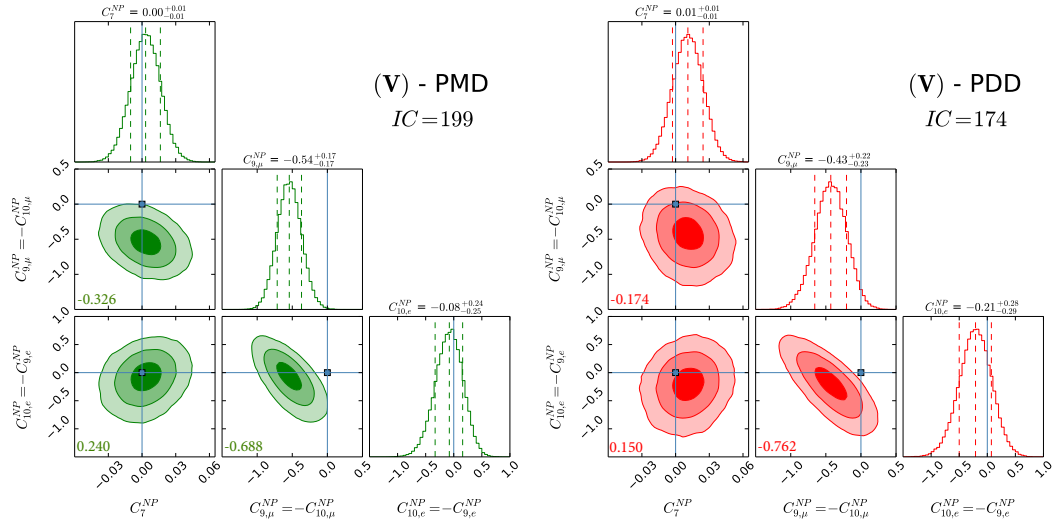


Figure 5.12: The fit result for the scenario involving C_7^{NP} , $C_{9,\mu}^{NP}$, $C_{9,e}^{NP}$ and $C_{10,\mu,e}^{NP} = -C_{9,e}^{NP}$. See caption of figure 5.11 for the colour coding and further details.

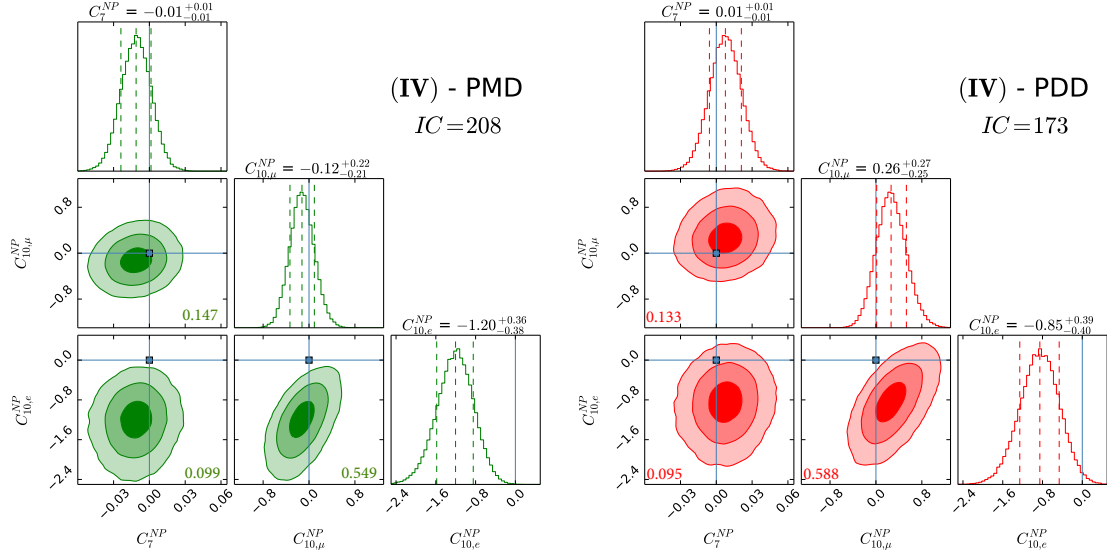


Figure 5.13: The fit result for the scenario involving C_7^{NP} , $C_{10,\mu}^{NP}$ and $C_{10,e}^{NP}$. See caption of figure 5.11 for the colour coding and further details.

the approaches we obtained values compatible with zero for both C_7^{NP} (which is mainly constrained by the inclusive $B \rightarrow X_s \gamma$ Branching Fraction, as shown in Ref. [225]) and for $C_{9,e}^{NP} = -C_{10,e}^{NP}$, since the anomalies in the angular observables for $B \rightarrow K^* \mu^+ \mu^-$ require NP effects in the muonic sector: therefore, all the evidence of NP resides in $C_{9,\mu}^{NP} = -C_{10,\mu}^{NP}$, which is found to be different from zero at 3σ , with allowed values compatible with the ones found in Refs. [214, 216]. Once again, as expected, the PDD approach softens the evidence for NP (the WC now sits only 2σ away from the null value), with a sizably lower value for the IC . It is worth to mention that, while the PDD IC value is compatible with the ones obtained for both approaches in the previous scenario, this is not the case for the PMD approach: this implies that, while under the PDD approach both scenarios are equally preferred by data, this is not the case for the PMD approach, where the “uncorrelated” scenario is preferred in comparison with the one where the condition $C_{9,\mu}^{NP} = -C_{10,\mu}^{NP}$ is required.

As a third scenario, we decided to test a set of NP WCs that had not yet been taken in consideration by previous global fits, since it does not involve the presence of $C_{9,\mu}^{NP}$: indeed, we performed a fit for a NP scenario involving only C_7^{NP} and $C_{10,\mu,e}^{NP}$ (indicated as the scenario **(IV)** in Ref. [11]). The results for this scenario are shown in Fig. 5.13, as usually for both the PMD and the PDD approach, and are very informative. NP effects in the dipole operator and in the axial semi-leptonic currents cannot address at the same time both the BF ratios

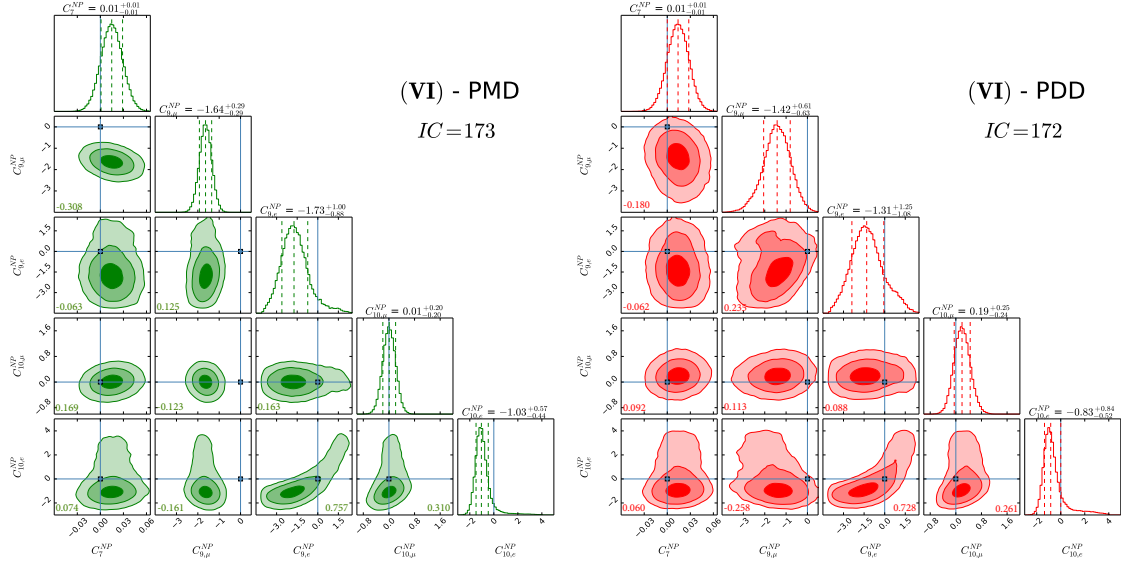


Figure 5.14: The fit result for the scenario involving C_7^{NP} , $C_{9,\mu}^{NP}$, $C_{9,e}^{NP}$, $C_{10,\mu}^{NP}$ and $C_{10,e}^{NP}$. See caption of figure 5.11 for the colour coding and further details.

R_{K,K^*} and the angular observable P'_5 , without allowing for large non-factorizable power corrections. Indeed, the fit does not perform well in the PMD scenario, as can be easily inferred by looking at the IC value and comparing it with the ones obtained for the previous scenarios. Most likely this is the reason why this scenario have not been tested by any other collaboration so far, given its bad performance. However, the situation dramatically changes once a more conservative handling of hadronic power correction is employed, following the prescriptions of the PDD approach. In fact, allowing for a larger size for the non-factorizable contribution, it is possible to rely upon them to reproduce the $B \rightarrow K^* \mu^+ \mu^-$ angular observables data, as was shown in our previous work [8]. Therefore, once the muonic angular observables are taken into account, it is possible to accommodate for the BF ratios R_K and R_{K^*} by means of NP effects in the axial semi-electronic current. We therefore obtained evidence for a $C_{10,e}^{NP}$ at $\sim 2\sigma$, but most importantly an IC value of the same order of the ones obtained for the previous scenarios, hence showing that also this *axial solution* is viable, under the PDD approach.

As a final scenario, we also performed a fit with all 5 NP WCs switched on, without imposing any relation between them: this is the scenario indicated as **(VI)** in Ref. [11], and the results of the fit are shown in Fig. 5.14. The IC values for the two scenarios are compatible both among themselves and with the previous well-fitting cases. It is interesting to notice that current experimental data are informative enough to constrain, at the same time, all the NP WCs in

both approaches. Moreover, the PDD approach employed in this scenario, thanks to a nontrivial interplay among the NP effects encoded both in $C_{9,\mu}^{NP}$ and $C_{10,e}^{NP}$ and the hadronic contributions, produces the weakest NP evidence provided by our global analysis – sitting between 2σ and 3σ level – while allowing for a very good description of the entire data set.

The numerical values for the mean and standard deviation for the NP WCs together with the absolute values of h_λ can be found in Tabs. 5.2–5.3 for the PMD and PDD approach respectively, for all the scenarios analyzed above⁴. Analogously, the results for the observables of main interest, i.e. the BF ratios R_K and R_{K^*} and the angular observable P'_5 , are reported in Tabs. 5.4–5.5 for all the NP scenarios, along with the experimental measurements, for the PMD and PDD approach respectively.

⁴Since h_0 enters the decay amplitude of Eq. (4.39) with an additional factor of $\sqrt{q^2}$ with respect to h_\pm due to Eq. (4.49), we dropped $h_0^{(2)}$ in all our analysis in Ref. [11].

Par.	(II)	(IV)	(V)	(VI)
C_7^{NP}	–	-0.011 ± 0.013	0.003 ± 0.013	0.015 ± 0.014
$C_{9,\mu}^{NP}$	-1.53 ± 0.25	–	-0.54 ± 0.17	-1.64 ± 0.29
$C_{9,e}^{NP}$	–	–	0.09 ± 0.25	-1.6 ± 1.0
$C_{10,\mu}^{NP}$	0.03 ± 0.16	-0.12 ± 0.22	0.54 ± 0.17	0.009 ± 0.200
$C_{10,e}^{NP}$	–	-1.22 ± 0.37	-0.09 ± 0.25	-0.91 ± 0.76
$ h_0^{(0)} \cdot 10^4$	2.0 ± 1.2	1.8 ± 1.2	1.3 ± 1.0	2.0 ± 1.3
$ h_+^{(0)} \cdot 10^4$	0.079 ± 0.067	0.083 ± 0.069	0.086 ± 0.072	0.076 ± 0.064
$ h_-^{(0)} \cdot 10^4$	0.54 ± 0.19	0.56 ± 0.20	0.60 ± 0.21	0.52 ± 0.19
$ h_0^{(1)} \cdot 10^4$	0.30 ± 0.22	0.45 ± 0.26	0.32 ± 0.24	0.28 ± 0.22
$ h_+^{(1)} \cdot 10^4$	0.22 ± 0.19	0.21 ± 0.19	0.26 ± 0.22	0.22 ± 0.19
$ h_-^{(1)} \cdot 10^4$	0.23 ± 0.19	0.30 ± 0.21	0.32 ± 0.22	0.23 ± 0.19
$ h_+^{(2)} \cdot 10^4$	0.053 ± 0.045	0.046 ± 0.042	0.064 ± 0.053	0.050 ± 0.044
$ h_-^{(2)} \cdot 10^4$	0.046 ± 0.039	0.092 ± 0.050	0.070 ± 0.047	0.045 ± 0.038

Table 5.2: Results from the fit for NP WCs and hadronic contributions in the PMD approach, for the 4 NP scenarios analyzed in the text.

Par.	(II)	(IV)	(V)	(VI)
C_7^{NP}	–	0.008 ± 0.014	0.011 ± 0.014	0.014 ± 0.014
$C_{9,\mu}^{\text{NP}}$	-1.17 ± 0.46	–	-0.43 ± 0.23	-1.43 ± 0.64
$C_{9,e}^{\text{NP}}$	–	–	0.21 ± 0.29	-1.2 ± 1.2
$C_{10,\mu}^{\text{NP}}$	0.26 ± 0.23	0.27 ± 0.26	0.43 ± 0.23	0.20 ± 0.25
$C_{10,e}^{\text{NP}}$	–	-0.86 ± 0.4	-0.21 ± 0.29	-0.60 ± 0.99
$ h_0^{(0)} \cdot 10^4$	2.3 ± 1.4	1.7 ± 1.3	1.7 ± 1.3	2.6 ± 1.6
$ h_+^{(0)} \cdot 10^4$	0.081 ± 0.070	0.086 ± 0.075	0.087 ± 0.075	0.077 ± 0.067
$ h_-^{(0)} \cdot 10^4$	0.55 ± 0.22	0.60 ± 0.23	0.59 ± 0.23	0.53 ± 0.21
$ h_0^{(1)} \cdot 10^4$	0.41 ± 0.34	0.50 ± 0.36	0.46 ± 0.37	0.40 ± 0.33
$ h_+^{(1)} \cdot 10^4$	0.42 ± 0.30	0.39 ± 0.29	0.42 ± 0.30	0.41 ± 0.30
$ h_-^{(1)} \cdot 10^4$	0.52 ± 0.38	0.82 ± 0.46	0.73 ± 0.43	0.50 ± 0.37
$ h_+^{(2)} \cdot 10^4$	0.160 ± 0.099	0.139 ± 0.094	0.160 ± 0.100	0.145 ± 0.095
$ h_-^{(2)} \cdot 10^4$	0.126 ± 0.098	0.190 ± 0.100	0.170 ± 0.110	0.124 ± 0.094

Table 5.3: Results from the fit for WCs and hadronic contributions in the PDD approach, for the 4 NP scenarios analyzed in the text.

Obs.	Exp. value	(II)	(IV)	(V)	(VI)
$R_{K[1,6]}$	0.753 ± 0.090	0.703 ± 0.047	0.781 ± 0.055	0.740 ± 0.061	0.724 ± 0.067
$R_{K^*[0.045,1.1]}$	0.680 ± 0.093	0.881 ± 0.016	0.839 ± 0.024	0.858 ± 0.019	0.843 ± 0.030
$R_{K^*[1.1,6]}$	0.707 ± 0.102	0.786 ± 0.049	0.713 ± 0.065	0.740 ± 0.060	0.717 ± 0.067
$P_{5[4,6]}^{\text{LHCb}}$	-0.301 ± 0.160	-0.427 ± 0.061	-0.556 ± 0.063	-0.587 ± 0.053	-0.431 ± 0.061
$P_{5[6,8]}^{\text{LHCb}}$	-0.505 ± 0.124	-0.607 ± 0.061	-0.677 ± 0.066	-0.704 ± 0.057	-0.61 ± 0.06
$P_{5[4,6]}^{\text{ATLAS}}$	-0.26 ± 0.39	-0.427 ± 0.061	-0.556 ± 0.063	-0.587 ± 0.053	-0.431 ± 0.061
$P_{5[4.3,6]}^{\text{CMS}}$	-0.955 ± 0.268	-0.447 ± 0.061	-0.572 ± 0.063	-0.603 ± 0.053	-0.451 ± 0.061
$P_{5[6,8.68]}^{\text{CMS}}$	-0.660 ± 0.220	-0.626 ± 0.061	-0.688 ± 0.067	-0.711 ± 0.058	-0.63 ± 0.06
$P_{5[4,8]}^{\text{Belle}}$	-0.025 ± 0.318	-0.524 ± 0.059	-0.620 ± 0.063	-0.649 ± 0.053	-0.528 ± 0.059
$P_{5,e[4,8]}^{\text{Belle}}$	-0.510 ± 0.272	-0.794 ± 0.039	-0.536 ± 0.063	-0.710 ± 0.044	-0.42 ± 0.23

Table 5.4: Experimental results (with symmetrized errors) and results from the fit for key observables in the PMD approach, for the 4 NP scenarios analyzed in the text.

Obs.	Exp. value	(II)	(IV)	(V)	(VI)
$R_{K[1,6]}$	0.753 ± 0.090	0.714 ± 0.064	0.775 ± 0.057	0.740 ± 0.062	0.719 ± 0.073
$R_{K^*[0.045,1.1]}$	0.680 ± 0.093	0.873 ± 0.016	0.842 ± 0.024	0.861 ± 0.019	0.847 ± 0.030
$R_{K^*[1.1,6]}$	0.707 ± 0.102	0.777 ± 0.053	0.714 ± 0.066	0.755 ± 0.059	0.722 ± 0.069
$P_{5[4,6]}^{\text{LHCb}}$	-0.301 ± 0.160	-0.405 ± 0.068	-0.435 ± 0.065	-0.421 ± 0.068	-0.417 ± 0.068
$P_{5[6,8]}^{\text{LHCb}}$	-0.505 ± 0.124	-0.521 ± 0.083	-0.521 ± 0.080	-0.508 ± 0.082	-0.545 ± 0.083
$P_{5[4,6]}^{\text{ATLAS}}$	-0.26 ± 0.39	-0.405 ± 0.068	-0.435 ± 0.065	-0.421 ± 0.068	-0.417 ± 0.068
$P_{5[4,3,6]}^{\text{CMS}}$	-0.955 ± 0.268	-0.420 ± 0.068	-0.447 ± 0.066	-0.434 ± 0.068	-0.433 ± 0.068
$P_{5[6,8,68]}^{\text{CMS}}$	-0.660 ± 0.220	-0.531 ± 0.086	-0.529 ± 0.084	-0.514 ± 0.085	-0.556 ± 0.086
$P_{5[4,8]}^{\text{Belle}}$	-0.025 ± 0.318	-0.467 ± 0.072	-0.481 ± 0.070	-0.467 ± 0.072	-0.486 ± 0.072
$P_{5,e[4,8]}^{\text{Belle}}$	-0.510 ± 0.272	-0.664 ± 0.095	-0.424 ± 0.063	-0.570 ± 0.066	-0.41 ± 0.22

Table 5.5: Experimental results (with symmetrized errors) and results from the fit for key observables in the PDD approach, for the 4 NP scenarios analyzed in the text.

Chapter 6

A Systematic Analysis of the $b \rightarrow s$ Anomalies Employing the SMEFT Framework

In Chapter 5 I have reviewed the status of the anomalies affecting the $b \rightarrow s$ transitions and the mainstream NP interpretation advocated to address such a pattern. Moreover, I have also shown how a cautious handling of the hadronic uncertainties might yield to a broader range of viable NP scenarios. All these studies have been carried out in a WET framework. The goal of the final chapter of this Part is therefore to reinterpret these results within the SMEFT framework, trying to constrain in the most systematic way the $SU(2) \times U(1)$ WCs.

The first part of this chapter will be devoted to identifying the SMEFT operators involved in $b \rightarrow s$ transitions, and matching them to the WET ones. Subsequently, the global fit discussed in Sec. 5.5 will be performed again, after the change of basis has been applied. Finally, an analysis of the results is shown, with an eye on possible future generalizations.

6.1 The Operators Involved

The list of SMEFT operators that can affect the dynamics of $b \rightarrow s$ transitions has already been known for a few years [136, 226]. It contains operators coming from three of the eight classes defined in Sec. 3.2.1, and can be therefore catalogued accordingly. Here and in the following, the chiral fermions subscripts will indicate their flavour content in the basis where the down-type quark mass matrix is diagonal. It is obviously possible to choose a different basis, but given that the observables of interest involve down-type quarks this choice minimize the number of operators involved.

The first sub-list of operators comes from class 6, containing the dipole operators:

$$Q_{dW} = (\bar{q}_s \sigma^{\mu\nu} d_b) \tau^I \varphi W_{\mu\nu}^I, \quad (6.1)$$

$$Q'_{dW} = \varphi^\dagger \tau^I (\bar{d}_b \sigma^{\mu\nu} q_s) W_{\mu\nu}^I, \quad (6.2)$$

$$Q_{dB} = (\bar{q}_s \sigma^{\mu\nu} d_b) \varphi B_{\mu\nu}, \quad (6.3)$$

$$Q'_{dB} = \varphi^\dagger (\bar{d}_b \sigma^{\mu\nu} q_s) B_{\mu\nu}. \quad (6.4)$$

The second sub-list of operators stems from class 7, and includes operators involving a fermion current and an Higgs current:

$$Q_{Hq}^{(1)} = (\varphi^\dagger i \overleftrightarrow{D}_\mu \varphi) (\bar{q}_s \gamma^\mu q_b), \quad (6.5)$$

$$Q_{Hq}^{(3)} = (\varphi^\dagger i \overleftrightarrow{D}_\mu^I \varphi) (\bar{q}_s \tau^I \gamma^\mu q_b), \quad (6.6)$$

$$Q_{Hd} = (\varphi^\dagger i \overleftrightarrow{D}_\mu \varphi) (\bar{d}_s \gamma^\mu d_b). \quad (6.7)$$

The final sub-list is by far the largest one, and is a sub-set of the class 8, four-quark operators; this is the only sub-list not blind to lepton content, and therefore these operators can be further divided in according to the lepton involved. The electron operators are:

$$Q_{lq}^{(1),e} = (\bar{l}_e \gamma^\mu l_e) (\bar{q}_s \gamma^\mu q_b), \quad (6.8)$$

$$Q_{lq}^{(3),e} = (\bar{l}_e \gamma^\mu \tau^I l_e) (\bar{q}_s \gamma^\mu \tau^I q_b), \quad (6.9)$$

$$Q_{qe}^e = (\bar{q}_s \gamma^\mu q_b) (\bar{e}_e \gamma^\mu e_e), \quad (6.10)$$

$$Q_{ld}^e = (\bar{l}_e \gamma^\mu l_e) (\bar{d}_s \gamma^\mu d_b), \quad (6.11)$$

$$Q_{ed}^e = (\bar{e}_e \gamma^\mu e_e) (\bar{d}_s \gamma^\mu d_b), \quad (6.12)$$

$$Q_{ledq}^e = (\bar{e}_e l_e) (\bar{q}_s d_b), \quad (6.13)$$

$$Q'_{ledq}^e = (\bar{l}_e e_e) (\bar{d}_s q_b), \quad (6.14)$$

while the analogous muonic operators are:

$$Q_{lq}^{(1),\mu} = (\bar{l}_\mu \gamma^\mu l_\mu) (\bar{q}_s \gamma^\mu q_b), \quad (6.15)$$

$$Q_{lq}^{(3),\mu} = (\bar{l}_\mu \gamma^\mu \tau^I l_\mu) (\bar{q}_s \gamma^\mu \tau^I q_b), \quad (6.16)$$

$$Q_{qe}^\mu = (\bar{q}_s \gamma^\mu q_b) (\bar{e}_\mu \gamma^\mu e_\mu), \quad (6.17)$$

$$Q_{ld}^\mu = (\bar{l}_\mu \gamma^\mu l_\mu) (\bar{d}_s \gamma^\mu d_b), \quad (6.18)$$

$$Q_{ed}^\mu = (\bar{e}_\mu \gamma^\mu e_\mu) (\bar{d}_s \gamma^\mu d_b), \quad (6.19)$$

$$Q_{ledq}^\mu = (\bar{e}_\mu l_\mu) (\bar{q}_s d_b), \quad (6.20)$$

$$Q'_{ledq}^\mu = (\bar{l}_\mu e_\mu) (\bar{d}_s q_b). \quad (6.21)$$

Now that we have all the ingredients needed to address the anomalies, it is necessary to perform the matching at the scale M_W between the SMEFT and the WET [136, 226]. For the dipole operator O_7 , blind to lepton indices, the matching reads

$$C_7^{(\prime)} = \frac{8\pi^2 v^2}{y_b \lambda_t \Lambda^2} \left(C_{dB}^{(\prime)} - C_{dW}^{(\prime)} \right), \quad (6.22)$$

where y_b is the bottom Yukawa coupling and the presence of the CKM factor λ_t is induced by going from the flavour basis to the mass one in the SMEFT. For the current-current operators, one obtains

$$C_9^\ell = \frac{4\pi^2 v^2}{e^2 \lambda_t \Lambda^2} \left(C_{qe}^\ell + C_{\ell q}^{(1),\ell} + C_{\ell q}^{(3),\ell} - (1 - 4s_W^2)(C_{Hq}^{(1)} + C_{Hq}^{(3)}) \right), \quad (6.23)$$

$$C_{10}^\ell = \frac{4\pi^2 v^2}{e^2 \lambda_t \Lambda^2} \left(C_{qe}^\ell - C_{\ell q}^{(1),\ell} - C_{\ell q}^{(3),\ell} + (C_{Hq}^{(1)} + C_{Hq}^{(3)}) \right), \quad (6.24)$$

$$C_9^{\prime\ell} = \frac{4\pi^2 v^2}{e^2 \lambda_t \Lambda^2} \left(C_{ed}^\ell + C_{\ell d}^\ell - (1 - 4s_W^2)C_{Hd} \right), \quad (6.25)$$

$$C_{10}^{\prime\ell} = \frac{4\pi^2 v^2}{e^2 \lambda_t \Lambda^2} \left(C_{ed}^\ell - C_{\ell d}^\ell + C_{Hd} \right), \quad (6.26)$$

where ℓ can be either an electron or a muon. Finally, for the scalar and tensor operators one gets

$$C_S^\ell = -C_P^\ell = \frac{4\pi^2 v^2}{e^2 \lambda_{ts} \Lambda^2} C_{\ell edq}^\ell, \quad (6.27)$$

$$C_S^{\prime\ell} = C_P^{\prime\ell} = \frac{4\pi^2 v^2}{e^2 \lambda_{ts} \Lambda^2} C_{\ell edq}^{\prime\ell}, \quad (6.28)$$

$$C_T^\ell = C_{T5}^\ell = 0, \quad (6.29)$$

where again ℓ can be either an electron or a muon. It is interesting to notice that the requirement of U(1) invariance prevents on the one hand the presence of tensorial operators (in this channel) also in the SMEFT, while imposes on the other hand precise relations between the scalar and pseudo-scalar WET operators.

A few observations are now in order. A WET global fit taking into account all possible NP contributions to WCs would allow for 18 different free parameters¹, while a SMEFT requires 21 free ones. However, as we have already said, the inclusive radiative Branching Fraction of $B \rightarrow X_s \gamma$ severely constraints the $C_7^{(\prime)}$ WCs [225]: hence, it is safe to remove the operators in Eq. (6.22) from a fit meant to address the anomalies, reducing the number of relevant free parameters to 16

¹The tensor operators are usually neglected in these kind of analysis, since they are not even present in the SM.

in the WET, and to 17 in the SMEFT. Moreover, the operators in Eqs. (6.5)-(6.7) are lepton-blind, and therefore not able to address a set of anomalies involving LFUV processes. In addition, they would be heavily correlated to the hadronic contributions h_λ , since they would appear in all the analysed processes on the same footing. For this reason, it is reasonable to exclude also these operators from the fit, reducing the number of SMEFT free parameters to 14. Finally, looking at the way $Q_{lq}^{(1),\ell}$ and $Q_{lq}^{(3),\ell}$ contribute to the matching, it is easy to infer a 100% correlation between the two operators, with no possibility to disentangle their contribution with a tree-level matching. It is therefore acceptable to merge the two operators into a single one, Q_{lq}^ℓ , with a reduction of the total SMEFT free parameters to 12.

Summarizing, the nature of the problem we are interested in, together with the present status of theoretical and experimental uncertainties, allows us to simplify the matching conditions from Eqs. (6.22)-(6.29) to the following set:

$$C_9^\ell = \frac{4\pi^2 v^2}{e^2 \lambda_t} (C_{qe}^\ell + C_{lq}^\ell), \quad (6.30)$$

$$C_{10}^\ell = \frac{4\pi^2 v^2}{e^2 \lambda_t} (C_{qe}^\ell - C_{lq}^\ell), \quad (6.31)$$

$$C_9^{\prime\ell} = \frac{4\pi^2 v^2}{e^2 \lambda_t} (C_{ed}^\ell + C_{ld}^\ell), \quad (6.32)$$

$$C_{10}^{\prime\ell} = \frac{4\pi^2 v^2}{e^2 \lambda_t} (C_{ed}^\ell - C_{ld}^\ell), \quad (6.33)$$

$$C_S^\ell = -C_P^\ell = \frac{4\pi^2 v^2}{e^2 \lambda_t} C_{ledq}^\ell, \quad (6.34)$$

$$C_S^{\prime\ell} = C_P^{\prime\ell} = \frac{4\pi^2 v^2}{e^2 \lambda_t} C_{ledq}^{\prime\ell}, \quad (6.35)$$

where we have absorbed the NP scale Λ^2 in the definition of the SMEFT WCs. In conclusion, in the current-current sector we have 8 free parameters both in the WET and in the SMEFT, while in the scalar sector we have 8 free ones for the former and only 4 for the latter.

6.2 Previous Studies

We have now all the ingredients needed to perform a SMEFT analyses. However, it is worth to mention that two analysis have already been performed in this framework: the first one appeared right after the announcement of the R_{K^*} anomaly [218], while a second one was performed a few days later [167]. Therefore I will first describe these two works, before going into the details of our analysis and its differences compared to these previous studies.

Regarding the analysis from Ref. [218], it consisted in a global fit performed in a basis analogous to the SMEFT one, except for a different normalization. However, only the eight current-current operators were taken into account. As a first step of their analysis, they performed a fit involving only “clean” observables (i.e. Branching Fraction ratios) and considering one coefficient at a time. Those fits showed that viable candidates to accommodate for the anomalies where the WC corresponding to the SMEFT $C_{\ell q}^\mu$, $C_{\ell q}^e$, C_{qe}^e and C_{ed}^e . However, once the “dirty”, angular observables were taken into account, only the scenario involving $C_{\ell q}^\mu$ produced a feasible fit. This was easily predictable, given their handling of hadronic uncertainties along the lines of the phenomenological model of Ref. [99]: the electron WCs are not capable to account for the $B \rightarrow K^* \mu^+ \mu^-$ angular anomalies, hence ruling them out as viable candidates to address the global anomalies pattern. Analogously, once a global fit was performed with all WCs taken in consideration, $C_{\ell q}^\mu$ was the only coefficient showing a significant evidence.

On the other hand, the analysis from Ref. [167] was mainly focused on the explanation of the “clean” anomalies. The starting point consisted in deriving approximate phenomenological formulae for R_K and R_{K^*} as functions of differences between muonic and electronic NP WC, with all SM parameters fixed. Subsequently, they performed a scan using one coefficient at a time and investigated which coefficient was capable to address the ratios anomalies simultaneously. Analogously to Ref. [218], the only difference between muonic and electronic WCs capable to account for the anomalies consisted in the one involving $C_{\ell q}^{\mu-e}$; they also performed scans involving couple of (differences of) WCs, and once again the only way for the anomalies to be addressed involved the presence of $C_{\ell q}^{\mu-e}$ in the couple of parameters scanned. Therefore, in the spirit of addressing the whole set of anomalies, they focused on the scenario where most of the NP content came from $C_{\ell q}^\mu$ and obtained bounds on this coefficient using the results from the global fit performed in Ref. [214].

In conclusion, the two studies already performed in the SMEFT framework agree on the need for a $C_{\ell q}^\mu$ different from zero in order to be able to consistently address the anomalies pattern. However, if only branching fraction ratios are taken into account, Ref. [218] showed how solutions involving electronic coefficients are viable as well; those solutions are no longer viable once the $B \rightarrow K^* \mu^+ \mu^-$ angular observables are included in the fit, if one sticks to the dispersion relation of Ref. [99] in order to describe the effect of hadronic contributions in the whole phenomenological region. Nevertheless, a more conservative approach along the lines of the PDD approach employed in Ref. [11] could preserve the viability of the electronic solutions as well, once a global fit is performed. Therefore, in the next section I will study all the SMEFT scenarios allowed by a more careful treatment of hadronic uncertainties and capable of addressing the current experimental data.

6.3 Constraining the Couplings by Means of a Bayesian Analysis

We can now proceed to perform the global fits in the SMEFT basis. As I have already said at the end of the previous section, these fits have been carried out following the guidelines of the PDD approach employed in Ref. [11] and explained in Sec. 5.5. The main feature of this approach consists in a conservative treatment of hadronic uncertainties, relying on the LCSR computations from Ref. [99] only at low q^2 and allowing for larger effects approaching the $c\bar{c}$ threshold.

As a first step, I have performed global fits where only one SMEFT WC at a time was included. Out of the twelve operators individuated at the end of Sec. 6.1, only four were found to be capable of addressing the anomalies producing a good fit: namely, the ones relative to $C_{\ell q}^\mu$, $C_{\ell q}^e$, C_{qe}^e and C_{ed}^e . This result is consistent with what was already found in Ref. [218]. However, in that analysis those coefficients were found viable only when angular observables were not included in the fit; once a global fit was performed, all the electron solutions had to be discarded, given their inability to address the “dirty” observables. On the other hand, as was already pointed out in Ref. [11], once the PDD approach is employed this is no longer the case: an hadronic contribution larger than, but in the same ballpark of, the one predicted by dispersion relations applied to LCSR computations is indeed capable of accounting for the angular anomalies, allowing electronic solutions to be able to explain the ratio anomalies.

Let us now take a closer look to this four viable scenarios.

- $C_{\ell q}^\mu$

This first case has already been studied in the literature [167, 218], as I have already reviewed in Sec. 6.2. Moreover, it corresponds to the $C_{9,\mu}^{NP} = -C_{10,\mu}^{NP}$ scenario in the WET basis, already advocated in several analysis [11, 214–217]. The fit is well-behaving, producing results for the anomalous observables compatible with experimental data. The fitted value for the WC is

$$C_{\ell q}^\mu = (0.86 \pm 0.22) \cdot 10^{-3} \text{ TeV}^{-2}, \quad (6.36)$$

expressed in terms of mean and s.t.d extracted from the probability distribution function (p.d.f.) produced by the fit. Going from the SMEFT basis to the WET basis, this solution can be read as

$$C_{9,\mu}^{NP} = -C_{10,\mu}^{NP} = -0.54 \pm 0.14, \quad (6.37)$$

in agreement with the results obtain in Refs. [11, 214–217].

In order to allow for a model comparison, the IC (defined at Eq. (5.8)) for this model is 157. The p.d.f. for $C_{\ell q}^\mu$, showing the 1σ , 2σ and 3σ regions, can be found in the left panel of Fig. 6.1

- $C_{\ell q}^e$

This is the first case where all the NP content stems from an electron operator. It corresponds to the $C_{9,e}^{NP} = -C_{10,e}^{NP}$ scenario in the WET basis, and is first studied here thanks to the features of the PDD approach. The fit is again well-behaving, with all the anomalous observables showing compatibility with experimental data. The fitted value for the WC is

$$C_{\ell q}^e = -(0.99 \pm 0.31) \cdot 10^{-3} \text{ TeV}^{-2}, \quad (6.38)$$

expressed in terms of mean and s.t.d extracted from the fit-produced p.d.f.. Rotating from the SMEFT basis to the WET basis, this solution can be read as

$$C_{9,e}^{NP} = -C_{10,e}^{NP} = 0.63 \pm 0.20. \quad (6.39)$$

The IC for this model is 158, perfectly compatible with the one produced for the previous case. The p.d.f. for $C_{\ell q}^e$, showing the 1σ , 2σ and 3σ regions, can be found in the right panel of Fig. 6.1

- C_{qe}^e

This is the second case where all NP effects are induced by means of an electron operator, and it corresponds to the $C_{9,e}^{NP} = C_{10,e}^{NP}$ scenario in the WET basis. Also this fit is well-behaving, displaying high compatibility between the results for the anomalous observables and the experimental data. The fitted value for the WC is

$$C_{qe}^e = (2.22 \pm 0.84) \cdot 10^{-3} \text{ TeV}^{-2}, \quad (6.40)$$

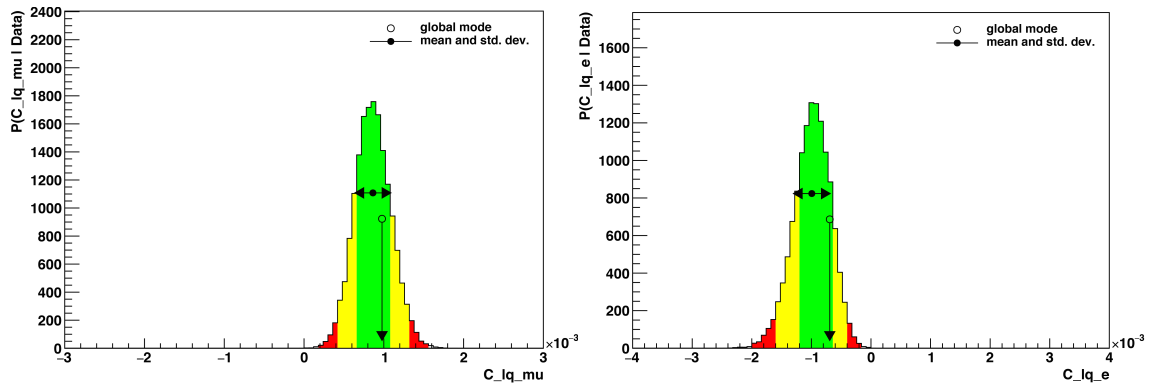


Figure 6.1: Left: p.d.f. for $C_{\ell q}^{\mu}$ from a single-coefficient global fit. Here and in the following, the green zone is the 1σ region, the yellow zone is the 2σ region and the red one is the 3σ region. Right: p.d.f. for $C_{\ell q}^e$ from a single-coefficient global fit.

expressed in terms of mean and s.t.d extracted from the fit-produced p.d.f.. It is interesting to notice that a second, (very) small mode can be found for $C_{qe}^e \simeq -5 \cdot 10^{-3}$: the byproduct of this second mode is the presence of a (again very small) second mode in the results for the BELLE P'_5 observables, relatively to the electron channel. However, since the main C_{qe}^e mode is the one producing the value for the electronic P'_5 compatible with BELLE measurements, we will focus only on this mode disregarding the other one. Rotating from the SMEFT basis to the WET basis, this solution can be read as

$$C_{9,e}^{NP} = C_{10,e}^{NP} = -1.41 \pm 0.53. \quad (6.41)$$

The IC for this model is 161, compatible with the ones previously produced. The p.d.f. for C_{qe}^e , showing the 1σ , 2σ and 3σ regions, can be found in the left panel of Fig. 6.2

- C_{ed}^e
This is the last case featuring NP contributions in the electron sector, and it is the only one involving right-handed quarks. It corresponds to the $C'_{9,e}{}^{NP} = C'_{10,e}{}^{NP}$ scenario in the WET basis. This fit, too, is well-behaving, with results for the anomalous observables compatible with experimental data. The fitted WC value is

$$C_{ed}^e = -(2.9 \pm 1.3) \cdot 10^{-3} \text{ TeV}^{-2}, \quad (6.42)$$

expressed in terms of mean and s.t.d extracted from the fit-produced p.d.f.. Similarly to the previous case, a second small mode is present at $C_{ed}^e \simeq 3.5 \cdot 10^{-3}$; once again, it produces a second mode in the results for the

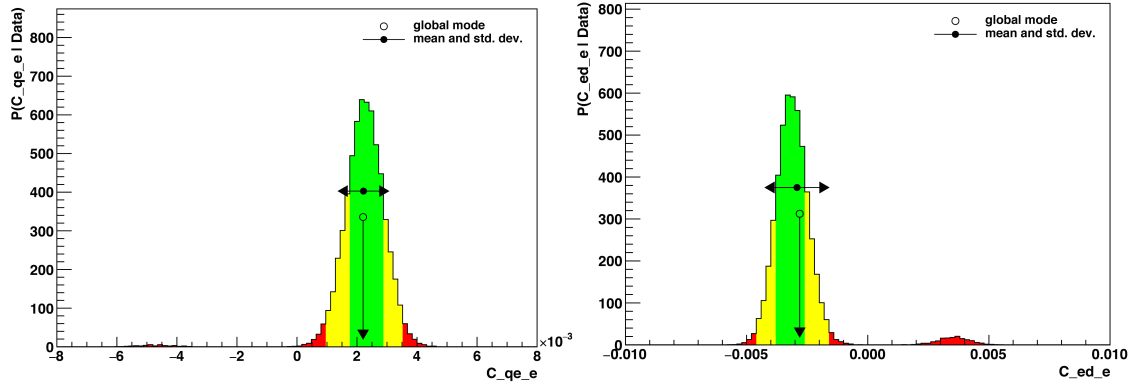


Figure 6.2: Left: p.d.f. for C_{qe}^e from a single-coefficient global fit. Right: p.d.f. for C_{ed}^e from a single-coefficient global fit. Coloring follows the prescriptions of Fig. 6.1.

BELLE electron P'_5 observables distant from the experimental measurement. Therefore, we will focus again only on the main mode. Rotating from the SMEFT basis to the WET basis, this solution can be read as

$$C'_{9,e}{}^{NP} = C'_{10,e}{}^{NP} = 1.85 \pm 0.83. \quad (6.43)$$

The IC for this model is 158, perfectly compatible with all the ones obtained in the previous case. The p.d.f. for $C'_{ed}{}^e$, showing the 1σ , 2σ and 3σ regions, can be found in the right panel of Fig. 6.2

In conclusion, these single-coefficient global fits pointed out different NP scenarios able to address the anomalies pattern. According to the IC they are all equally-compatible, with no reason to prefer a muonic solution instead of an electronic one if one follows the conservative prescriptions of the PDD approach.

As a second step of this analysis, it is interesting to perform a global fit allowing for NP effects in all the relevant SMEFT operators, i.e. a global fit with a total of 12 floating WCs. Such a fit has never been carried out before in the literature, and in particular within the PDD approach. The output of the fit, in the form of p.d.f. for all the NP WCs and correlation plots for all pairs of WCs, can be found in Figs. 6.3-6.7. As a first observation, it is worth to notice that there is enough experimental data to constrain all the 12 WCs at the same time. Given the high non-triviality of the decays under scrutiny, this was not easily predictable a priori. Starting from the muonic sector, the main NP evidence among the current-current operators is found in $C'_{\ell q}{}^\mu$; regarding the scalar operators, they are strictly correlated due to the anatomy of the $B_s \rightarrow \mu\mu$ branching fraction, as was already observed in Ref. [136]. On the other hand, in the electron sector evidence for NP can be found in $C'_{\ell q}{}^e$ and $C'_{ed}{}^e$; moreover, these coefficients display a really peculiar correlation, induced by the BELLE electron P'_5 in a similar fashion as what happened for the single-coefficient global fits. However, contrarily to what happened in those scenarios, here we are not in presence of a multimodality, where a particular mode can be preferred due to specific reasons: as it is manifest looking at the 2D correlation plot, we are in the presence of a broad, continuous mode. It is reasonable to assume that such a situation is due to the limited data present in the electron channel; therefore, it will be interesting to check if the electron sector will behave in a similar fashion as the muon one, once an amount of data comparable with the one relative to the muonic case will be available in the future.

Concluding, it is interesting to notice that, analogously to what was observed for the scenario **(VI)** of Ref. [11], a global fit performed allowing for NP effects in all the relevant WCs displays a larger evidence of NP contributions in the muonic sector, although the presence of NP in the electronic sector is still possible thanks to the conservative handling of hadronic uncertainties induced by the PDD approach.

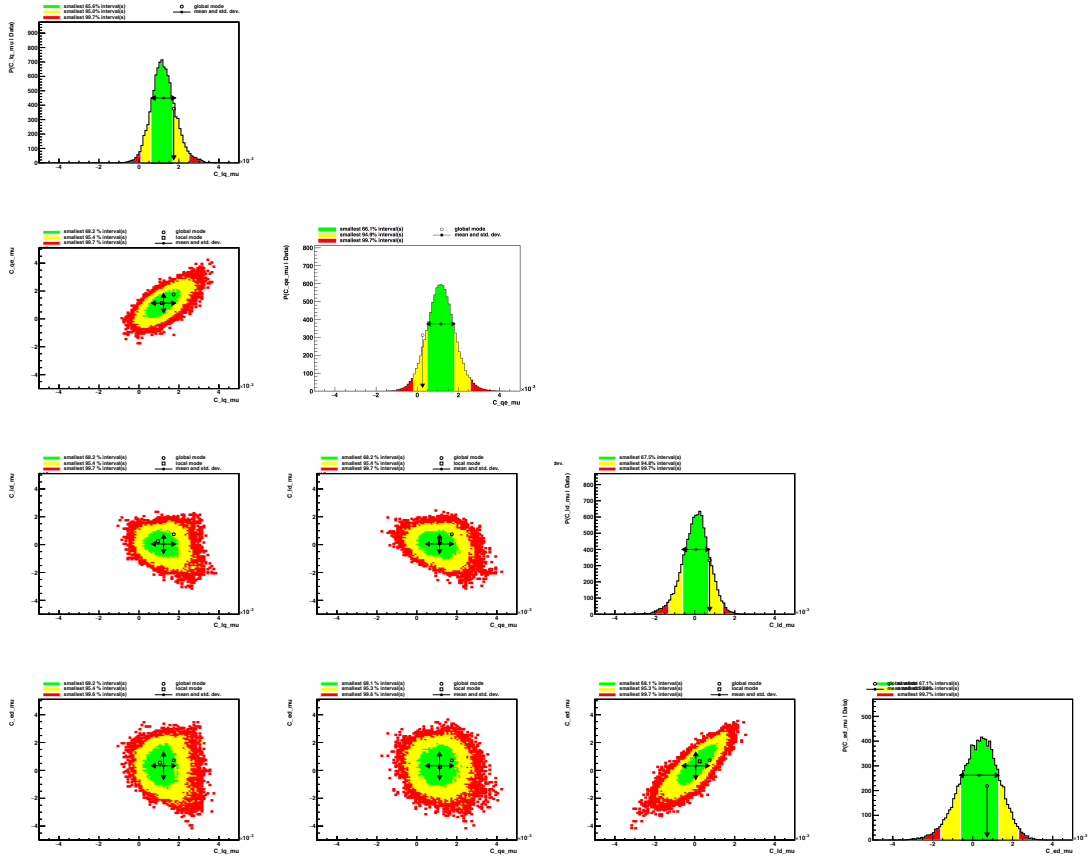


Figure 6.3: p.d.f. for C_{lq}^μ , C_{qe}^μ , C_{ld}^μ and C_{ed}^μ (respectively from the upper corner to the lower right corner), and relative correlations. Coloring follows the prescriptions of Fig. 6.1.

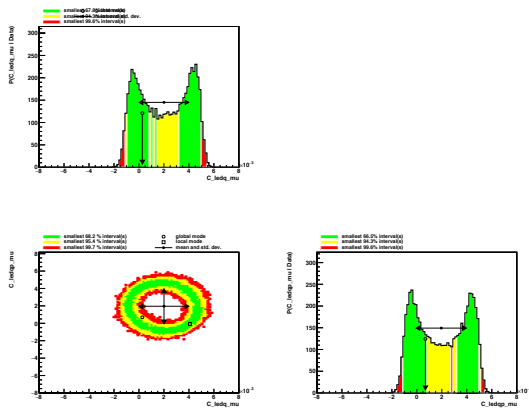


Figure 6.4: p.d.f. for C_{ledq}^μ and C_{ledq}^μ , and relative correlations. Coloring follows the prescriptions of Fig. 6.1.

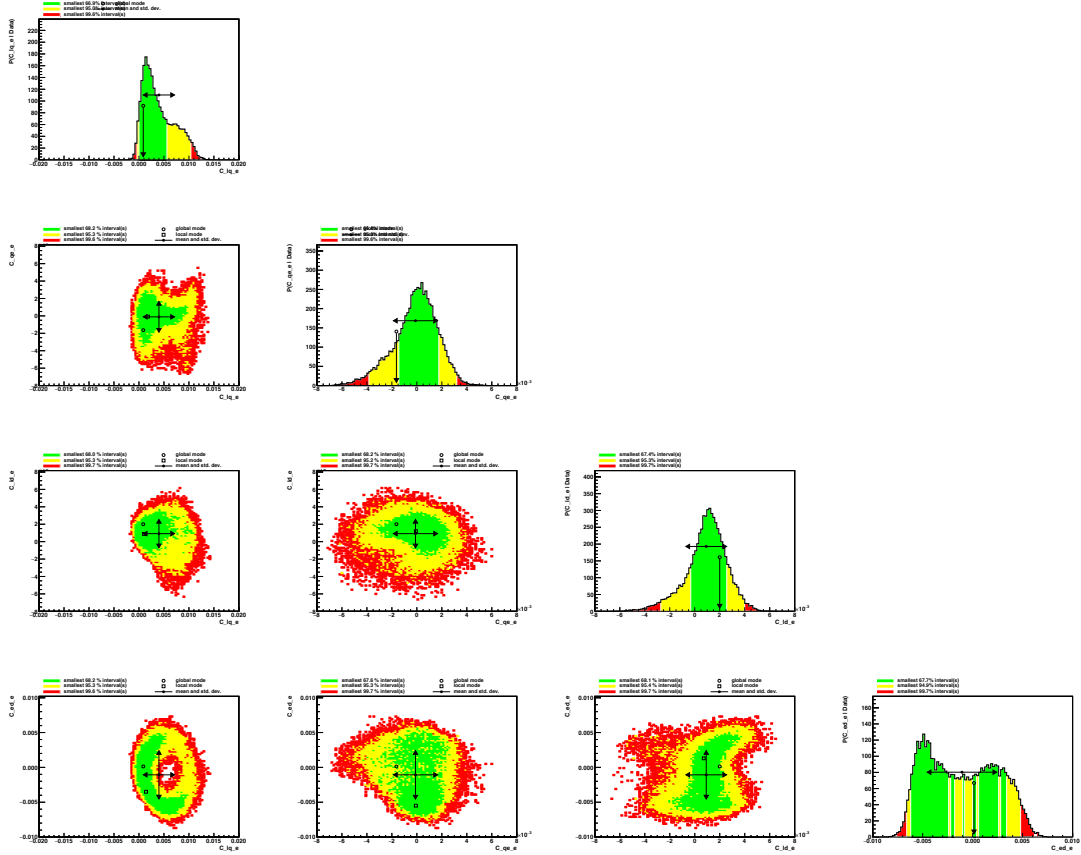


Figure 6.5: p.d.f. for C_{lq}^e , C_{qe}^e , C_{ld}^e and C_{ed}^e (respectively from the upper corner to the lower right corner), and relative correlations. Coloring follows the prescriptions of Fig. 6.1.

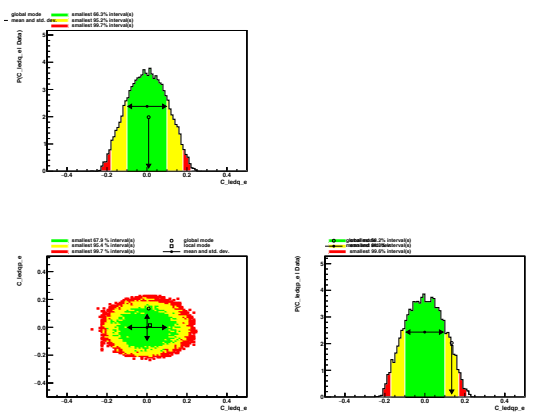


Figure 6.6: p.d.f. for C_{ledq}^e and C_{ledq}^{ie} , and relative correlations. Coloring follows the prescriptions of Fig. 6.1.

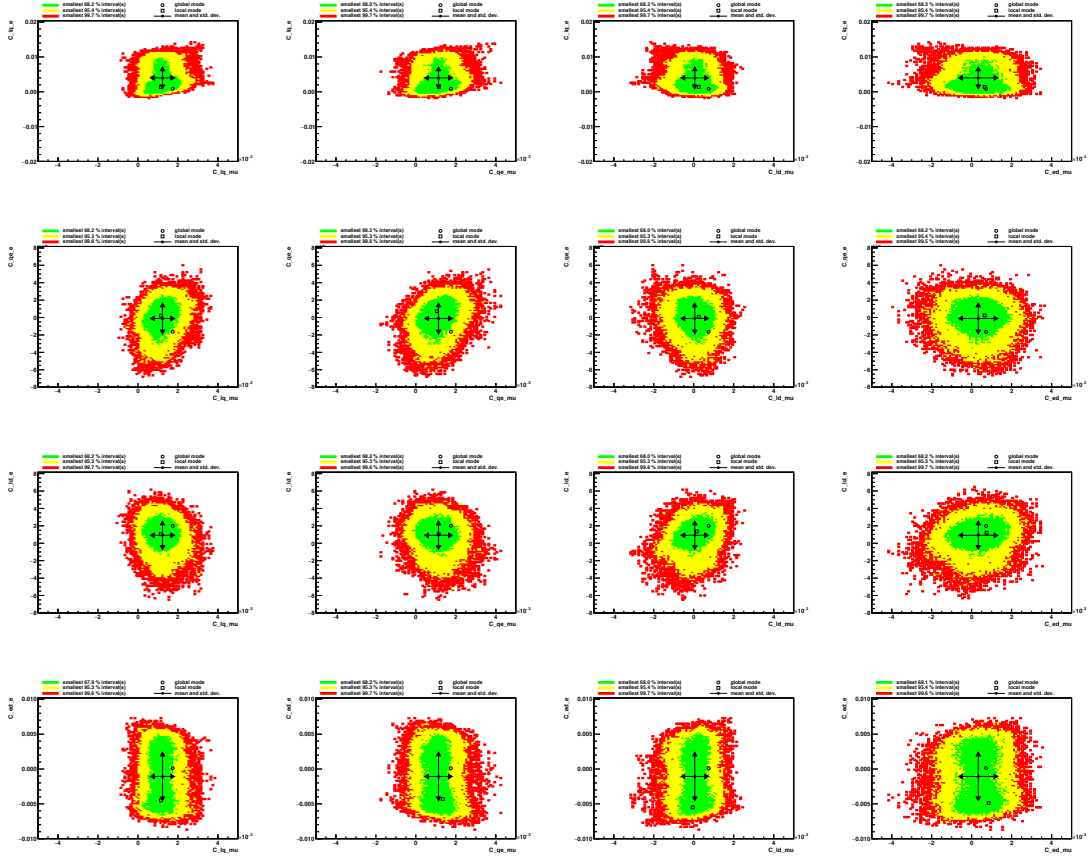


Figure 6.7: p.d.f. for the correlations between the muonic current-current operators (C_{lq}^μ , C_{qe}^μ , C_{ld}^μ and C_{ed}^μ , from left to right) and the electronic ones (C_{lq}^e , C_{qe}^e , C_{ld}^e and C_{ed}^e , from top to bottom).

6.4 Future Perspectives

In the final section of this chapter, I want to spend a few words describing what could be the possible future perspectives in this research field.

A first, possible generalization would consist in the addition of the other $\Delta B = 1$ anomalies, namely the ones affecting $b \rightarrow c$ transitions. Indeed, R_K and R_{K^*} were not the only anomalous branching fraction ratios measured in the last few years: the R_D and the R_D^* ratios, defined as the ratio between the tauonic and the sum of the electronic and muonic branching fraction of $B \rightarrow D^{(*)} \ell \nu$, have been found above the SM prediction of 2.2σ and 3.3σ , respectively [227–230]. Moreover, also t2 recent measure of the analogously defined $R_{J/\psi}$ ratio was found $\sim 2\sigma$ above the

SM prediction². Given the different kind of WET operators involved in the $b \rightarrow c$ transition, they have generally be addressed separately by global fits. However, the operator $Q_{lq}^{(3)}$ can give raise to both neutral and charged currents, depending on the Pauli matrix considered. Therefore, it is possible to perform a SMEFT global fit that addresses all the present $\Delta B = 1$ anomalies in a coherent framework.

A second, natural generalization for this kind of SMEFT global fits would be the inclusion of dimension 6 loop induced effects, i.e. including the running for the WC from the NP scale Λ to the matching scale of the WET, M_W . However, this analysis could not only consider flavour observables: the mixing between the various dimension 6 operators showed in Refs. [4–7] implies the presence of several new operators that do not contribute to $b \rightarrow s$ transitions at tree-level, while they might give raise to tree-level contributions in other channels. Therefore, a large quantity of high energy physics phenomena should be taken into account in order to properly constrain all the WC involved in such an analysis. Nevertheless, the outcome of this analysis could be highly unpredictable: on the one hand, the inclusion of all the relevant processes might generate problems with the convergence of the fit, resulting in numerically unstable results which might therefore be unreliable on the physical point of view. On the other hand, assuming a feasible computation, there is no guarantee that such an analysis could yield to meaningful constrains on all the considered WC. A possible solution would again be the requirement of some kind of symmetry to reduce the number of operators under scrutiny; however, such a choice would put at stakes the Bottom-Up approach proper of the SMEFT framework, hence potentially invalidating the validity of such an approach for this kind of analysis.

²https://indico.cern.ch/event/658856/contributions/2686351/attachments/1522412/2379024/talk_LHCb_MFontana.pdf

Part III

Is the EFT Approach the Only Way?

The Higgs boson observed at the Large Hadron Collider (LHC) [1, 2] behaves in accordance with the SM predictions, *i.e.*, it is a scalar CP-even state whose coupling to the other known particles has a SM-like structure and a strength proportional to their masses [231–233]. Presently, the analysis based on the combination of the 7 and 8 TeV LHC data sets [233] shows that the couplings with the vector bosons are found to be compatible with those expected from the SM within a $\sim 10\%$ uncertainty; on the other hand, concerning the heaviest SM fermions (the top and the bottom quarks, and the τ lepton) the compatibility is found with a slightly greater uncertainty, equal to $\sim 15 - 20\%$. The situation is going to get better in the future, with the best present estimates [234–236] indicating that at the end of the LHC Run 2 at $\sqrt{s} = 13 - 14$ TeV center-of-mass-energy and with a 300 fb^{-1} integrated luminosity, the measurement of the couplings between the Higgs boson and the vector bosons is expected to reach a few percent precision, while the corresponding ones for the fermions, with the exception of the μ lepton, can reach $\sim 8 - 12\%$ precision. Moreover, looking at the end of the High Luminosity phase, we can expect a reduction of these numbers by a factor ~ 2 .

However, similar levels of precision will not be reached regarding the study of the Higgs self interactions, stemming from the scalar potential in the SM Lagrangian. In the SM, the Higgs potential in the unitary gauge reads

$$V(\phi_1) = \frac{m_H^2}{2}\phi_1^2 + \lambda_3 v \phi_1^3 + \frac{\lambda_4}{4}\phi_1^4, \quad (\text{IV.1})$$

where the Higgs mass (m_H) and the trilinear (λ_3) and quartic (λ_4) interactions are linked by the relations $\lambda_4^{\text{SM}} = \lambda_3^{\text{SM}} = \lambda = m_H^2/(2v^2)$, where $v = (\sqrt{2}G_\mu)^{-1/2}$ is the vacuum expectation value, and λ is the coefficient of the $(\Phi^\dagger\Phi)^2$ interaction, with Φ being the Higgs doublet field.

The experimental verification of these relations relies on the measurements of processes featuring at least two Higgs bosons in the final state. However, due to the smallness of the cross section for this kind of processes, constraining the Higgs self couplings with a relative uncertainty of a few hundreds of percents is already extremely challenging. In particular, information on λ_3 can be obtained from Higgs pair production; however, the bounds on this decay channel, stemming from 8 TeV data, allowed us to constrain λ_3 only within $\mathcal{O}(\pm(15 - 20)\lambda_3^{\text{SM}})$ [237–240]. At $\sqrt{s} = 13$ TeV, the SM Higgs pair production cross section is around 35 fb in the gluon-fusion channel [241–243] and even smaller in other production mechanisms [244, 245]: the present 13 TeV data allows to restrict the allowed values for λ_3 in the range $\lambda_3 < -8 \lambda_3^{\text{SM}}$ and $\lambda_3 > 15 \lambda_3^{\text{SM}}$ [246], and the most updated estimates predict that, at the end of the High Luminosity Phase, it will be possible to exclude at the LHC only values in the range $\lambda_3 < -0.8 \lambda_3^{\text{SM}}$ and $\lambda_3 > 7.7 \lambda_3^{\text{SM}}$ via the $b\bar{b}\gamma\gamma$ signatures [247, 248] or $\lambda_3 < -4 \lambda_3^{\text{SM}}$ and $\lambda_3 > 12 \lambda_3^{\text{SM}}$ including also $b\bar{b}\tau\bar{\tau}$ signatures [249]. Moreover, concerning the quartic Higgs self-

coupling λ_4 , the abysmal smallness of the triple Higgs production cross section (around 0.1 fb) [242] suggests that its measurement seems beyond the reach of the LHC [250, 251].

Given these premise, one might wonder if the EFT approach is viable to study NP effects in the Higgs self couplings. Following the approach of Ref. [252], it is possible to parametrize such effects at the weak scale via a single parameter κ_λ , i.e. the rescaling of the SM trilinear coupling λ_3^{SM} , so that the ϕ_1^3 interaction in the potential is given by

$$V_{\phi_1^3} = \lambda_3 v \phi_1^3 \equiv \kappa_\lambda \lambda_3^{\text{SM}} v \phi_1^3, \quad \lambda_3^{\text{SM}} \equiv \frac{G_\mu}{\sqrt{2}} m_H^2. \quad (\text{IV.2})$$

On the other hand, working in the SMEFT framework, the modified Higgs potential looks like [253, 254]

$$V_{\phi_1^3} = V^{\text{SM}} + \frac{c_6}{v^2} (\phi_1^\dagger \phi_1)^3, \quad (\text{IV.3})$$

meaning that it is possible to write the following relation between the two formalisms:

$$\kappa_\lambda = 1 + \frac{2v^2}{m_H^2} c_6. \quad (\text{IV.4})$$

However, requiring that $\phi_1 = v/\sqrt{2}$ is still a global minimum of the potential constrains $\kappa_\lambda < 3$ [255]. This means that the EFT framework is, presently, not interesting from a phenomenological point of view, given the bound that can be imposed on κ_λ , both now and in the near future.

However, given the large room for NP effects in the Higgs self-coupling sector, trying to constrain such interactions can be a really interesting probe for the search of BSM effects. This is the reason why, during my PhD experience, I decided to devote some time to the study of possible new ways to put bounds on the Higgs trilinear self-coupling. The results of such studies, summarized in Ref. [12], are illustrated in the following chapter.

Chapter 7

Constraining the Trilinear Higgs Self-Coupling by Means of Precision Electroweak Measurements

As I have stated in the introduction of this section, constraining the Higgs self coupling by means of direct searches, i.e. by measuring processes featuring at least two Higgs bosons in the final state, is a quite challenging task [244]. As

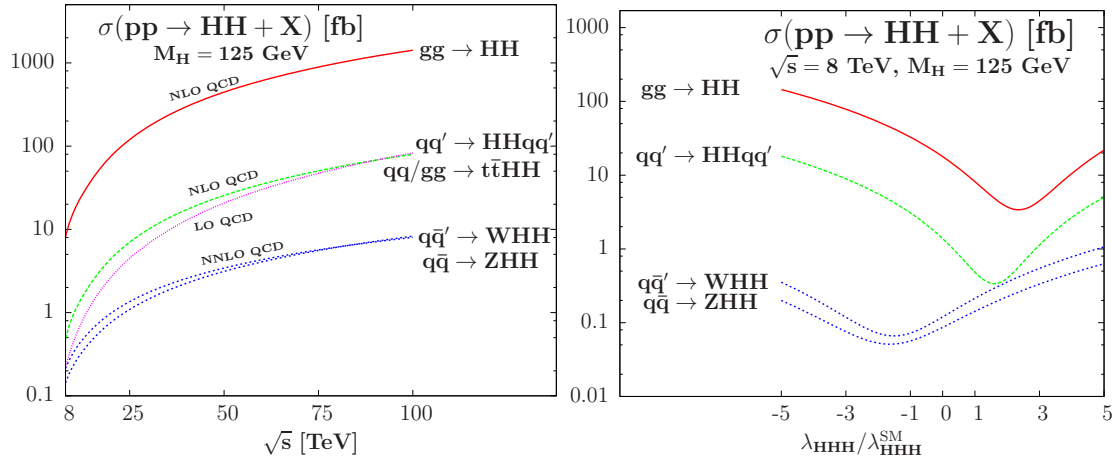


Figure 7.1: Left: total cross section for Higgs pair production at LHC in the main channels as a function of the center-of-mass-energy [244]. Right: sensitivity of the total cross section for the various production channels to the trilinear Higgs self-coupling, at a center-of-mass-energy equal to $\sqrt{s} = 8$ GeV [244].

shown in the left panel of Fig. 7.1, the total cross section for Higgs pair production at LHC will not be higher than a few tens of fb in the gluon-fusion channel (and even smaller in other production mechanisms), hence questioning the observation itself of such decay channels. However, as can be inferred looking at the right panel of Fig. 7.1, the size of the trilinear Higgs self-coupling heavily affects such cross sections. Therefore, setting bounds on the observation of decay channels stemming from double Higgs production can be translated into constraints on the trilinear Higgs self-coupling, subsequently reinterpreted in the light of the κ_λ formalism introduced in Eq. (IV.2).

Nevertheless, given the present bounds stemming from Run 1 data, this approach allowed the community to constrain κ_λ only within $\mathcal{O}(\pm(15-20))$ [237–240], as can be seen looking e.g. at Fig. 7.2. Moreover, even at the end of the High Luminosity Phase, it will be possible to exclude at the LHC only values in the range $\kappa_\lambda < -0.8$ and $\kappa_\lambda > 7.7$ via the $b\bar{b}\gamma\gamma$ signatures [247, 248].

Therefore, in the latest years arose the need for a complementary strategy in order to further constrain the trilinear self-coupling. A new idea was developed in 2013 by M. McCullough [256]. In this approach, the focus was set to elec-

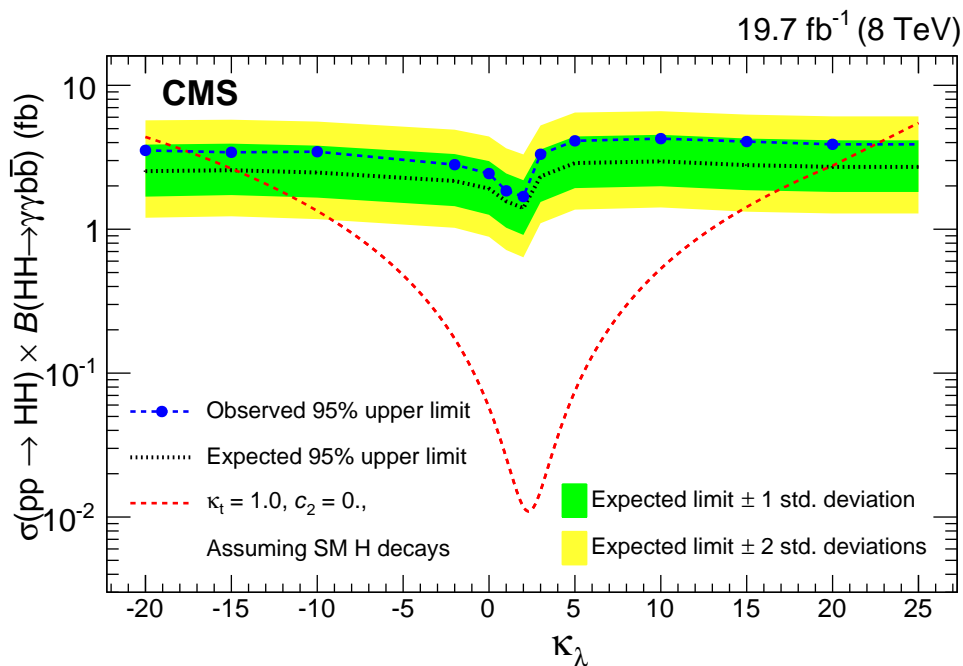


Figure 7.2: Observed and expected 95% CL upper limits on the product of cross section and the branching fraction $\sigma(pp \rightarrow HH) \times B(HH \rightarrow \gamma\gamma b\bar{b})$, performed by the CMS collaboration [239].

troneak corrections to precise measurements of single Higgs production and decay processes: in fact, if the channel of interest is measured with a sufficient precision, it can be sensitive to the effects induced by the presence of an anomalous trilinear self-coupling, introduced by loop corrections to Higgs propagators¹. This strategy, first applied to ZH production at an e^+e^- collider in Ref. [256] and later on to Higgs production and decay modes at the LHC [252–254], was capable to obtain constrains on κ_λ comparable with the ones stemming from direct searches.

In this chapter I will review my contribution to the field, consisting of applying the κ_λ formalism to the computation of the W boson mass, m_W , and the effective sine, $\sin^2 \theta_{\text{eff}}^{\text{lep}}$, and obtaining bounds on the anomalous self-coupling stemming by the loop-induced effects on such electroweak precision observables [12].

7.1 λ_3 -dependent Contributions in m_W and $\sin^2 \theta_{\text{eff}}^{\text{lep}}$

The \overline{MS} formulation of the radiative corrections [257–259] prescribes that the theoretical predictions of m_W and $\sin^2 \theta_{\text{eff}}^{\text{lep}}$ are expressed in terms of the pole mass of the particles, the \overline{MS} Weinberg angle $\hat{\theta}_W(\mu)$ and the \overline{MS} electromagnetic coupling $\hat{\alpha}(\mu)$, defined at the 't-Hooft mass scale μ , usually chosen to be equal to m_Z . In this formulation it is possible to define the radiative parameters $\Delta\hat{r}_W$, $\Delta\hat{\alpha}$, $Y_{\overline{MS}}$ through the following relations ($\sin^2 \hat{\theta}_W(m_Z) \equiv \hat{s}^2$) [260]:

$$\begin{aligned} \frac{G_\mu}{\sqrt{2}} &= \frac{\pi\hat{\alpha}(m_Z)}{2m_W^2\hat{s}^2} (1 + \Delta\hat{r}_W), & \hat{\alpha}(m_Z) &= \frac{\alpha}{1 - \Delta\hat{\alpha}(m_Z)}, \\ \hat{\rho} &\equiv \frac{m_W^2}{m_Z^2\hat{c}^2} = \frac{1}{1 - Y_{\overline{MS}}}, \end{aligned} \quad (7.1)$$

with $\hat{c}^2 = 1 - \hat{s}^2$. It is now possible to define m_W starting from the definition of m_Z , α and G_μ via the following relation,

$$m_W^2 = \frac{\hat{\rho} m_Z^2}{2} \left\{ 1 + \left[1 - \frac{4\hat{A}^2}{m_Z^2\hat{\rho}} (1 + \Delta\hat{r}_W) \right]^{1/2} \right\}, \quad (7.2)$$

where $\hat{A} = (\pi\hat{\alpha}(m_Z)/(\sqrt{2}G_\mu))^{1/2}$, while the effective sine is similarly related to \hat{s}^2 via the relations

$$\sin^2 \theta_{\text{eff}}^{\text{lep}} = \hat{k}_\ell(m_Z^2)\hat{s}^2, \quad \hat{k}_\ell(m_Z^2) = 1 + \delta\hat{k}_\ell(m_Z^2), \quad (7.3)$$

¹ It is worth to note that this approach builds on the assumption that NP couples to the SM via the Higgs potential in such a way that only the Higgs self-coupling is sizably affected, while the remaining couplings to the other fields of the SM (and in particular to the top quark and vector bosons) are either still given by the SM prescriptions or, equivalently, affected in a negligible way in the loop effects one is considering.

where $\hat{k}_\ell(q^2)$ is an electroweak form factor² (see Ref. [261]) and

$$\hat{s}^2 = \frac{1}{2} \left\{ 1 - \left[1 - \frac{4\hat{A}^2}{m_Z^2 \hat{\rho}} (1 + \Delta\hat{r}_W) \right]^{1/2} \right\}. \quad (7.4)$$

Our modified Higgs potential induces modifications to the radiative parameters $\Delta\hat{r}_W$ and $Y_{\overline{MS}}$ at the two-loop level, while $\Delta\hat{\alpha}$ and $\delta\hat{k}_\ell(m_Z^2)$ are going to be affected only at three loops. Given that the present knowledge of m_W and $\sin^2\theta_{\text{eff}}^{\text{lep}}$ in the SM includes the complete two-loop corrections, while the three-loops corrections are not fully known yet, we are going to discuss only the effects induced by the anomalous trilinear self-coupling in $\Delta\hat{r}_W$ and $Y_{\overline{MS}}$. The two-loop contribution to these observables can be expressed as [260]

$$\Delta\hat{r}_W^{(2)} = \frac{\text{Re } A_{WW}^{(2)}(m_W^2)}{m_W^2} - \frac{A_{WW}^{(2)}(0)}{m_W^2} + \dots \quad (7.5)$$

$$Y_{\overline{MS}}^{(2)} = \text{Re} \left[\frac{A_{WW}^{(2)}(m_W^2)}{m_W^2} - \frac{A_{ZZ}^{(2)}(m_Z^2)}{m_Z^2} \right] + \dots \quad (7.6)$$

where A_{WW} (A_{ZZ}) is the term proportional to the metric tensor in the W (Z) self energy with the superscript indicating the loop order, and the dots represent additional two-loop contributions that are not sensitive to a modification of the scalar potential.

For the reader convenience, it is possible to translate the additional contributions induced in $\Delta\hat{r}_W^{(2)}$ and $Y_{\overline{MS}}^{(2)}$ to the ones one would obtain for the On-Shell (OS) scheme [262] radiative parameters Δr and $\kappa_e(m_Z^2)$. The former, entering the interdependence between m_W and m_Z , can be written as

$$\Delta r^{(2)} = \Delta\hat{r}_W^{(2)} - \frac{c^2}{s^2} Y_{\overline{MS}}^{(2)}, \quad (7.7)$$

where $c^2 \equiv m_W^2/m_Z^2$, $s^2 = 1 - c^2$, while for the latter, relating the effective sine to s^2 in the OS scheme via $\sin^2\theta_{\text{eff}}^{\text{lep}} = \kappa_e(m_Z^2)s^2$, one can write

$$\kappa_e^{(2)}(m_Z^2) = 1 - \frac{c^2}{s^2} Y_{\overline{MS}}^{(2)}. \quad (7.8)$$

Employing the κ_λ formalism described at the beginning of this Part in Eq. (IV.2), it is now possible to compute the NP contributions to the self energies present in

²In our \overline{MS} formulation the top contribution is not decoupled. Then \hat{k} is very close to 1 and $\sin^2\theta_{\text{eff}}^{\text{lep}}$ can be safely identified with \hat{s}^2 [261].

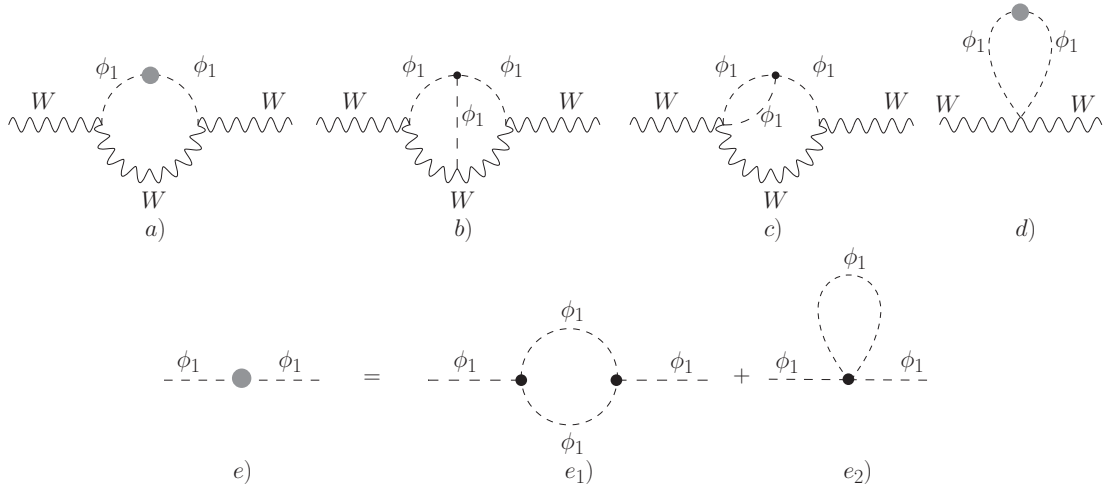


Figure 7.3: Unitary gauge two-loop λ_3 -and- λ_4 -dependent diagrams in the W self-energy. The grey blob represent the insertion of the modified diagrams in the one-loop Higgs self energy, shown in the second row, or in the mass counterterm. The black point represents either an anomalous λ_3 or λ_4 .

Eqs. (7.5)-(7.6) due to the anomalous self-coupling. In order to correctly identify the effects related to the ϕ_1^3 interaction we followed Ref. [252] and worked in the unitary gauge. I'll now discuss the procedure we used to compute the W self energy, which can be also applied for the Z self energy, following the same guidelines.

In Fig. 7.3 we report the W self energy two-loop diagrams that are affected by a modification of the Higgs self-couplings. The grey blob in diagrams 7.3a) and 7.3d) represents the insertion of the NP terms present in the one-loop Higgs self energy, stemming from the unitary gauge diagrams in fig. 7.3e), or in the correspondent one-loop Higgs mass counterterm. The analytical computation proceeded as follows: first, the amplitudes of the diagrams in fig. 7.3 were generated using the Mathematica package FEYNARTS [56]; subsequently, the obtained tensorial integrals were reduced to scalar Master Integrals using both private codes and the packages FeynCalc [263, 264] and Tarcer [265], in order to cross-check our results. After the reduction to scalar integrals we were left with two kind of contributions to evaluate: two-loop vacuum integrals and two-loop self-energy diagrams with external momenta different from zero. The former integrals were evaluated analytically using the results of Ref. [266], while the latter ones were further reduced to the set of loop-integral basis functions introduced in Ref. [267] and then numerically evaluated by means of the C program TSIL [268]. Our Higgs mass counterterm was fixed expressing our results in terms of the OS Higgs mass.

Before closing this section, a few remarks may be useful to the reader:

- since the observables of interest involve only differences of self energies, (see

Eqs. (7.5)-(7.6)), the contribution given by the diagram 7.3d) always vanishes in such differences;

- contributions proportional to the quartic Higgs self-couplings (on which we did not make any assumption) arise once the diagram 7.3e₂) is inserted in diagrams 7.3a) and 7.3d). However, this contribution is exactly cancelled by the corresponding Higgs mass counterterm diagram, in such a way that the final result does not depend on λ_4 . It is important to stress that this is a general finding, not dependent on the particular scheme used to define the Higgs mass. Using a different Higgs mass definition, like, e.g., the \overline{MS} Higgs mass \hat{m}_H , an explicit λ_4 dependence will appear in the expression for the W self-energy. However, an analogous dependence on λ_4 will appear in \hat{m}_H as well (when the latter is extracted from a physical quantity like the OS mass), resulting in a global cancellation of such dependences;
- further contributions, proportional to interaction between more than 4 ϕ_1 fields (e.g. quintic, sextic, etc. interactions), may arise from our modified potential. However, none of these interactions is going to contribute to the W self energy at the two-loop level³. Hence, the new contributions induced by our BSM scalar potential at the two-loop level are indeed only functions of κ_λ .

Analogously to what was obtained in the case of single Higgs processes [252], the anomalous contributions can be divided into two parts for both observables: a first one, linearly proportional to κ_λ and given by diagrams 7.3b), 7.3c); and a second one, quadratically dependent on κ_λ , due to the insertion of diagrams 7.3e₁) and of its corresponding Higgs mass counterterm in diagram 7.3a).

7.2 Analytic Expressions

Here I report the analytic expressions for the additional contributions induced in $\Delta\hat{r}_W^{(2)}$ and $Y_{\overline{MS}}^{(2)}$ by an anomalous λ_3 . In the formulae below

$$\zeta_w = \frac{m_H^2}{m_w^2}, \quad \overline{\ln}(x) = \log\left(\frac{x}{\mu}\right), \quad (7.9)$$

with μ the 't-Hooft mass scale. We find for the κ_λ contributions

$$\Delta\hat{r}_W^{(2,\kappa_\lambda)} = \left(\frac{\hat{\alpha}}{4\pi s^2}\right)^2 \left\{ \left[\frac{1}{64}\zeta_w (-12\zeta_w^2 + 49\zeta_w + 18) + \zeta_w \frac{4\zeta_w^2 - 7\zeta_w + 6}{16(\zeta_w - 1)} \overline{\ln}(m_w^2) \right] \right.$$

³A quintic self interaction does give rise to a two-loop tadpole; however, tadpole contributions cancel in Eqs. (7.5,7.6).

$$\begin{aligned}
& + \left(\frac{10 - 13\zeta_w}{16(\zeta_w - 1)} \zeta_w^2 + \frac{-2\zeta_w^4 + 9\zeta_w^3 - 46\zeta_w + 60}{32(\zeta_w - 1)^2} \zeta_w \bar{\ln}(m_w^2) \right) \bar{\ln}(m_H^2) \\
& + \frac{2\zeta_w^4 - 9\zeta_w^3 + 46\zeta_w - 60}{64(\zeta_w - 1)^2} \zeta_w \bar{\ln}(m_w^2)^2 \\
& + 3 \frac{2\zeta_w^4 - 3\zeta_w^3 - 4\zeta_w^2 + 18\zeta_w - 20}{64(\zeta_w - 1)^2} \zeta_w \bar{\ln}(m_H^2)^2 \\
& + \left(\frac{1}{8} (\zeta_w^2 - 3\zeta_w - 2) \zeta_w + \frac{1}{8} (\zeta_w - 2) \zeta_w \bar{\ln}(m_w^2) \right. \\
& \left. - \frac{1}{8} (\zeta_w - 2) \zeta_w^2 \bar{\ln}(m_H^2) \right) B_0(m_w^2, m_H^2, m_w^2) \\
& + \frac{1}{8} (\zeta_w - 2) \zeta_w B_0(m_w^2, m_H^2, m_w^2)^2 + \frac{\zeta_w - 2}{8m_w^2} \zeta_w S_0(m_w^2, m_w^2, m_H^2, m_H^2) \\
& - \frac{1}{2} (\zeta_w - 1) \zeta_w^2 T_0(m_w^2, m_H^2, m_w^2, m_H^2) \\
& + \frac{1}{4} (\zeta_w - 2) \zeta_w U_0(m_w^2, m_H^2, m_w^2, m_H^2, m_w^2) \\
& - \frac{1}{8} \zeta_w (\zeta_w^2 + \zeta_w - 6) U_0(m_w^2, m_w^2, m_H^2, m_H^2, m_H^2) \\
& + \frac{1}{16} m_H^2 (\zeta_w^3 - 12\zeta_w + 24) M_0(m_w^2, m_H^2, m_H^2, m_w^2, m_w^2, m_H^2) \\
& + 3 \frac{-2\zeta_w^3 + \zeta_w^2 + 4\zeta_w + 24}{64(\zeta_w - 1)^2} \zeta_w^2 \phi\left(\frac{1}{4}\right) + 3 \frac{4\zeta_w^2 - 41\zeta_w + 10}{32(\zeta_w - 1)^2} \zeta_w \phi\left(\frac{1}{4\zeta_w}\right) \\
& \left. - \frac{\zeta_w (2\zeta_w^4 - 13\zeta_w^3 + 18\zeta_w^2 + 40\zeta_w - 128)}{64(\zeta_w - 1)^2} \phi\left(\frac{\zeta_w}{4}\right) \right] \kappa_\lambda \\
& + \left[\frac{(-476\zeta_w^4 + 2403\zeta_w^3 - 4995\zeta_w^2 + 1652\zeta_w + 120)}{256(\zeta_w - 4)(\zeta_w - 1)} \zeta_w \right. \\
& + 3 \frac{(\zeta_w^4 - 6\zeta_w^3 + 39\zeta_w^2 - 100\zeta_w + 12)}{32(\zeta_w - 4)(\zeta_w - 1)^2} \zeta_w \bar{\ln}(m_w^2) \\
& + 9 \left(\frac{5\zeta_w^4 - 31\zeta_w^3 + 80\zeta_w^2 - 84\zeta_w + 48}{32(\zeta_w - 4)(\zeta_w - 1)^2} \zeta_w^2 - \frac{27\zeta_w^2}{32(\zeta_w - 1)^2} \bar{\ln}(m_w^2) \right) \bar{\ln}(m_H^2) \\
& \left. - 3 \frac{7\zeta_w^4 - 45\zeta_w^3 + 117\zeta_w^2 - 145\zeta_w + 120}{64(\zeta_w - 4)(\zeta_w - 1)^2} \zeta_w^2 \bar{\ln}(m_H^2)^2 \right]
\end{aligned}$$

$$\begin{aligned}
& + \left(\frac{1}{32} \zeta_w (\zeta_w^2 - 4\zeta_w + 12) - \frac{1}{16} \zeta_w (\zeta_w^2 - 4\zeta_w + 12) \bar{\ln}(m_H^2) \right. \\
& - 9 \frac{(\zeta_w - 2)^3}{32 (\zeta_w - 4)} \zeta_w B_0(m_H^2, m_H^2, m_H^2) \left. \right) B_0(m_W^2, m_H^2, m_W^2) \\
& + \left(9 \frac{2\zeta_w^4 - 13\zeta_w^3 + 33\zeta_w^2 - 36\zeta_w + 32}{64 (\zeta_w - 4) (\zeta_w - 1)} \zeta_w \right. \\
& + 9 \frac{\zeta_w^4 - 6\zeta_w^3 + 14\zeta_w^2 - 8\zeta_w + 8}{32 (\zeta_w - 4) (\zeta_w - 1)^2} \zeta_w \bar{\ln}(m_W^2) \\
& - 9 \frac{\zeta_w^4 - 7\zeta_w^3 + 19\zeta_w^2 - 24\zeta_w + 20}{32 (\zeta_w - 4) (\zeta_w - 1)^2} \zeta_w^2 \bar{\ln}(m_H^2) \left. \right) B_0(m_H^2, m_H^2, m_H^2) \\
& + 9 \frac{\zeta_w^2 - 4\zeta_w + 8}{32 m_W^2 (\zeta_w - 4)} \zeta_w S_0(m_W^2, m_W^2, m_H^2, m_H^2) \\
& - \frac{\zeta_w^3 - 5\zeta_w^2 + 16\zeta_w - 12}{4 (\zeta_w - 4)} \zeta_w T_0(m_W^2, m_H^2, m_W^2, m_H^2) \\
& + \frac{7\zeta_w^3 - 38\zeta_w^2 + 52\zeta_w + 24}{32 (\zeta_w - 4)} \zeta_w U_0(m_W^2, m_W^2, m_H^2, m_H^2, m_H^2) \\
& + 3 \frac{7\zeta_w^4 - 45\zeta_w^3 + 99\zeta_w^2 - 64\zeta_w + 84}{64 (\zeta_w - 4) (\zeta_w - 1)^2} \zeta_w^2 \phi\left(\frac{1}{4}\right) \\
& + 27 \frac{4\zeta_w - 1}{64 (\zeta_w - 1)^2} \zeta_w^2 \phi\left(\frac{1}{4\zeta_w}\right) \left. \right] \kappa_\lambda^2 \Bigg\}, \tag{7.10}
\end{aligned}$$

and

$$\begin{aligned}
Y_{\overline{MS}}^{(2, \kappa_\lambda)} & = \left(\frac{\hat{\alpha}}{4\pi s^2} \right)^2 \left\{ \left[f_1\left(\frac{m_H^2}{m_W^2}\right) - \frac{1}{c^4} f_1\left(\frac{m_H^2}{m_Z^2}\right) \right] \kappa_\lambda \right. \\
& \quad \left. + \left[f_2\left(\frac{m_H^2}{m_W^2}\right) - \frac{1}{c^4} f_2\left(\frac{m_H^2}{m_Z^2}\right) \right] \kappa_\lambda^2 \right\}, \tag{7.11}
\end{aligned}$$

where we have defined the functions f_1, f_2 as

$$\begin{aligned}
f_1(\zeta \equiv m_H^2/m^2) & = \frac{1}{32} \left[- (6\zeta^2 - 11\zeta - 15) \zeta + 4(2\zeta - 3) \zeta \bar{\ln}(m^2) + (\zeta - 4) \zeta^2 \bar{\ln}(m^2)^2 \right. \\
& \quad \left. - 2 \left(10\zeta^2 + (\zeta - 4) \zeta^2 \bar{\ln}(m^2) \right) \bar{\ln}(m_H^2) + 3\zeta^3 \bar{\ln}(m_H^2)^2 \right]
\end{aligned}$$

$$\begin{aligned}
& +4 \left(-2 - 3\zeta + \zeta^2 + (\zeta - 2)\overline{\ln}(m^2) \right. \\
& \left. - (\zeta - 2)\zeta\overline{\ln}(m_H^2) \right) \zeta B_0(m^2, m_H^2, m^2) \\
& +4(\zeta - 2)\zeta B_0(m^2, m_H^2, m^2)^2 \\
& +4(\zeta - 2)\frac{\zeta^2}{m_H^2} S_0(m^2, m^2, m_H^2, m_H^2) \\
& -16(\zeta - 1)\zeta^2 T_0(m^2, m_H^2, m^2, m_H^2) \\
& +8(\zeta - 2)\zeta U_0(m^2, m_H^2, m^2, m_H^2, m^2) \\
& -4(\zeta^2 + \zeta - 6)\zeta U_0(m^2, m^2, m_H^2, m_H^2, m_H^2) \\
& +2(\zeta^3 - 12\zeta + 24)m_H^2 M_0(m^2, m_H^2, m_H^2, m^2, m^2, m_H^2) \\
& \left. -3\zeta^3 \phi\left(\frac{1}{4}\right) - (\zeta - 4)(\zeta - 2)\zeta \phi\left(\frac{\zeta}{4}\right) \right], \tag{7.12}
\end{aligned}$$

$$\begin{aligned}
f_2(\zeta \equiv m_H^2/m^2) = & \frac{1}{128} \left[-\frac{(238\zeta^3 - 941\zeta^2 + 1660\zeta + 60)\zeta}{\zeta - 4} + \frac{12(\zeta^2 - 4\zeta + 12)\zeta}{\zeta - 4} \zeta\overline{\ln}(m^2) \right. \\
& +36\frac{5\zeta^2 - 20\zeta + 32}{\zeta - 4} \zeta^2\overline{\ln}(m_H^2) - 6\frac{7\zeta^2 - 28\zeta + 36}{\zeta - 4} \zeta^2\overline{\ln}(m_H^2)^2 \\
& +36 \left(\frac{\zeta^3 - 5\zeta^2 + 12\zeta - 16}{\zeta - 4} \zeta + \frac{\zeta^2 - 4\zeta + 8}{\zeta - 4} \zeta\overline{\ln}(m^2) \right. \\
& \left. - \frac{(\zeta - 2)^2}{\zeta - 4} \zeta^2\overline{\ln}(m_H^2) - \frac{(\zeta - 2)^3}{\zeta - 4} \zeta B_0(m^2, m_H^2, m^2) \right) B_0(m_H^2, m_H^2, m_H^2) \\
& +4(\zeta^2 - 4\zeta + 12) \left(1 - 2\overline{\ln}(m_H^2) \right) \zeta B_0(m^2, m_H^2, m^2) \\
& +36\frac{\zeta^2 - 4\zeta + 8}{m_H^2(\zeta - 4)} \zeta^2 S_0(m^2, m^2, m_H^2, m_H^2) \\
& -32\frac{\zeta^3 - 5\zeta^2 + 16\zeta - 12}{\zeta - 4} \zeta T_0(m^2, m_H^2, m^2, m_H^2) \\
& +4\frac{7\zeta^3 - 38\zeta^2 + 52\zeta + 24}{\zeta - 4} \zeta U_0(m^2, m^2, m_H^2, m_H^2, m_H^2) \\
& \left. +6\frac{7\zeta^2 - 28\zeta + 36}{\zeta - 4} \zeta^2 \phi\left(\frac{1}{4}\right) \right]. \tag{7.13}
\end{aligned}$$

In Eqs. (7.10)-(7.13)

$$\phi(x) = 4\sqrt{\frac{x}{1-x}} \operatorname{Im}(\operatorname{Li}_2(e^{i2\arcsin(\sqrt{x})})), \quad (7.14)$$

and, following Refs. [267, 268], we define the d -dimensional functions

$$B_0(s, x, y) = \lim_{\epsilon \rightarrow 0} \left[B(s, x, y) - \frac{1}{\epsilon} \right] = - \int_0^1 dt \overline{\ln}[tx + (1-t)y - t(1-t)s], \quad (7.15)$$

$$S_0(s, x, y, z) = \lim_{\epsilon \rightarrow 0} \left[S(s, x, y, z) + \frac{x+y+z}{2\epsilon^2} + \frac{\frac{s}{2} - x - y - z}{2\epsilon} - \frac{A(x) + A(y) + A(z)}{\epsilon} \right], \quad (7.16)$$

$$T_0(s, x, y, z) = -\frac{\partial}{\partial x} S_0(s, x, y, z), \quad (7.17)$$

$$U_0(s, x, y, z, u) = \lim_{\epsilon \rightarrow 0} \left[U(s, x, y, z, u) + \frac{1}{2\epsilon^2} - \frac{1}{2\epsilon} - \frac{B(s, x, y)}{\epsilon} \right], \quad (7.18)$$

$$M_0(s, x, y, z, u, v) = \lim_{\epsilon \rightarrow 0} [M(s, x, y, z, u, v)], \quad (7.19)$$

with $d = 4 - 2\epsilon$ and

$$A(x) = -i \frac{(2\pi\mu)^{2\epsilon}}{\pi^2} \int \frac{d^d k_1}{(k_1^2 - x)}, \quad (7.20)$$

$$B(s, x, y) = -i \frac{(2\pi\mu)^{2\epsilon}}{\pi^2} \int \frac{d^d k_1}{(k_1^2 - x)(k_3^2 - y)}, \quad (7.21)$$

$$S(s, x, y, z) = - \left(\frac{(2\pi\mu)^{2\epsilon}}{\pi^2} \right)^2 \iint \frac{d^d k_1 d^d k_2}{(k_1^2 - x)(k_3^2 - y)(k_4^2 - z)}, \quad (7.22)$$

$$U(s, x, y, z, u) = - \left(\frac{(2\pi\mu)^{2\epsilon}}{\pi^2} \right)^2 \iint \frac{d^d k_1 d^d k_2}{(k_5^2 - u)(k_2^2 - x)(k_3^2 - z)(k_4^2 - y)}, \quad (7.23)$$

$$M(s, x, y, z, u, v) = - \left(\frac{(2\pi\mu)^{2\epsilon}}{\pi^2} \right)^2 \iint \frac{d^d k_1 d^d k_2}{(k_1^2 - x)(k_2^2 - y)(k_3^2 - z)(k_4^2 - u)(k_5^2 - v)}, \quad (7.24)$$

where we introduced the notation

$$k_3 = k_1 - p, \quad k_4 = k_2 - p, \quad k_5 = k_1 - k_2, \quad (7.25)$$

with $p^2 = s$.

7.3 Resulting Bounds on the Trilinear Higgs Self-Coupling

Given the results obtained in the previous section and summarized in Eqs. (7.10)-(7.11), it is now possible to investigate their effect on the SM predictions for m_W and $\sin^2 \theta_{\text{eff}}^{\text{lep}}$ via Eqs. (7.1)-(7.4).

Denoting as O either m_W or $\sin^2 \theta_{\text{eff}}^{\text{lep}}$ one can write

$$O = O^{\text{SM}} [1 + (\kappa_\lambda - 1)C_1 + (\kappa_\lambda^2 - 1)C_2] , \quad (7.26)$$

with the values of the coefficients C_1 and C_2 reported in Tab. 7.1. The validity of such equation is due to the fact that the computation has been carried out at the two-loop level. This implies that, at this order, only finite contributions stemming from an anomalous trilinear Higgs coupling will affect the precision observables (check Tab. 7.1 or Eqs. (7.10)-(7.11)); moreover, these contributions are not sensitive to the NP scale Λ associated with the modification of the potential. This behavior is analogous to what happens when new contributions induced by an anomalous λ_3 coupling are considered in single Higgs processes at NLO [252]. In a similar fashion compared to NNLO effects in single Higgs processes, once tree- or more-loops diagrams are included in the computation, the modified potential is going to induce contributions not only proportional to the trilinear Higgs self-interactions, but also to the quartic, quintic etc. ones; moreover, these contributions will be also sensitive to the NP scale.

Before starting to analyse the bounds that can be obtained on κ_λ , a further clarification regarding our approach is necessary: throughout our study, we assumed the validity of the perturbative approach. Therefore, we assume that any high-order contribution should be subdominant with respect to the ones we considered in this analysis: hence, we expect that these higher-order contributions should not contain any large amplifying factor related to the scale Λ , which can be in turn interpreted as the requirement that Λ cannot be too far from the Electroweak scale. An estimate of this scale can be obtained by looking when perturbative unitarity is lost in processes like e.g. the annihilation of longitudinal vector bosons into n Higgs bosons, $V_L V_L \rightarrow n \phi_1$ [269]. A preliminary study on this subject indicates that $\Lambda \sim 1 - 3$ TeV [270].

	C_1	C_2
m_W	6.27×10^{-6}	-1.72×10^{-6}
$\sin^2 \theta_{\text{eff}}^{\text{lep}}$	-1.56×10^{-5}	4.55×10^{-6}

Table 7.1: Values of the coefficients C_1 and C_2 .

Moreover, following the same reasoning as the one at the end of Sec. 7.1, it is correct to assume that at the three-loop level the precision observables will obtain anomalous contributions up to order κ_λ^4 : hence, in order to not spoil the perturbative approach, a restricted range of κ_λ should also be imposed. Following Ref. [252] we therefore considered $|\kappa_\lambda| \lesssim 20$ as a range of validity of our perturbative approach. However, it is worth to notice that the subsequent study of [271], based both on the partial-wave unitarity of the $hh \rightarrow hh$ scattering and on the loop corrections to tree-level vertices, restricted the above range to $|\kappa_\lambda| \lesssim 6$.

We are now ready to study the bounds set on κ_λ from the analysis of precision observables. In order to accomplish such task, we performed the following simplified fit: the best value for κ_λ has been defined as the one that minimizes the $\chi^2(\kappa_\lambda)$ function defined as

$$\chi^2(\kappa_\lambda) \equiv \sum \frac{(O_{\text{exp}} - O_{\text{the}})^2}{(\delta)^2}, \quad (7.27)$$

where O_{exp} refers to the experimental measurement of the observable O , O_{the} is its theoretical value obtained from Eq. (7.26) and δ is the total uncertainty, set to be equal to the sum in quadrature of the experimental and theory errors. The goodness of our fit was ascertained by also computing the p -value as a function of κ_λ :

$$p\text{-value}(\kappa_\lambda) = 1 - F_{\chi_{(n)}^2}(\chi^2(\kappa_\lambda)), \quad (7.28)$$

where $F_{\chi_{(n)}^2}(\chi^2(\kappa_\lambda))$ is the cumulative distribution function for a χ^2 distribution with n degrees of freedom, computed at $\chi^2(\kappa_\lambda)$.

This procedure is analogous to the one employed by my collaborators in their previous study on signal strength parameter for single Higgs production [252]. In that analysis, the most promising set of observables consisted of the signal strength parameters in gluon fusion (ggF) and vector boson fusion (VBF): indicated as the P_2 set in Ref. [252], it was shown that it was the scenario providing the most stringent bound on κ_λ . Therefore, we decided to include these observables in our fits as well, studying a total of three different scenarios, differentiated by the considered set of data:

- The P_2 set in Ref. [252], using the experimental results presented in Tab. 8 of Ref. [233].
- The W mass and the effective sine. For the W mass we decided to use the latest result by the ATLAS collaboration $m_W = 80.370 \pm 0.019$ GeV [272]. This number, albeit showing a slightly larger uncertainty with respect to the world average $m_W = 80.385 \pm 0.015$ GeV [273], was chosen because closer to

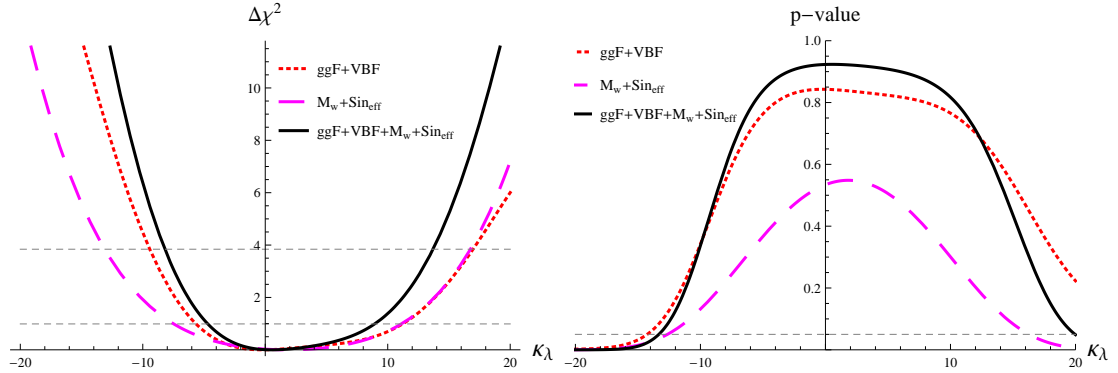


Figure 7.4: Left: χ^2 for two different sets of observables (electroweak precision observables, in purple, and signal strength parameter for single Higgs production, in red) and their combination (in black); the two horizontal dashed lines represent $\Delta\chi^2 = 1$ and $\Delta\chi^2 = 3.84$. Right: corresponding p -value, following the same colour scheme; the horizontal line is $p = 0.05$.

the SM prediction $m_W = 80.357 \pm 0.009 \pm 0.003$, with the errors referring to the parametric and the theoretical uncertainties [260]. Regarding the effective sine, we use the average of the CDF [274] and D0 [275] combinations $\sin^2 \theta_{\text{eff}}^{\text{lep}} = 0.23185 \pm 0.00035$ [273], to compare to the SM result $\sin^2 \theta_{\text{eff}}^{\text{lep}} = 0.23145 \pm 0.00012 \pm 0.00005$, where again the errors refer to parametric and theoretical uncertainties respectively [260, 276].

- The combination of these two sets of data.

The $\chi^2(\kappa_\lambda)$ for the three scenarios are reported in the left panel of Fig. 7.4, while the p -value functions are shown in the right one. In particular, in the third scenario (i.e. the combination of electroweak precision observables and signal strength parameter for single Higgs production) we found the following bounds:

$$\kappa_\lambda^{\text{best}} = 0.5, \quad \kappa_\lambda^{1\sigma} = [-4.7, 8.9], \quad \kappa_\lambda^{2\sigma} = [-8.2, 13.7], \quad (7.29)$$

where the $\kappa_\lambda^{\text{best}}$ is the best value and $\kappa_\lambda^{1\sigma}$, $\kappa_\lambda^{2\sigma}$ are respectively the 1σ and 2σ intervals, identified assuming a χ^2 distribution. It is interesting to compare the results obtained in Eq. (7.29) with the corresponding ones for the P_2 set of [252], where no precision observables was included. Recalling that such results were

$$\kappa_\lambda^{\text{best}} = -0.24, \quad \kappa_\lambda^{1\sigma} = [-5.6, 11.2], \quad \kappa_\lambda^{2\sigma} = [-9.4, 17.0], \quad (7.30)$$

it is straightforward to observe that the inclusion of the precision observables reduces the allowed range for κ_λ , resulting in a better constrain on the Higgs

trilinear self-coupling. Similarly, looking at the solid black line in the right panel of Fig. 7.4, we can now exclude at more than 2σ models with κ_λ in the regions $\kappa_\lambda < -13.3$ and $\kappa_\lambda > 20.0$.

These results are already comparable in size with the ones obtained by direct search, showing the utility of this alternative approach as a further way to constrain the Higgs trilinear self-coupling. Therefore, when more accurate measurements will be available in the future, the combination on m_W and $\sin^2 \theta_{\text{eff}}^{\text{lep}}$ with single Higgs processes could be very powerful in constraining the allowed region for κ_λ , in particular the region of positive κ_λ .

7.4 On the Equivalence with a $(\Phi^\dagger \Phi)^n$ Theory

The closing section of this chapter is devoted to showing that the results presented in Sec. 7.1 and obtained in the unitary gauge, with no specific assumption on the BSM scalar potential (and, in particular, no EFT assumption either), can be obtained starting from the SM Lagrangian, with a scalar potential of the form

$$V^{NP} = \sum_{n=1}^N c_{2n} (\Phi^\dagger \Phi)^n, \quad \Phi = \frac{1}{\sqrt{2}} \begin{pmatrix} \sqrt{2} \phi^+ \\ v + \phi_1 + i\phi_2 \end{pmatrix}. \quad (7.31)$$

The series can be either finite or infinite, with the requirement that in the latter case we assume it to be convergent. This is the only constraint we require from the c_{2n} coefficients: hence, an EFT scaling, i.e. $c_{2n+2} \sim c_{2n}/\Lambda^2$, is not required. Eq. (7.31) can be used also to describe the SM, setting $N = 2$ and defining $c_2 = -m^2$ and $c_4 = \lambda$, where $-m^2$ is the Higgs mass term in the SM Lagrangian in the unbroken phase.

Defining $\phi_{2u} = \phi^+ \phi^- + \frac{1}{2} \phi_2^2$ the n -th term in the series can be written as

$$(\Phi^\dagger \Phi)^n = \sum_{k=0}^n \sum_{j=0}^k \sum_{h=0}^j \binom{n}{k} \binom{k}{j} \binom{j}{h} \phi_{2u}^{n-k} \left(\frac{v^2}{2}\right)^{k-j} \left(\frac{\phi_1^2}{2}\right)^{j-h} (v\phi_1)^h, \quad (7.32)$$

with

$$\binom{n}{k} \binom{k}{j} \binom{j}{h} = \frac{n!}{(n-k)!(k-j)!(j-h)!h!}. \quad (7.33)$$

It is therefore possible to identify the contribution from the potential to any Higgs self-interaction by means of the triplet $\{k, j, h\}$. For example, the minimum of the potential can be obtained looking at the triplet $\{n, 1, 1\}$, which is the one that identifies the term of the potential linear in ϕ_1 :

$$\left. \frac{dV^{NP}}{d\phi_1} \right|_{\phi_1=0} = v \sum_{n=1}^N c_{2n} n \left(\frac{v^2}{2}\right)^{n-1} = 0. \quad (7.34)$$

Following the same reasoning, the Higgs mass is given by the two triplets $\{n, 1, 0\}$ and $\{n, 2, 2\}$, since these are the triplets that identify the term of the potential quadratic in ϕ_1 . However the first triplet yields a vanishing term, since it is proportional to the minimum condition from Eq. (7.34), so that only the second triplet contributes to the definition

$$m_H^2 = v^2 \sum_{n=1}^N c_{2n} n(n-1) \left(\frac{v^2}{2}\right)^{n-2}. \quad (7.35)$$

Starting from this general potential, it is possible to write down the potential V^{NP} up to quartic interactions as

$$\begin{aligned} V_{4\phi}^{NP} = & \frac{m_H^2}{2v^2} \left[\phi^+ \phi^- (\phi^+ \phi^- + \phi_2^2) + \frac{1}{4} \phi_2^4 \right] + \left(\frac{m_H^2}{2v^2} + d\lambda_4 \right) \frac{1}{4} \phi_1^4 \\ & + \left(\frac{m_H^2}{2v^2} + 3d\lambda_3 \right) \phi_1^2 \left[\phi^+ \phi^- + \frac{1}{2} \phi_2^2 \right] + \left(\frac{m_H^2}{2v} + v d\lambda_3 \right) \phi_1^3 \\ & + \frac{m_H^2}{2v} \phi_1 (\phi_2^2 + 2\phi^+ \phi^-) + \frac{1}{2} m_H^2 \phi_1^2, \end{aligned} \quad (7.36)$$

where the following relations are implied:

$$d\lambda_3 = \frac{1}{3} \sum_{n=3}^N c_{2n} n(n-1)(n-2) \left(\frac{v^2}{2}\right)^{n-2}, \quad (7.37)$$

$$d\lambda_4 = \frac{2}{3} \sum_{n=3}^N c_{2n} n^2(n-1)(n-2) \left(\frac{v^2}{2}\right)^{n-2}. \quad (7.38)$$

One remarkable feature of Eq. (7.36) is that only few couplings are modified with respect to their SM values. In particular, concerning the unphysical scalars, the only modified coupling is the one relative to the $\phi_{2u} \phi_1^2$ interaction, with a deformation that is related to the deformation of λ_3 .

We have now all the necessary ingredients to show that the result for the two-loop W self energy obtained in Sec. 7.1, assuming an anomalous λ_3 and working in the unitary gauge, is equal to the one that can be obtained using V^{NP} (and analogously for the Z self-energy). In order to do so, we have to analyze the two-loop diagrams that are modified with respect to their SM result working in a generic R_ξ gauge. Therefore, besides computing the diagrams in Fig. 7.3 in an R_ξ gauge, new diagrams will have to be taken into account. First, one should also consider the diagrams containing unphysical scalars: such diagrams are shown in Fig. 7.5, where the grey blob represents the insertion of the relevant one-loop self energy or the corresponding mass counterterm. Moreover, new diagrams (involving

again unphysical scalars) will be included in the various self energies as well: such diagrams (along with the tadpole one), affected by the modification with respect to their SM result due to the new scalar potential V^{NP} , are shown in Fig. 7.6.

Similarly to what was observed for diagram 7.3e₂), the cactus diagrams 7.6a) are cancelled against the corresponding Higgs counterterms once inserted in diagrams 7.3a), 7.3d) or 7.5a). Furthermore, both the sum of diagrams 7.3a) and 7.5a) and the sum of diagrams 7.3b), 7.3c), 7.5b), and 7.5c) are gauge invariant: hence, going from the unitary gauge to a generic R_ξ gauge and adding the diagrams 7.5a)–7.5c) and 7.6a) does not add further, gauge-dependent terms to the result. Therefore, in order to complete our equivalence proof, we have to show that the additional contributions with respect to the SM results in the diagrams 7.5d)–7.5h) and in the corresponding counterterm diagrams must vanish.

Diagram 7.5d) is automatically zero, while all the remaining diagrams display an insertion of a self energy of an unphysical scalar, or of the correspondent counterterm. According to Eq. (7.36), diagrams 7.6c₁) and 7.6d₁) are the only modified contributions in the one-loop self energies of the unphysical scalars. The counterterm associated to the renormalization of the mass of an unphysical scalar contains two terms: the first one is related to the mass of the corresponding vector boson, while the second one is related to the renormalization of the vacuum. The former is not affected by our modified scalar potential, while the latter, when v is identified with the minimum of the radiatively corrected potential, is given by the tadpole contribution [277]. Therefore, the only modified contribution in the

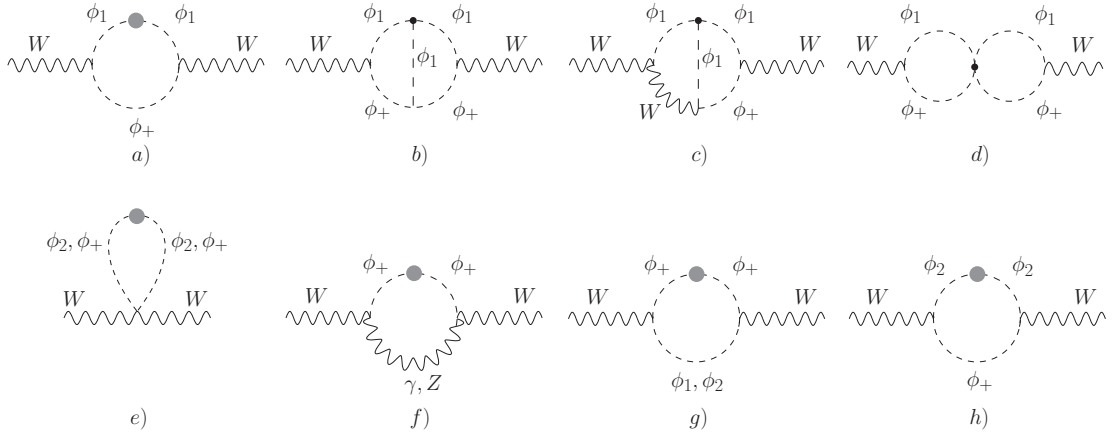


Figure 7.5: Two-loop diagrams in the W self-energy, involving unphysical scalars where modified couplings (black points) from $V_{4\phi}^{NP}$ appear. The grey blob represents the insertion of the modified diagrams in the one-loop self energy (see fig. 7.6), or in the mass counterterm.

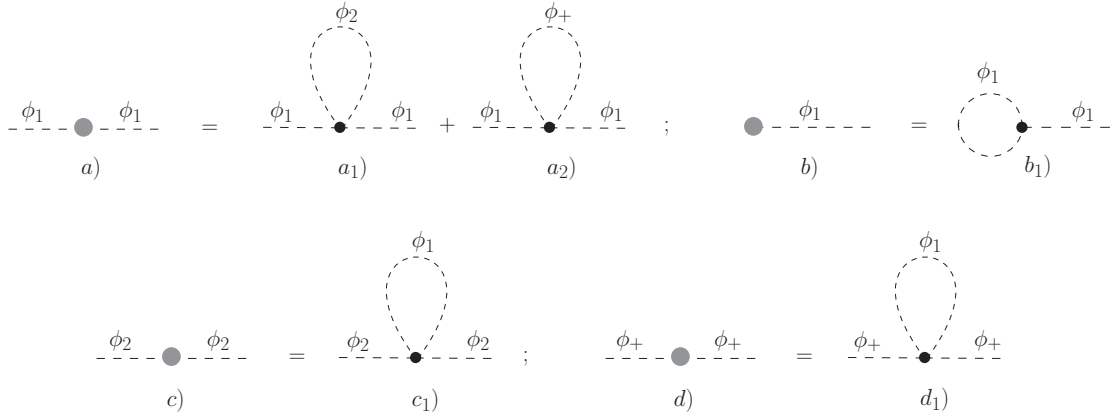


Figure 7.6: One-loop self energy and tadpole diagrams that contain modified couplings with respect to the SM.

mass renormalization of the unphysical scalars is given by the tadpole diagram 7.6 b_1). Observing now Eq. (7.36), it is easy to notice that the modification to the vertices 7.6 c_1) and 7.6 d_1) are related by a factor $3/v$ to the one of the vertex 7.6 b_1). Remarkably, when the Feynman rule for the latter vertex is computed, a factor of 3 is generated due to combinatorics. Therefore, one obtains that diagrams 7.5 d)–7.5 h) are equal if one inserts either a self-energy or a counterterm: hence, once the differences of the two are taken into account, the total contribution vanishes.

This concludes our equivalence proof: a theory with a scalar potential given by Eq. (7.31) modifies the two-loop W self energy in a gauge-invariant way. Therefore, directly computing such modification in the unitary gauge does not introduce gauge-dependent terms: the results obtained in the two methods are equivalent, once the identification $\kappa_\lambda = 1 + 2v^2/m_H^2 d\lambda_3$ is made.

Conclusions

The Standard Model has been providing an excellent description of all available data in particle physics for a few decades. Yet, we have several reasons to believe that it is only a low energy effective theory valid up to the TeV scale, with Beyond Standard Model physics still hidden at higher scales. However, the amazing efforts put in the LHC still have to succeed in the production of BSM particles, and hence we have no particular clue on what the UV completion of the SM could look like. In such a context, the SMEFT framework can be particularly useful, given its peculiar feature to describe BSM effects in a model-independent way. The BSM fields can in fact be integrated out of the theory in such a way that, at the EWSB scale, their effects appear in the couplings of the SMEFT. Performing global fits of experimental data in this framework allows to bound such couplings; subsequently, these bounds can be reinterpreted as bounds on the NP scale and masses once the SMEFT is mapped on the desired UV completion of the theory. Given this context, my PhD thesis was carried out employing the SMEFT framework.

As a first step in my PhD program, I recomputed several of the entries of the SMEFT AD from Refs. [4–7], namely all those stemming from 1PI diagrams. This computation was performed since a systematic cross-check of such computation was lacking in the literature, and it involved only the 1PI diagrams because a complete check of the AD would have been lengthy, and beyond the scope of this thesis. All the obtained results were found in perfect agreement with the ones from Refs. [4–7].

Subsequently, I devoted most of my time to flavour Physics. The recent years of experimental results in B physics have been indeed characterized by the emergence of a striking pattern of anomalies, observed in multiple independent studies of some rare $b \rightarrow s$ transitions [125]. The main characters of such a pattern are the angular observables of the $B \rightarrow K^* \mu^+ \mu^-$ decay [74, 78, 80, 82, 126], the Branching Fractions of the $B \rightarrow \phi \mu^+ \mu^-$ [77] and $B \rightarrow K \mu^+ \mu^-$ [75, 81] decays, and the Branching Fraction ratios R_K [76] and R_{K^*} [83]. As I have argued in Refs. [8–10], the “pollution” induced by a non-perfect knowledge of the hadronic contribution in the angular observables produces an entanglement between these contributions and NP effects (usually advocated in the muonic vector current), in such a way

that it is not possible to ascertain the presence of BSM physics looking at the angular observables only. However, the emergence of LUV in Branching Fraction ratios points toward an ineluctable requirement for NP effects in $b \rightarrow s$ transitions, if these anomalies are indeed to stay in future measurements. Nevertheless, as I have illustrated in Ref. [11], a careful treatment of the hadronic contribution could yield to a parallel, equally viable NP scenario involving BSM effects in the electronic axial current. Moreover, I have reinterpreted all my findings in the SMEFT framework, being able to put bounds on several NP WCs by means of a Bayesian global fit. Hopefully, Run 2 results from LHCb will help to shed some light on the NP shape, but most likely we will have to wait until the first results from Belle II to clarify the experimental situation.

Last but not least, I have spent some time working on the study of the trilinear Higgs self-coupling as well. Given the large room for NP effects in this coupling, compatible with the present status of the experimental constraints, the SMEFT framework is, presently, not interesting from a phenomenological point of view. Nevertheless, trying to constrain such interactions can be a really interesting probe for the search of BSM effects: hence, I decided to devote some time to the study of possible new ways to put bounds on the Higgs trilinear self-coupling. The results of such studies, summarized in Ref. [12], are obtained employing the κ_λ formalism [256] to electroweak precision observables, namely the W boson mass and the effective sine. Indeed, we were able to obtain bounds on the anomalous self-coupling stemming by the loop-induced effects on such electroweak precision observables; such bounds turned out to be comparable with the ones obtained from direct searches, therefore proving that this can be a complementary tool in a combined effort to constrain the last SM coupling allowing for large NP effects.

Bibliography

- [1] CMS collaboration, S. Chatrchyan et al., *Observation of a new boson at a mass of 125 GeV with the CMS experiment at the LHC*, *Phys. Lett.* **B716** (2012) 30–61, [1207.7235].
- [2] ATLAS collaboration, G. Aad et al., *Observation of a new particle in the search for the Standard Model Higgs boson with the ATLAS detector at the LHC*, *Phys.Lett.* **B716** (2012) 1–29, [1207.7214].
- [3] B. Grzadkowski, M. Iskrzynski, M. Misiak and J. Rosiek, *Dimension-Six Terms in the Standard Model Lagrangian*, *JHEP* **10** (2010) 085, [1008.4884].
- [4] C. Grojean, E. E. Jenkins, A. V. Manohar and M. Trott, *Renormalization Group Scaling of Higgs Operators and $\Gamma(h \rightarrow \gamma\gamma)$* , *JHEP* **04** (2013) 016, [1301.2588].
- [5] E. E. Jenkins, A. V. Manohar and M. Trott, *Renormalization Group Evolution of the Standard Model Dimension Six Operators I: Formalism and lambda Dependence*, *JHEP* **10** (2013) 087, [1308.2627].
- [6] E. E. Jenkins, A. V. Manohar and M. Trott, *Renormalization Group Evolution of the Standard Model Dimension Six Operators II: Yukawa Dependence*, *JHEP* **01** (2014) 035, [1310.4838].
- [7] R. Alonso, E. E. Jenkins, A. V. Manohar and M. Trott, *Renormalization Group Evolution of the Standard Model Dimension Six Operators III: Gauge Coupling Dependence and Phenomenology*, *JHEP* **04** (2014) 159, [1312.2014].
- [8] M. Ciuchini, M. Fedele, E. Franco, S. Mishima, A. Paul, L. Silvestrini et al., *$B \rightarrow K^* \ell^+ \ell^-$ decays at large recoil in the Standard Model: a theoretical reappraisal*, *JHEP* **06** (2016) 116, [1512.07157].

- [9] M. Ciuchini, M. Fedele, E. Franco, S. Mishima, A. Paul, L. Silvestrini et al., *B* → *K** $\ell^+\ell^-$ in the Standard Model: Elaborations and Interpretations, *PoS ICHEP2016* (2016) 584, [1611.04338].
- [10] M. Ciuchini, M. Fedele, E. Franco, S. Mishima, A. Paul, L. Silvestrini et al., *Knowns and Unknowns in the Predictions for B* → *K** $\mu^+\mu^-$, *Nucl. Part. Phys. Proc.* **285-286** (2017) 45–49.
- [11] M. Ciuchini, A. M. Coutinho, M. Fedele, E. Franco, A. Paul, L. Silvestrini et al., *On Flavourful Easter eggs for New Physics hunger and Lepton Flavour Universality violation*, *Eur. Phys. J.* **C77** (2017) 688, [1704.05447].
- [12] G. Degrossi, M. Fedele and P. P. Giardino, *Constraints on the trilinear Higgs self coupling from precision observables*, *JHEP* **04** (2017) 155, [1702.01737].
- [13] P. W. Higgs, *Broken symmetries, massless particles and gauge fields*, *Phys.Lett.* **12** (1964) 132–133.
- [14] P. W. Higgs, *Broken Symmetries and the Masses of Gauge Bosons*, *Phys.Rev.Lett.* **13** (1964) 508–509.
- [15] P. W. Higgs, *Spontaneous Symmetry Breakdown without Massless Bosons*, *Phys.Rev.* **145** (1966) 1156–1163.
- [16] N. Cabibbo, *Unitary Symmetry and Leptonic Decays*, *Phys.Rev.Lett.* **10** (1963) 531–533.
- [17] M. Kobayashi and T. Maskawa, *CP Violation in the Renormalizable Theory of Weak Interaction*, *Prog.Theor.Phys.* **49** (1973) 652–657.
- [18] L.-L. Chau and W.-Y. Keung, *Comments on the Parametrization of the Kobayashi-Maskawa Matrix*, *Phys.Rev.Lett.* **53** (1984) 1802.
- [19] L. Wolfenstein, *Parametrization of the Kobayashi-Maskawa Matrix*, *Phys.Rev.Lett.* **51** (1983) 1945.
- [20] A. J. Buras, *Weak Hamiltonian, CP violation and rare decays*, in *Probing the standard model of particle interactions. Proceedings, Summer School in Theoretical Physics, NATO Advanced Study Institute, 68th session, Les Houches, France, July 28-September 5, 1997. Pt. 1, 2*, pp. 281–539, 1998. hep-ph/9806471.

- [21] G. 't Hooft and M. Veltman, *Regularization and Renormalization of Gauge Fields*, *Nucl.Phys.* **B44** (1972) 189–213.
- [22] G. 't Hooft, *Dimensional regularization and the renormalization group*, *Nucl.Phys.* **B61** (1973) 455–468.
- [23] E. Fermi, *An attempt of a theory of beta radiation. 1.*, *Z. Phys.* **88** (1934) 161–177.
- [24] K. G. Wilson, *Nonlagrangian models of current algebra*, *Phys.Rev.* **179** (1969) 1499–1512.
- [25] K. Wilson and W. Zimmermann, *Operator product expansions and composite field operators in the general framework of quantum field theory*, *Commun.Math.Phys.* **24** (1972) 87–106.
- [26] S. Weinberg, *Baryon- and lepton-nonconserving processes*, *Physical Review Letters* **43** (1979) 1566–1570.
- [27] A. de Gouvea, J. Herrero-Garcia and A. Kobach, *Neutrino Masses, Grand Unification, and Baryon Number Violation*, *Phys. Rev.* **D90** (2014) 016011, [1404.4057].
- [28] A. Kobach, *Baryon Number, Lepton Number, and Operator Dimension in the Standard Model*, *Phys. Lett.* **B758** (2016) 455–457, [1604.05726].
- [29] P. Minkowski, $\mu \rightarrow e\gamma$ at a Rate of One Out of 10^9 Muon Decays?, *Phys. Lett.* **67B** (1977) 421–428.
- [30] T. Yanagida, *HORIZONTAL SYMMETRY AND MASSES OF NEUTRINOS*, *Conf. Proc.* **C7902131** (1979) 95–99.
- [31] S. L. Glashow, *The Future of Elementary Particle Physics*, *NATO Sci. Ser. B* **61** (1980) 687.
- [32] M. Gell-Mann, P. Ramond and R. Slansky, *Complex Spinors and Unified Theories*, *Conf. Proc.* **C790927** (1979) 315–321, [1306.4669].
- [33] B. Henning, X. Lu and H. Murayama, *How to use the Standard Model effective field theory*, *JHEP* **01** (2016) 023, [1412.1837].
- [34] W. Buchmuller and D. Wyler, *Effective Lagrangian Analysis of New Interactions and Flavor Conservation*, *Nucl. Phys.* **B268** (1986) 621–653.
- [35] G. F. Giudice, C. Grojean, A. Pomarol and R. Rattazzi, *The Strongly-Interacting Light Higgs*, *JHEP* **06** (2007) 045, [hep-ph/0703164].

- [36] K. Hagiwara, S. Ishihara, R. Szalapski and D. Zeppenfeld, *Low-energy effects of new interactions in the electroweak boson sector*, *Phys. Rev.* **D48** (1993) 2182–2203.
- [37] R. F. Dashen, E. E. Jenkins and A. V. Manohar, *The $1/N(c)$ expansion for baryons*, *Phys. Rev.* **D49** (1994) 4713, [[hep-ph/9310379](#)].
- [38] R. F. Dashen, E. E. Jenkins and A. V. Manohar, *Spin flavor structure of large $N(c)$ baryons*, *Phys. Rev.* **D51** (1995) 3697–3727, [[hep-ph/9411234](#)].
- [39] E. Braaten, C.-S. Li and T.-C. Yuan, *The Evolution of Weinberg’s Gluonic CP Violation Operator*, *Phys. Rev. Lett.* **64** (1990) 1709.
- [40] G. Boyd, A. K. Gupta, S. P. Trivedi and M. B. Wise, *Effective Hamiltonian for the Electric Dipole Moment of the Neutron*, *Phys. Lett.* **B241** (1990) 584–588.
- [41] C. Arzt, M. B. Einhorn and J. Wudka, *Effective Lagrangian approach to precision measurements: The Anomalous magnetic moment of the muon*, *Phys. Rev.* **D49** (1994) 1370–1377, [[hep-ph/9304206](#)].
- [42] K. Hagiwara, R. Szalapski and D. Zeppenfeld, *Anomalous Higgs boson production and decay*, *Phys. Lett.* **B318** (1993) 155–162, [[hep-ph/9308347](#)].
- [43] S. Alam, S. Dawson and R. Szalapski, *Low-energy constraints on new physics revisited*, *Phys. Rev.* **D57** (1998) 1577–1590, [[hep-ph/9706542](#)].
- [44] F. Borzumati, C. Greub, T. Hurth and D. Wyler, *Gluino contribution to radiative B decays: Organization of QCD corrections and leading order results*, *Phys. Rev.* **D62** (2000) 075005, [[hep-ph/9911245](#)].
- [45] A. J. Buras, M. Misiak and J. Urban, *Two loop QCD anomalous dimensions of flavor changing four quark operators within and beyond the standard model*, *Nucl. Phys.* **B586** (2000) 397–426, [[hep-ph/0005183](#)].
- [46] Z. Han and W. Skiba, *Effective theory analysis of precision electroweak data*, *Phys. Rev.* **D71** (2005) 075009, [[hep-ph/0412166](#)].
- [47] G. Degrossi, E. Franco, S. Marchetti and L. Silvestrini, *QCD corrections to the electric dipole moment of the neutron in the MSSM*, *JHEP* **11** (2005) 044, [[hep-ph/0510137](#)].
- [48] J. Gao, C. S. Li and C. P. Yuan, *NLO QCD Corrections to dijet Production via Quark Contact Interactions*, *JHEP* **07** (2012) 037, [[1204.4773](#)].

- [49] H. Mebane, N. Greiner, C. Zhang and S. Willenbrock, *Effective Field Theory of Precision Electroweak Physics at One Loop*, *Phys. Lett.* **B724** (2013) 259–263, [1304.1789].
- [50] C. Zhang and F. Maltoni, *Top-quark decay into Higgs boson and a light quark at next-to-leading order in QCD*, *Phys. Rev.* **D88** (2013) 054005, [1305.7386].
- [51] H. Mebane, N. Greiner, C. Zhang and S. Willenbrock, *Constraints on Electroweak Effective Operators at One Loop*, *Phys. Rev.* **D88** (2013) 015028, [1306.3380].
- [52] J. Brod, U. Haisch and J. Zupan, *Constraints on CP-violating Higgs couplings to the third generation*, *JHEP* **11** (2013) 180, [1310.1385].
- [53] F. J. Gilman and M. B. Wise, *Effective Hamiltonian for $\Delta S = 1$ Weak Nonleptonic Decays in the Six Quark Model*, *Phys. Rev.* **D20** (1979) 2392.
- [54] H. Georgi, *Weak Interactions and Modern Particle Theory*. 1984.
- [55] A. Alloul, N. D. Christensen, C. Degrande, C. Duhr and B. Fuks, *FeynRules 2.0 - A complete toolbox for tree-level phenomenology*, *Comput. Phys. Commun.* **185** (2014) 2250–2300, [1310.1921].
- [56] T. Hahn, *Generating Feynman diagrams and amplitudes with FeynArts 3*, *Comput. Phys. Commun.* **140** (2001) 418–431, [hep-ph/0012260].
- [57] G. Passarino and M. J. G. Veltman, *One Loop Corrections for e^+e^- annihilation into $\mu^+\mu^-$ in the Weinberg Model*, *Nucl. Phys.* **B160** (1979) 151.
- [58] R. K. Ellis, Z. Kunszt, K. Melnikov and G. Zanderighi, *One-loop calculations in quantum field theory: from Feynman diagrams to unitarity cuts*, *Phys. Rept.* **518** (2012) 141–250, [1105.4319].
- [59] L. Lehman, *Extending the Standard Model Effective Field Theory with the Complete Set of Dimension-7 Operators*, *Phys. Rev.* **D90** (2014) 125023, [1410.4193].
- [60] L. Lehman and A. Martin, *Low-derivative operators of the Standard Model effective field theory via Hilbert series methods*, *JHEP* **02** (2016) 081, [1510.00372].

- [61] B. Henning, X. Lu, T. Melia and H. Murayama, *2, 84, 30, 993, 560, 15456, 11962, 261485, ...: Higher dimension operators in the SM EFT*, 1512.03433.
- [62] L. Lehman and A. Martin, *Hilbert Series for Constructing Lagrangians: expanding the phenomenologist's toolbox*, *Phys. Rev.* **D91** (2015) 105014, [1503.07537].
- [63] R. Contino, A. Falkowski, F. Goertz, C. Grojean and F. Riva, *On the Validity of the Effective Field Theory Approach to SM Precision Tests*, *JHEP* **07** (2016) 144, [1604.06444].
- [64] Y. Amhis et al., *Averages of b -hadron, c -hadron, and τ -lepton properties as of summer 2016*, 1612.07233.
- [65] A. J. Buras, *Climbing NLO and NNLO Summits of Weak Decays*, 1102.5650.
- [66] F. Beaujean, C. Bobeth and D. van Dyk, *Comprehensive Bayesian analysis of rare (semi)leptonic and radiative B decays*, *Eur.Phys.J.* **C74** (2014) 2897, [1310.2478].
- [67] T. Blake, G. Lanfranchi and D. M. Straub, *Rare B Decays as Tests of the Standard Model*, *Prog. Part. Nucl. Phys.* **92** (2017) 50–91, [1606.00916].
- [68] S. L. Glashow, J. Iliopoulos and L. Maiani, *Weak Interactions with Lepton-Hadron Symmetry*, *Phys. Rev.* **D2** (1970) 1285–1292.
- [69] BELLE collaboration, T. Saito et al., *Measurement of the $\bar{B} \rightarrow X_s \gamma$ Branching Fraction with a Sum of Exclusive Decays*, *Phys. Rev.* **D91** (2015) 052004, [1411.7198].
- [70] BELLE collaboration, A. Abdesselam et al., *Measurement of the inclusive $B \rightarrow X_{s+d} \gamma$ branching fraction, photon energy spectrum and HQE parameters*, in *Proceedings, 38th International Conference on High Energy Physics (ICHEP 2016): Chicago, IL, USA, August 3-10, 2016*, 2016. 1608.02344.
- [71] BABAR collaboration, J. P. Lees et al., *Precision Measurement of the $B \rightarrow X_s \gamma$ Photon Energy Spectrum, Branching Fraction, and Direct CP Asymmetry $A_{CP}(B \rightarrow X_{s+d} \gamma)$* , *Phys. Rev. Lett.* **109** (2012) 191801, [1207.2690].

- [72] LHCb collaboration, R. Aaij et al., *Differential branching fraction and angular analysis of the decay $B^0 \rightarrow K^{*0} \mu^+ \mu^-$* , *JHEP* **08** (2013) 131, [1304.6325].
- [73] LHCb collaboration, *Angular analysis of the $B^0 \rightarrow K^{*0} \mu^+ \mu^-$ decay*, *LHCb-CONF-2015-002, CERN-LHCb-CONF-2015-002* (2015) .
- [74] LHCb collaboration, R. Aaij et al., *Measurement of Form-Factor-Independent Observables in the Decay $B^0 \rightarrow K^{*0} \mu^+ \mu^-$* , *Phys.Rev.Lett.* **111** (2013) 191801, [1308.1707].
- [75] LHCb collaboration, R. Aaij et al., *Differential branching fractions and isospin asymmetries of $B \rightarrow K^{(*)} \mu^+ \mu^-$ decays*, *JHEP* **06** (2014) 133, [1403.8044].
- [76] LHCb collaboration, R. Aaij et al., *Test of lepton universality using $B^+ \rightarrow K^+ \ell^+ \ell^-$ decays*, *Phys. Rev. Lett.* **113** (2014) 151601, [1406.6482].
- [77] LHCb collaboration, R. Aaij et al., *Angular analysis and differential branching fraction of the decay $B_s^0 \rightarrow \phi \mu^+ \mu^-$* , *JHEP* **09** (2015) 179, [1506.08777].
- [78] LHCb collaboration, R. Aaij et al., *Angular analysis of the $B^0 \rightarrow K^{*0} \mu^+ \mu^-$ decay using 3 fb^{-1} of integrated luminosity*, *JHEP* **02** (2016) 104, [1512.04442].
- [79] BELLE collaboration, A. Abdesselam et al., *Angular analysis of $B^0 \rightarrow K^*(892)^0 \ell^+ \ell^-$* , in *Proceedings, LHCSki 2016 - A First Discussion of 13 TeV Results: Obergurgl, Austria, April 10-15, 2016*, 2016. 1604.04042.
- [80] BELLE collaboration, S. Wehle et al., *Lepton-Flavor-Dependent Angular Analysis of $B \rightarrow K^* \ell^+ \ell^-$* , *Phys. Rev. Lett.* **118** (2017) 111801, [1612.05014].
- [81] LHCb collaboration, R. Aaij et al., *Measurement of the phase difference between short- and long-distance amplitudes in the $B^+ \rightarrow K^+ \mu^+ \mu^-$ decay*, *Eur. Phys. J.* **C77** (2017) 161, [1612.06764].
- [82] ATLAS collaboration, *Angular analysis of $B_d^0 \rightarrow K^* \mu^+ \mu^-$ decays in pp collisions at $\sqrt{s} = 8 \text{ TeV}$ with the ATLAS detector*, Tech. Rep. ATLAS-CONF-2017-023, CERN, Geneva, Apr, 2017.
- [83] LHCb collaboration, R. Aaij et al., *Test of lepton universality with $B^0 \rightarrow K^{*0} \ell^+ \ell^-$ decays*, *JHEP* **08** (2017) 055, [1705.05802].

- [84] K. G. Chetyrkin, M. Misiak and M. Munz, *Weak radiative B meson decay beyond leading logarithms*, *Phys.Lett.* **B400** (1997) 206–219, [[hep-ph/9612313](#)].
- [85] A. J. Buras and M. Munz, *Effective Hamiltonian for $B \rightarrow X_s e^+ e^-$ beyond leading logarithms in the NDR and HV schemes*, *Phys.Rev.* **D52** (1995) 186–195, [[hep-ph/9501281](#)].
- [86] M. Ciuchini, G. Degrossi, P. Gambino and G. Giudice, *Next-to-leading QCD corrections to $B \rightarrow X_s \gamma$: Standard model and two Higgs doublet model*, *Nucl.Phys.* **B527** (1998) 21–43, [[hep-ph/9710335](#)].
- [87] P. Ball and R. Zwicky, *$B_{d,s} \rightarrow \rho, \omega, K^*, \phi$ decay form-factors from light-cone sum rules revisited*, *Phys.Rev.* **D71** (2005) 014029, [[hep-ph/0412079](#)].
- [88] A. Bharucha, D. M. Straub and R. Zwicky, *$B \rightarrow V \ell^+ \ell^-$ in the Standard Model from Light-Cone Sum Rules*, 1503.05534.
- [89] F. Kruger and J. Matias, *Probing new physics via the transverse amplitudes of $B_0 \rightarrow K^{*0}(\rightarrow K^- \pi^+) \ell^+ \ell^-$ at large recoil*, *Phys.Rev.* **D71** (2005) 094009, [[hep-ph/0502060](#)].
- [90] W. Altmannshofer, P. Ball, A. Bharucha, A. J. Buras, D. M. Straub et al., *Symmetries and Asymmetries of $B \rightarrow K^* \mu^+ \mu^-$ Decays in the Standard Model and Beyond*, *JHEP* **0901** (2009) 019, [[0811.1214](#)].
- [91] J. Matias, F. Mescia, M. Ramon and J. Virto, *Complete Anatomy of $\bar{B}_d \rightarrow \bar{K}^{*0}(\rightarrow K \pi) \ell^+ \ell^-$ and its angular distribution*, *JHEP* **1204** (2012) 104, [[1202.4266](#)].
- [92] LHCb collaboration, R. Aaij et al., *Measurement of the $B^0 \rightarrow K^{*0} e^+ e^-$ branching fraction at low dilepton mass*, *JHEP* **05** (2013) 159, [[1304.3035](#)].
- [93] LHCb collaboration, R. Aaij et al., *Angular analysis of the $B^0 \rightarrow K^{*0} e^+ e^-$ decay in the low- q^2 region*, *JHEP* **04** (2015) 064, [[1501.03038](#)].
- [94] S. Descotes-Genon, J. Matias, M. Ramon and J. Virto, *Implications from clean observables for the binned analysis of $B \rightarrow K^* \mu^+ \mu^-$ at large recoil*, *JHEP* **1301** (2013) 048, [[1207.2753](#)].
- [95] S. Descotes-Genon, T. Hurth, J. Matias and J. Virto, *Optimizing the basis of $B \rightarrow K^* \ell^+ \ell^-$ observables in the full kinematic range*, *JHEP* **1305** (2013) 137, [[1303.5794](#)].

- [96] J. Matias and N. Serra, *Symmetry relations between angular observables in $B^0 \rightarrow K^* \mu^+ \mu^-$ and the LHCb P'_5 anomaly*, *Phys.Rev.* **D90** (2014) 034002, [1402.6855].
- [97] J. Lyon and R. Zwicky, *Resonances gone topsy turvy - the charm of QCD or new physics in $b \rightarrow sl^+ \ell^-$?*, 1406.0566.
- [98] S. Descotes-Genon, L. Hofer, J. Matias and J. Virto, *Global analysis of $b \rightarrow sll$ anomalies*, *JHEP* **06** (2016) 092, [1510.04239].
- [99] A. Khodjamirian, T. Mannel, A. Pivovarov and Y.-M. Wang, *Charm-loop effect in $B \rightarrow K^{(*)} \ell^+ \ell^-$ and $B \rightarrow K^* \gamma$* , *JHEP* **1009** (2010) 089, [1006.4945].
- [100] M. Beneke and T. Feldmann, *Symmetry breaking corrections to heavy to light B meson form-factors at large recoil*, *Nucl.Phys.* **B592** (2001) 3–34, [hep-ph/0008255].
- [101] M. Beneke, T. Feldmann and D. Seidel, *Systematic approach to exclusive $B \rightarrow V l^+ l^-$, $V \gamma$ decays*, *Nucl.Phys.* **B612** (2001) 25–58, [hep-ph/0106067].
- [102] M. Beneke, G. Buchalla, M. Neubert and C. Sachrajda, *Penguins with Charm and Quark-Hadron Duality*, *Eur.Phys.J.* **C61** (2009) 439–449, [0902.4446].
- [103] N. Isgur and M. B. Wise, *Relationship Between Form-factors in Semileptonic \bar{B} and D Decays and Exclusive Rare \bar{B} Meson Decays*, *Phys.Rev.* **D42** (1990) 2388–2391.
- [104] J. Charles, A. Le Yaouanc, L. Oliver, O. Pene and J. Raynal, *Heavy to light form-factors in the heavy mass to large energy limit of QCD*, *Phys.Rev.* **D60** (1999) 014001, [hep-ph/9812358].
- [105] B. Grinstein and D. Pirjol, *Symmetry breaking corrections to heavy meson form-factor relations*, *Phys.Lett.* **B533** (2002) 8–16, [hep-ph/0201298].
- [106] U. Egede, T. Hurth, J. Matias, M. Ramon and W. Reece, *New observables in the decay mode $\bar{B}_d \rightarrow \bar{K}^{*0} l^+ l^-$* , *JHEP* **0811** (2008) 032, [0807.2589].
- [107] P. Colangelo, F. De Fazio, P. Santorelli and E. Scrimieri, *QCD sum rule analysis of the decays $B \rightarrow K l^+ l^-$ and $B \rightarrow K^* l^+ l^-$* , *Phys.Rev.* **D53** (1996) 3672–3686, [hep-ph/9510403].
- [108] P. Ball and R. Zwicky, *New results on $B \rightarrow \pi, K, \eta$ decay form factors from light-cone sum rules*, *Phys.Rev.* **D71** (2005) 014015, [hep-ph/0406232].

- [109] A. Khodjamirian, T. Mannel and N. Offen, *Form-factors from light-cone sum rules with B-meson distribution amplitudes*, *Phys.Rev.* **D75** (2007) 054013, [[hep-ph/0611193](#)].
- [110] R. Horgan, Z. Liu, S. Meinel and M. Wingate, *Rare B decays using lattice QCD form factors*, *PoS LATTICE2014* (2015) 372, [[1501.00367](#)].
- [111] U. Egede, T. Hurth, J. Matias, M. Ramon and W. Reece, *New physics reach of the decay mode $\bar{B} \rightarrow \bar{K}^{*0} \ell^+ \ell^-$* , *JHEP* **1010** (2010) 056, [[1005.0571](#)].
- [112] D. Bečirević and E. Schneider, *On transverse asymmetries in $B \rightarrow K^* \ell^+ \ell^-$* , *Nucl.Phys.* **B854** (2012) 321–339, [[1106.3283](#)].
- [113] D. Das and R. Sinha, *New Physics Effects and Hadronic Form Factor Uncertainties in $B \rightarrow K^* \ell^+ \ell^-$* , *Phys.Rev.* **D86** (2012) 056006, [[1205.1438](#)].
- [114] S. Jäger and J. Martin Camalich, *On $B \rightarrow V \ell \ell$ at small dilepton invariant mass, power corrections, and new physics*, *JHEP* **1305** (2013) 043, [[1212.2263](#)].
- [115] S. Descotes-Genon, J. Matias and J. Virto, *Understanding the $B \rightarrow K^* \mu^+ \mu^-$ Anomaly*, *Phys.Rev.* **D88** (2013) 074002, [[1307.5683](#)].
- [116] S. Descotes-Genon, L. Hofer, J. Matias and J. Virto, *On the impact of power corrections in the prediction of $B \rightarrow K^* \mu^+ \mu^-$ observables*, *JHEP* **1412** (2014) 125, [[1407.8526](#)].
- [117] S. Jäger and J. Martin Camalich, *Reassessing the discovery potential of the $B \rightarrow K^* \ell^+ \ell^-$ decays in the large-recoil region: SM challenges and BSM opportunities*, [1412.3183](#).
- [118] S. W. Bosch and G. Buchalla, *The Radiative decays $B \rightarrow V$ gamma at next-to-leading order in QCD*, *Nucl. Phys.* **B621** (2002) 459–478, [[hep-ph/0106081](#)].
- [119] T. Hurth, F. Mahmoudi and S. Neshatpour, *On the anomalies in the latest LHCb data*, *Nucl. Phys.* **B909** (2016) 737–777, [[1603.00865](#)].
- [120] J. Martin Camalich, *Hadronic uncertainties in semileptonic B decays*, *PoS BEAUTY2016* (2016) 037.
- [121] B. Capdevila, S. Descotes-Genon, L. Hofer and J. Matias, *Hadronic uncertainties in $B \rightarrow K^* \mu^+ \mu^-$: a state-of-the-art analysis*, *JHEP* **04** (2017) 016, [[1701.08672](#)].

- [122] V. G. Chobanova, T. Hurth, F. Mahmoudi, D. Martinez Santos and S. Neshatpour, *Large hadronic power corrections or new physics in the rare decay $B \rightarrow K^* \ell \ell$?*, 1702.02234.
- [123] C. Bobeth, M. Chrzaszcz, D. van Dyk and J. Virto, *Long-distance effects in $B \rightarrow K^* \ell \ell$ from Analyticity*, 1707.07305.
- [124] T. Blake, U. Egede, P. Owen, G. Pomery and K. A. Petridis, *An empirical model of the long-distance contributions to $\bar{B}^0 \rightarrow \bar{K}^{*0} \mu^+ \mu^-$ transitions*, 1709.03921.
- [125] T. Blake, M. Gersabeck, L. Hofer, S. Jäger, Z. Liu and R. Zwicky, *Round table: Flavour anomalies in $b \rightarrow sl^+l$ processes*, *EPJ Web Conf.* **137** (2017) 01001, [1703.10005].
- [126] CMS collaboration, *Measurement of the P_1 and P'_5 angular parameters of the decay $B^0 \rightarrow K^{*0} \mu^+ \mu^-$ in proton-proton collisions at $\sqrt{s} = 8$ TeV*, Tech. Rep. CMS-PAS-BPH-15-008, CERN, Geneva, 2017.
- [127] T. Hurth and F. Mahmoudi, *On the LHCb anomaly in $B \rightarrow K^* \ell^+ \ell^-$* , *JHEP* **1404** (2014) 097, [1312.5267].
- [128] W. Altmannshofer and D. M. Straub, *New physics in $b \rightarrow s$ transitions after LHC run 1*, *Eur. Phys. J.* **C75** (2015) 382, [1411.3161].
- [129] B. Capdevila, S. Descotes-Genon, J. Matias and J. Virto, *Assessing lepton-flavour non-universality from $B \rightarrow K^* \ell \ell$ angular analyses*, *JHEP* **10** (2016) 075, [1605.03156].
- [130] C. Bobeth, G. Hiller, D. van Dyk and C. Wacker, *The Decay $B \rightarrow Kl^+l^-$ at Low Hadronic Recoil and Model-Independent $\Delta B = 1$ Constraints*, *JHEP* **1201** (2012) 107, [1111.2558].
- [131] A. Khodjamirian, T. Mannel and Y. M. Wang, *$B \rightarrow K \ell^+ \ell^-$ decay at large hadronic recoil*, *JHEP* **02** (2013) 010, [1211.0234].
- [132] G. Hiller and F. Kruger, *More model-independent analysis of $b \rightarrow s$ processes*, *Phys. Rev.* **D69** (2004) 074020, [hep-ph/0310219].
- [133] M. Bordone, G. Isidori and A. Pattori, *On the Standard Model predictions for R_K and R_{K^*}* , *Eur. Phys. J.* **C76** (2016) 440, [1605.07633].
- [134] N. Serra, R. Silva Coutinho and D. van Dyk, *Measuring the breaking of lepton flavor universality in $B \rightarrow K^* \ell^+ \ell^-$* , *Phys. Rev.* **D95** (2017) 035029, [1610.08761].

- [135] W. Altmannshofer, C. Niehoff, P. Stangl and D. M. Straub, *Status of the $B \rightarrow K^* \mu^+ \mu^-$ anomaly after Moriond 2017*, 1703.09189.
- [136] R. Alonso, B. Grinstein and J. Martin Camalich, *$SU(2) \times U(1)$ gauge invariance and the shape of new physics in rare B decays*, *Phys. Rev. Lett.* **113** (2014) 241802, [1407.7044].
- [137] G. Hiller and M. Schmaltz, *R_K and future $b \rightarrow sll$ physics beyond the standard model opportunities*, *Phys. Rev.* **D90** (2014) 054014, [1408.1627].
- [138] D. Ghosh, M. Nardecchia and S. A. Renner, *Hint of Lepton Flavour Non-Universality in B Meson Decays*, *JHEP* **12** (2014) 131, [1408.4097].
- [139] S. L. Glashow, D. Guadagnoli and K. Lane, *Lepton Flavor Violation in B Decays?*, *Phys. Rev. Lett.* **114** (2015) 091801, [1411.0565].
- [140] G. Hiller and M. Schmaltz, *Diagnosing lepton-nonuniversality in $b \rightarrow sll$* , *JHEP* **02** (2015) 055, [1411.4773].
- [141] B. Gripaios, M. Nardecchia and S. A. Renner, *Composite leptoquarks and anomalies in B -meson decays*, *JHEP* **05** (2015) 006, [1412.1791].
- [142] S. Sahoo and R. Mohanta, *Scalar leptoquarks and the rare B meson decays*, *Phys. Rev.* **D91** (2015) 094019, [1501.05193].
- [143] A. Crivellin, G. D'Ambrosio and J. Heeck, *Addressing the LHC flavor anomalies with horizontal gauge symmetries*, *Phys. Rev.* **D91** (2015) 075006, [1503.03477].
- [144] A. Crivellin, L. Hofer, J. Matias, U. Nierste, S. Pokorski and J. Rosiek, *Lepton-flavour violating B decays in generic Z' models*, *Phys. Rev.* **D92** (2015) 054013, [1504.07928].
- [145] A. Celis, J. Fuentes-Martin, M. Jung and H. Serodio, *Family nonuniversal Z models with protected flavor-changing interactions*, *Phys. Rev.* **D92** (2015) 015007, [1505.03079].
- [146] R. Alonso, B. Grinstein and J. Martin Camalich, *Lepton universality violation and lepton flavor conservation in B -meson decays*, *JHEP* **10** (2015) 184, [1505.05164].
- [147] A. Greljo, G. Isidori and D. Marzocca, *On the breaking of Lepton Flavor Universality in B decays*, *JHEP* **07** (2015) 142, [1506.01705].

- [148] L. Calibbi, A. Crivellin and T. Ota, *Effective Field Theory Approach to $b \rightarrow sll^{(\prime)}$, $B \rightarrow K^{(*)}\nu\bar{\nu}$ and $B \rightarrow D^{(*)}\tau\nu$ with Third Generation Couplings*, *Phys. Rev. Lett.* **115** (2015) 181801, [1506.02661].
- [149] A. Falkowski, M. Nardecchia and R. Ziegler, *Lepton Flavor Non-Universality in B-meson Decays from a $U(2)$ Flavor Model*, *JHEP* **11** (2015) 173, [1509.01249].
- [150] A. Carmona and F. Goertz, *Lepton Flavor and Nonuniversality from Minimal Composite Higgs Setups*, *Phys. Rev. Lett.* **116** (2016) 251801, [1510.07658].
- [151] C.-W. Chiang, X.-G. He and G. Valencia, *Z model for $b \rightarrow s\bar{\ell}\ell$ flavor anomalies*, *Phys. Rev.* **D93** (2016) 074003, [1601.07328].
- [152] D. Bečirević, O. Sumensari and R. Zukanovich Funchal, *Lepton flavor violation in exclusive $b \rightarrow s$ decays*, *Eur. Phys. J.* **C76** (2016) 134, [1602.00881].
- [153] F. Feruglio, P. Paradisi and A. Pattori, *Revisiting Lepton Flavor Universality in B Decays*, *Phys. Rev. Lett.* **118** (2017) 011801, [1606.00524].
- [154] E. Megias, G. Panico, O. Pujolas and M. Quiros, *A Natural origin for the $LHCb$ anomalies*, *JHEP* **09** (2016) 118, [1608.02362].
- [155] D. Bečirević, N. Košnik, O. Sumensari and R. Zukanovich Funchal, *Palatable Leptoquark Scenarios for Lepton Flavor Violation in Exclusive $b \rightarrow s\ell_1\ell_2$ modes*, *JHEP* **11** (2016) 035, [1608.07583].
- [156] P. Arnan, L. Hofer, F. Mescia and A. Crivellin, *Loop effects of heavy new scalars and fermions in $b \rightarrow s\mu^+\mu^-$* , *JHEP* **04** (2017) 043, [1608.07832].
- [157] S. Sahoo, R. Mohanta and A. K. Giri, *Explaining the R_K and $R_{D^{(*)}}$ anomalies with vector leptoquarks*, *Phys. Rev.* **D95** (2017) 035027, [1609.04367].
- [158] R. Alonso, E. Fernandez Martinez, M. B. Gavela, B. Grinstein, L. Merlo and P. Quilez, *Gauged Lepton Flavour*, *JHEP* **12** (2016) 119, [1609.05902].
- [159] G. Hiller, D. Loose and K. Schonwald, *Leptoquark Flavor Patterns & B Decay Anomalies*, *JHEP* **12** (2016) 027, [1609.08895].
- [160] I. Galon, A. Kwa and P. Tanedo, *Lepton-Flavor Violating Mediators*, *JHEP* **03** (2017) 064, [1610.08060].

- [161] A. Crivellin, J. Fuentes-Martin, A. Greljo and G. Isidori, *Lepton Flavor Non-Universality in B decays from Dynamical Yukawas*, *Phys. Lett.* **B766** (2017) 77–85, [1611.02703].
- [162] I. García García, *LHCb anomalies from a natural perspective*, *JHEP* **03** (2017) 040, [1611.03507].
- [163] P. Cox, A. Kusenko, O. Sumensari and T. T. Yanagida, *SU(5) Unification with TeV-scale Leptoquarks*, *JHEP* **03** (2017) 035, [1612.03923].
- [164] S. Jäger, K. Leslie, M. Kirk and A. Lenz, *Charming new physics in rare B-decays and mixing?*, 1701.09183.
- [165] E. Megias, M. Quiros and L. Salas, *Lepton-flavor universality violation in R_K and $R_{D^{(*)}}$ from warped space*, *JHEP* **07** (2017) 102, [1703.06019].
- [166] A. Crivellin, D. Müller and T. Ota, *Simultaneous explanation of $R(D^{(*)})$ and $b \rightarrow s\mu^+\mu^-$: the last scalar leptoquarks standing*, *JHEP* **09** (2017) 040, [1703.09226].
- [167] A. Celis, J. Fuentes-Martin, A. Vicente and J. Virto, *Gauge-invariant implications of the LHCb measurements on lepton-flavor nonuniversality*, *Phys. Rev.* **D96** (2017) 035026, [1704.05672].
- [168] D. Bečirević and O. Sumensari, *A leptoquark model to accommodate $R_K^{\text{exp}} < R_K^{\text{SM}}$ and $R_{K^*}^{\text{exp}} < R_{K^*}^{\text{SM}}$* , *JHEP* **08** (2017) 104, [1704.05835].
- [169] Y. Cai, J. Gargalionis, M. A. Schmidt and R. R. Volkas, *Reconsidering the One Leptoquark solution: flavor anomalies and neutrino mass*, 1704.05849.
- [170] J. F. Kamenik, Y. Soreq and J. Zupan, *Lepton flavor universality violation without new sources of quark flavor violation*, 1704.06005.
- [171] S. Di Chiara, A. Fowlie, S. Fraser, C. Marzo, L. Marzola, M. Raidal et al., *Minimal flavor-changing Z' models and muon $g - 2$ after the R_{K^*} measurement*, *Nucl. Phys.* **B923** (2017) 245–257, [1704.06200].
- [172] D. Ghosh, *Explaining the R_K and R_{K^*} anomalies*, 1704.06240.
- [173] A. K. Alok, D. Kumar, J. Kumar and R. Sharma, *Lepton flavor non-universality in the B-sector: a global analyses of various new physics models*, 1704.07347.
- [174] A. K. Alok, B. Bhattacharya, A. Datta, D. Kumar, J. Kumar and D. London, *New Physics in $b \rightarrow s\mu^+\mu^-$ after the Measurement of R_{K^*}* , 1704.07397.

- [175] R. Alonso, P. Cox, C. Han and T. T. Yanagida, *Anomaly-free local horizontal symmetry and anomaly-full rare B-decays*, 1704.08158.
- [176] W. Wang and S. Zhao, *Implications of the R_K and R_{K^*} anomalies*, 1704.08168.
- [177] A. Greljo and D. Marzocca, *High- p_T dilepton tails and flavor physics*, *Eur. Phys. J.* **C77** (2017) 548, [1704.09015].
- [178] C. Bonilla, T. Modak, R. Srivastava and J. W. F. Valle, *$U(1)_{B_3-3L_\mu}$ gauge symmetry as the simplest description of $b \rightarrow s$ anomalies*, 1705.00915.
- [179] F. Feruglio, P. Paradisi and A. Pattori, *On the Importance of Electroweak Corrections for B Anomalies*, *JHEP* **09** (2017) 061, [1705.00929].
- [180] J. Ellis, M. Fairbairn and P. Tunney, *Anomaly-Free Models for Flavour Anomalies*, 1705.03447.
- [181] F. Bishara, U. Haisch and P. F. Monni, *Regarding light resonance interpretations of the B decay anomalies*, *Phys. Rev.* **D96** (2017) 055002, [1705.03465].
- [182] R. Alonso, P. Cox, C. Han and T. T. Yanagida, *Flavoured B – L Local Symmetry and Anomalous Rare B Decays*, 1705.03858.
- [183] E. Megias, G. Panico, O. Pujolas and M. Quiros, *A Natural extra-dimensional origin for the LHCb anomalies*, in *52nd Rencontres de Moriond on EW Interactions and Unified Theories (Moriond EW 2017) La Thuile, Italy, March 18-25, 2017*, 2017. 1705.04822.
- [184] Y. Tang and Y.-L. Wu, *Flavor Non-universality Gauge Interactions and Anomalies in B-Meson Decays*, 1705.05643.
- [185] T. Hurth, F. Mahmoudi, D. Martinez Santos and S. Neshatpour, *On lepton non-universality in exclusive $b \rightarrow s\ell\ell$ decays*, 1705.06274.
- [186] A. Datta, J. Kumar, J. Liao and D. Marfatia, *New light mediators for the R_K and R_{K^*} puzzles*, 1705.08423.
- [187] D. Das, C. Hati, G. Kumar and N. Mahajan, *Scrutinizing R-parity violating interactions in light of $R_{K^{(*)}}$ data*, 1705.09188.
- [188] D. N. Dinh, L. Merlo, S. T. Petcov and R. Vega-Álvarez, *Revisiting Minimal Lepton Flavour Violation in the Light of Leptonic CP Violation*, *JHEP* **07** (2017) 089, [1705.09284].

- [189] D. Bardhan, P. Byakti and D. Ghosh, *Role of Tensor operators in R_K and R_{K^*}* , *Phys. Lett.* **B773** (2017) 505–512, [1705.09305].
- [190] A. Crivellin, *New Physics in Flavour Observables*, in *52nd Rencontres de Moriond on EW Interactions and Unified Theories (Moriond EW 2017) La Thuile, Italy, March 18-25, 2017*, 2017. 1706.00929.
- [191] S. Matsuzaki, K. Nishiwaki and R. Watanabe, *Phenomenology of flavorful composite vector bosons in light of B anomalies*, *JHEP* **08** (2017) 145, [1706.01463].
- [192] L. Di Luzio and M. Nardecchia, *What is the scale of new physics behind the B -flavour anomalies?*, *Eur. Phys. J.* **C77** (2017) 536, [1706.01868].
- [193] C.-W. Chiang, X.-G. He, J. Tandean and X.-B. Yuan, *$R_{K^{(*)}}$ and related $b \rightarrow s\ell\bar{\ell}$ anomalies in minimal flavor violation framework with Z' boson*, 1706.02696.
- [194] B. Chauhan, B. Kindra and A. Narang, *A Leptoquark explanation for $(g-2)_\mu$, R_K , R_{K^*} and, IceCube PeV events*, 1706.04598.
- [195] S. F. King, *Flavourful Z models for $R_{K^{(*)}}$* , *JHEP* **08** (2017) 019, [1706.06100].
- [196] M. Blanke, *Theoretical implications of recent heavy flavour measurements at the LHC*, in *5th Large Hadron Collider Physics Conference (LHCP 2017) Shanghai, China, May 15-20, 2017*, 2017. 1706.06464.
- [197] R. S. Chivukula, J. Isaacson, K. A. Mohan, D. Sengupta and E. H. Simmons, *R_K anomalies and simplified limits on Z' models at the LHC*, 1706.06575.
- [198] S. Khalil, *Explaining the R_K and R_{K^*} Anomalies With Right-handed Sneutrino*, 1706.07337.
- [199] X.-G. He and G. Valencia, *Are the B -anomalies evidence for heavy neutrinos?*, 1706.07570.
- [200] I. Doršner, S. Fajfer, D. A. Faroughy and N. Košnik, *Saga of the two GUT leptoquarks in flavor universality and collider searches*, 1706.07779.
- [201] D. Buttazzo, A. Greljo, G. Isidori and D. Marzocca, *B -physics anomalies: a guide to combined explanations*, 1706.07808.

- [202] D. Choudhury, A. Kundu, R. Mandal and R. Sinha, *Minimal unified resolution to $R_{K^{(*)}}$ and $R(D^{(*)})$ anomalies with lepton mixing*, 1706.08437.
- [203] J. M. Cline and J. Martin Camalich, *B decay anomalies from nonabelian local horizontal symmetry*, 1706.08510.
- [204] A. Crivellin, D. Mueller, A. Signer and Y. Ulrich, *Correlating Lepton Flavour (Universality) Violation in B Decays with $\mu \rightarrow e\gamma$ using Leptoquarks*, 1706.08511.
- [205] S.-Y. Guo, Z.-L. Han, B. Li, Y. Liao and X.-D. Ma, *Interpreting the $R_{K^{(*)}}$ Anomaly in the Colored Zee-Babu Model*, 1707.00522.
- [206] C.-H. Chen and T. Nomura, *Penguin $b \rightarrow s\ell^+\ell^-$ and B-meson anomalies in a gauged $L_\mu - L_\tau$* , 1707.03249.
- [207] S. Baek, *Dark matter contribution to $b \rightarrow s\mu^+\mu^-$ anomaly in local $U(1)_{L_\mu - L_\tau}$ model*, 1707.04573.
- [208] L. Bian, S.-M. Choi, Y.-J. Kang and H. M. Lee, *A minimal flavored $U(1)'$ for B-meson anomalies*, 1707.04811.
- [209] E. Megias, M. Quiros and L. Salas, *Lepton-flavor universality limits in warped space*, 1707.08014.
- [210] H. M. Lee, *Gauged $U(1)$ Clockwork Theory*, 1708.03564.
- [211] N. Assad, B. Fornal and B. Grinstein, *Baryon Number and Lepton Universality Violation in Leptoquark and Diquark Models*, 1708.06350.
- [212] L. Di Luzio, A. Greljo and M. Nardecchia, *Gauge leptoquark as the origin of B-physics anomalies*, 1708.08450.
- [213] L. Calibbi, A. Crivellin and T. Li, *A model of vector leptoquarks in view of the B-physics anomalies*, 1709.00692.
- [214] B. Capdevila, A. Crivellin, S. Descotes-Genon, J. Matias and J. Virto, *Patterns of New Physics in $b \rightarrow s\ell^+\ell^-$ transitions in the light of recent data*, 1704.05340.
- [215] L.-S. Geng, B. Grinstein, S. Jäger, J. Martin Camalich, X.-L. Ren and R.-X. Shi, *Towards the discovery of new physics with lepton-universality ratios of $b \rightarrow s\ell\ell$ decays*, 1704.05446.

- [216] W. Altmannshofer, P. Stangl and D. M. Straub, *Interpreting Hints for Lepton Flavor Universality Violation*, *Phys. Rev.* **D96** (2017) 055008, [1704.05435].
- [217] G. Hiller and I. Nisandzic, *R_K and R_{K^*} beyond the standard model*, *Phys. Rev.* **D96** (2017) 035003, [1704.05444].
- [218] G. D’Amico, M. Nardecchia, P. Panci, F. Sannino, A. Strumia, R. Torre et al., *Flavour anomalies after the R_{K^*} measurement*, *JHEP* **09** (2017) 010, [1704.05438].
- [219] CLEO collaboration, T. E. Coan et al., *Study of exclusive radiative B meson decays*, *Phys. Rev. Lett.* **84** (2000) 5283–5287, [hep-ex/9912057].
- [220] BELLE collaboration, M. Nakao et al., *Measurement of the $B \rightarrow K^* \gamma$ branching fractions and asymmetries*, *Phys. Rev.* **D69** (2004) 112001, [hep-ex/0402042].
- [221] BABAR collaboration, B. Aubert et al., *Measurement of Branching Fractions and CP and Isospin Asymmetries in $B \rightarrow K^*(892)\gamma$ Decays*, *Phys. Rev. Lett.* **103** (2009) 211802, [0906.2177].
- [222] PARTICLE DATA GROUP collaboration, K. A. Olive et al., *Review of Particle Physics*, *Chin. Phys.* **C38** (2014) 090001.
- [223] T. Ando, *Predictive bayesian model selection*, *American Journal of Mathematical and Management Sciences* **31** (2011) 13–38.
- [224] A. Gelman, J. B. Carlin, H. S. Stern and D. B. Rubin, *Bayesian data analysis*. Texts in Statistical Science Series. Chapman & Hall/CRC, Boca Raton, FL, second ed., 2004.
- [225] A. Paul and D. M. Straub, *Constraints on new physics from radiative B decays*, *JHEP* **04** (2017) 027, [1608.02556].
- [226] J. Aebischer, A. Crivellin, M. Fael and C. Greub, *Matching of gauge invariant dimension-six operators for $b \rightarrow s$ and $b \rightarrow c$ transitions*, *JHEP* **05** (2016) 037, [1512.02830].
- [227] BABAR collaboration, J. P. Lees et al., *Evidence for an excess of $\bar{B} \rightarrow D^{(*)} \tau^- \bar{\nu}_\tau$ decays*, *Phys. Rev. Lett.* **109** (2012) 101802, [1205.5442].
- [228] BELLE collaboration, M. Huschle et al., *Measurement of the branching ratio of $\bar{B} \rightarrow D^{(*)} \tau^- \bar{\nu}_\tau$ relative to $\bar{B} \rightarrow D^{(*)} \ell^- \bar{\nu}_\ell$ decays with hadronic tagging at Belle*, *Phys. Rev.* **D92** (2015) 072014, [1507.03233].

- [229] BELLE collaboration, A. Abdesselam et al., *Measurement of the branching ratio of $\bar{B}^0 \rightarrow D^{*+}\tau^-\bar{\nu}_\tau$ relative to $\bar{B}^0 \rightarrow D^{*+}\ell^-\bar{\nu}_\ell$ decays with a semileptonic tagging method*, in *Proceedings, 51st Rencontres de Moriond on Electroweak Interactions and Unified Theories: La Thuile, Italy, March 12-19, 2016*, 2016. 1603.06711.
- [230] LHCb collaboration, R. Aaij et al., *Measurement of the ratio of branching fractions $\mathcal{B}(\bar{B}^0 \rightarrow D^{*+}\tau^-\bar{\nu}_\tau)/\mathcal{B}(\bar{B}^0 \rightarrow D^{*+}\mu^-\bar{\nu}_\mu)$* , *Phys. Rev. Lett.* **115** (2015) 111803, [1506.08614].
- [231] CMS collaboration, V. Khachatryan et al., *Precise determination of the mass of the Higgs boson and tests of compatibility of its couplings with the standard model predictions using proton collisions at 7 and 8 TeV*, *Eur. Phys. J.* **C75** (2015) 212, [1412.8662].
- [232] ATLAS collaboration, G. Aad et al., *Measurements of the Higgs boson production and decay rates and coupling strengths using pp collision data at $\sqrt{s} = 7$ and 8 TeV in the ATLAS experiment*, *Eur. Phys. J.* **C76** (2016) 6, [1507.04548].
- [233] ATLAS, CMS collaboration, G. Aad et al., *Measurements of the Higgs boson production and decay rates and constraints on its couplings from a combined ATLAS and CMS analysis of the LHC pp collision data at $\sqrt{s} = 7$ and 8 TeV*, 1606.02266.
- [234] CMS collaboration, *Projected Performance of an Upgraded CMS Detector at the LHC and HL-LHC: Contribution to the Snowmass Process*, in *Community Summer Study 2013: Snowmass on the Mississippi (CSS2013) Minneapolis, MN, USA, July 29-August 6, 2013*, 2013. 1307.7135.
- [235] M. E. Peskin, *Estimation of LHC and ILC Capabilities for Precision Higgs Boson Coupling Measurements*, in *Community Summer Study 2013: Snowmass on the Mississippi (CSS2013) Minneapolis, MN, USA, July 29-August 6, 2013*, 2013. 1312.4974.
- [236] ATLAS collaboration, *Projections for measurements of Higgs boson signal strengths and coupling parameters with the ATLAS detector at a HL-LHC*, Tech. Rep. ATL-PHYS-PUB-2014-016, CERN, Geneva, Oct, 2014.
- [237] ATLAS collaboration, G. Aad et al., *Searches for Higgs boson pair production in the $hh \rightarrow bb\tau\tau, \gamma\gamma WW^*, \gamma\gamma bb, bbbb$ channels with the ATLAS detector*, *Phys. Rev.* **D92** (2015) 092004, [1509.04670].

- [238] ATLAS collaboration, G. Aad et al., *Search for Higgs boson pair production in the $b\bar{b}b\bar{b}$ final state from pp collisions at $\sqrt{s} = 8$ TeV with the ATLAS detector*, *Eur. Phys. J.* **C75** (2015) 412, [1506.00285].
- [239] CMS collaboration, V. Khachatryan et al., *Search for two Higgs bosons in final states containing two photons and two bottom quarks*, 1603.06896.
- [240] ATLAS collaboration, *Search for pair production of Higgs bosons in the $b\bar{b}b\bar{b}$ final state using proton–proton collisions at $\sqrt{s} = 13$ TeV with the ATLAS detector*, Tech. Rep. ATLAS-CONF-2016-049, CERN, Geneva, Aug, 2016.
- [241] D. de Florian and J. Mazzitelli, *Higgs Boson Pair Production at Next-to-Next-to-Leading Order in QCD*, *Phys. Rev. Lett.* **111** (2013) 201801, [1309.6594].
- [242] F. Maltoni, E. Vryonidou and M. Zaro, *Top-quark mass effects in double and triple Higgs production in gluon-gluon fusion at NLO*, *JHEP* **11** (2014) 079, [1408.6542].
- [243] S. Borowka, N. Greiner, G. Heinrich, S. Jones, M. Kerner, J. Schlenk et al., *Higgs Boson Pair Production in Gluon Fusion at Next-to-Leading Order with Full Top-Quark Mass Dependence*, *Phys. Rev. Lett.* **117** (2016) 012001, [1604.06447].
- [244] J. Baglio, A. Djouadi, R. Gröber, M. Mühlleitner, J. Quevillon et al., *The measurement of the Higgs self-coupling at the LHC: theoretical status*, *JHEP* **1304** (2013) 151, [1212.5581].
- [245] R. Frederix, S. Frixione, V. Hirschi, F. Maltoni, O. Mattelaer, P. Torrielli et al., *Higgs pair production at the LHC with NLO and parton-shower effects*, *Phys. Lett.* **B732** (2014) 142–149, [1401.7340].
- [246] CMS collaboration, C. Collaboration, *Search for Higgs boson pair production in the final state containing two photons and two bottom quarks in proton-proton collisions at $\sqrt{s} = 13$ TeV*, .
- [247] *Prospects for measuring Higgs pair production in the channel $H(\rightarrow \gamma\gamma)H(\rightarrow b\bar{b})$ using the ATLAS detector at the HL-LHC*, Tech. Rep. ATL-PHYS-PUB-2014-019, CERN, Geneva, Oct, 2014.
- [248] ATLAS collaboration, *Study of the double Higgs production channel $H(\rightarrow b\bar{b})H(\rightarrow \gamma\gamma)$ with the ATLAS experiment at the HL-LHC*, Tech. Rep. ATL-PHYS-PUB-2017-001, CERN, Geneva, Jan, 2017.

- [249] *Higgs Pair Production in the $H(\rightarrow \tau\tau)H(\rightarrow b\bar{b})$ channel at the High-Luminosity LHC*, Tech. Rep. ATL-PHYS-PUB-2015-046, CERN, Geneva, Nov, 2015.
- [250] T. Plehn and M. Rauch, *The quartic higgs coupling at hadron colliders*, *Phys. Rev.* **D72** (2005) 053008, [[hep-ph/0507321](#)].
- [251] T. Binoth, S. Karg, N. Kauer and R. Ruckl, *Multi-Higgs boson production in the Standard Model and beyond*, *Phys. Rev.* **D74** (2006) 113008, [[hep-ph/0608057](#)].
- [252] G. Degrossi, P. P. Giardino, F. Maltoni and D. Pagani, *Probing the Higgs self coupling via single Higgs production at the LHC*, *JHEP* **12** (2016) 080, [[1607.04251](#)].
- [253] M. Gorbahn and U. Haisch, *Indirect probes of the trilinear Higgs coupling: $gg \rightarrow h$ and $h \rightarrow \gamma\gamma$* , *JHEP* **10** (2016) 094, [[1607.03773](#)].
- [254] W. Bizon, M. Gorbahn, U. Haisch and G. Zanderighi, *Constraints on the trilinear Higgs coupling from vector boson fusion and associated Higgs production at the LHC*, [1610.05771](#).
- [255] C. Grojean, G. Servant and J. D. Wells, *First-order electroweak phase transition in the standard model with a low cutoff*, *Phys. Rev.* **D71** (2005) 036001, [[hep-ph/0407019](#)].
- [256] M. McCullough, *An Indirect Model-Dependent Probe of the Higgs Self-Coupling*, *Phys. Rev.* **D90** (2014) 015001, [[1312.3322](#)].
- [257] A. Sirlin, *Role of $\sin^2 \theta_W(m_Z)$ at the Z^0 Peak*, *Phys. Lett.* **B232** (1989) 123–126.
- [258] S. Fanchiotti and A. Sirlin, *Accurate Determination of $\sin^2 \theta_W(m_Z)$* , *Phys. Rev.* **D41** (1990) 319.
- [259] G. Degrossi, S. Fanchiotti and A. Sirlin, *Relations Between the On-shell and \overline{MS} Frameworks and the m_W – m_Z Interdependence*, *Nucl. Phys.* **B351** (1991) 49–69.
- [260] G. Degrossi, P. Gambino and P. P. Giardino, *The m_W – m_Z interdependence in the Standard Model: a new scrutiny*, *JHEP* **05** (2015) 154, [[1411.7040](#)].
- [261] P. Gambino and A. Sirlin, *Relation between $\sin^2 \theta_W(m_Z)$ and $\sin^2 \theta_{\text{eff}}^{\text{lep}}$* , *Phys. Rev.* **D49** (1994) 1160–1162, [[hep-ph/9309326](#)].

- [262] A. Sirlin, *Radiative Corrections in the $SU(2)_L \times U(1)$ Theory: A Simple Renormalization Framework*, *Phys. Rev.* **D22** (1980) 971–981.
- [263] R. Mertig, M. Bohm and A. Denner, *FEYN CALC: Computer algebraic calculation of Feynman amplitudes*, *Comput. Phys. Commun.* **64** (1991) 345–359.
- [264] V. Shtabovenko, R. Mertig and F. Orellana, *New Developments in FeynCalc 9.0*, 1601.01167.
- [265] R. Mertig and R. Scharf, *TARCER: A Mathematica program for the reduction of two loop propagator integrals*, *Comput. Phys. Commun.* **111** (1998) 265–273, [hep-ph/9801383].
- [266] A. I. Davydychev and J. B. Tausk, *Two loop selfenergy diagrams with different masses and the momentum expansion*, *Nucl. Phys.* **B397** (1993) 123–142.
- [267] S. P. Martin, *Evaluation of two loop selfenergy basis integrals using differential equations*, *Phys. Rev.* **D68** (2003) 075002, [hep-ph/0307101].
- [268] S. P. Martin and D. G. Robertson, *TSIL: A Program for the calculation of two-loop self-energy integrals*, *Comput. Phys. Commun.* **174** (2006) 133–151, [hep-ph/0501132].
- [269] J. M. Cornwall, D. N. Levin and G. Tiktopoulos, *Derivation of Gauge Invariance from High-Energy Unitarity Bounds on the s Matrix*, *Phys. Rev.* **D10** (1974) 1145.
- [270] A. Falkowski, *Three slides on triple Higgs couplings*, Talk given at the LHC Higgs Cross Section Working Group, HH subgroup meeting, Geneva December 12th, 2016 .
- [271] L. Di Luzio, R. Gröber and M. Spannowsky, *Maxi-sizing the trilinear Higgs self-coupling: how large could it be?*, 1704.02311.
- [272] ATLAS collaboration, M. Aaboud et al., *Measurement of the W -boson mass in pp collisions at $\sqrt{s} = 7$ TeV with the ATLAS detector*, 1701.07240.
- [273] PARTICLE DATA GROUP collaboration, C. Patrignani et al., *Review of Particle Physics*, *Chin. Phys.* **C40** (2016) 100001.

- [274] CDF collaboration, T. A. Aaltonen et al., *Measurement of $\sin^2 \theta_{\text{eff}}^{\text{lept}}$ using e^+e^- pairs from γ^*/Z bosons produced in $p\bar{p}$ collisions at a center-of-momentum energy of 1.96 TeV*, *Phys. Rev.* **D93** (2016) 112016, [1605.02719].
- [275] D0 collaboration, V. M. Abazov et al., *Measurement of the effective weak mixing angle in $p\bar{p} \rightarrow Z/\gamma^* \rightarrow e^+e^-$ events*, *Phys. Rev. Lett.* **115** (2015) 041801, [1408.5016].
- [276] M. Awramik, M. Czakon and A. Freitas, *Bosonic corrections to the effective weak mixing angle at $\mathcal{O}(\alpha^2)$* , *Phys. Lett.* **B642** (2006) 563–566, [hep-ph/0605339].
- [277] A. Sirlin and R. Zucchini, *Dependence of the Quartic Coupling $h_{\text{MS}}(M)$ on m_h and the Possible Onset of New Physics in the Higgs Sector of the Standard Model*, *Nucl. Phys.* **B266** (1986) 389–409.